Monthly Notices
of the
ROYAL ASTRONOMICAL SOCIETY

MNRAS **465,** 3977–4015 (2017)
Advance Access publication 2016 November 17

doi:10.1093/mnras/stw2962

Blue diffuse dwarf galaxies: a clearer picture

Bethan L. James,[1,2,3★] Sergey E. Koposov,[1] Daniel P. Stark,[4] Vasily Belokurov,[1] Max Pettini,[1] Edward W. Olszewski[4] and Kristen B. W. McQuinn[5]

[1]*Institute of Astronomy, University of Cambridge, Madingley Road, Cambridge CB3 0HA, UK*
[2]*Cavendish Laboratory, University of Cambridge, 19 J.J. Thomson Avenue, Cambridge CB3 0HE, UK*
[3]*Kavli Institute for Cosmology, University of Cambridge, Madingley Road, Cambridge CB3 0HA, UK*
[4]*Steward Observatory, The University of Arizona, 933 N Cherry Avenue, Tucson, AZ 85721, USA*
[5]*University of Texas at Austin, McDonald Observatory, 2515 Speedway, Stop C1402, Austin, TX 78712, USA*

Accepted 2016 November 14. Received 2016 November 14; in original form 2016 August 11

ABSTRACT

The search for chemically unevolved galaxies remains prevalent in the nearby Universe, mostly because these systems provide excellent proxies for exploring in detail the physics of high-z systems. The most promising candidates are extremely metal-poor galaxies (XMPs), i.e. galaxies with $<1/10$ solar metallicity. However, due to the bright emission-line-based search criteria traditionally used to find XMPs, we may not be sampling the full XMP population. In 2014, we reoriented this search using only morphological properties and uncovered a population of ∼150 'blue diffuse dwarf (BDD) galaxies', and published a sub-sample of 12 BDD spectra. Here, we present optical spectroscopic observations of a larger sample of 51 BDDs, along with their Sloan Digital Sky Survey (SDSS) photometric properties. With our improved statistics, we use direct-method abundances to confirm that BDDs are chemically unevolved ($7.43 < 12 + \log(\mathrm{O/H}) < 8.01$), with ∼20 per cent of our sample classified as being XMP galaxies, and find that they are actively forming stars at rates of $\sim$1–33 $\times\ 10^{-2}$ $\mathrm{M}_\odot\ \mathrm{yr}^{-1}$ in H II regions randomly embedded in a blue, low-surface-brightness continuum. Stellar masses are calculated from population synthesis models and estimated to be in the range $\log(M_*/\mathrm{M}_\odot) \simeq 5$–9. Unlike other low-metallicity star-forming galaxies, BDDs are in agreement with the mass–metallicity relation at low masses, suggesting that they are not accreting large amounts of pristine gas relative to their stellar mass. BDD galaxies appear to be a population of actively star-forming dwarf irregular (dIrr) galaxies which fall within the class of low-surface-brightness dIrr galaxies. Their ongoing star formation and irregular morphology make them excellent analogues for galaxies in the early Universe.

Key words: galaxies: abundances – galaxies: dwarf – galaxies: evolution – galaxies: irregular – galaxies: star formation.

1 INTRODUCTION

According to hierarchical formation, dwarf ($M_\star \lesssim 10^9\ \mathrm{M}_\odot$) galaxies are the first systems to collapse and start forming stars, supplying the building blocks for the formation of more massive galaxies through merging and accretion. As remnants of this process, present-day dwarfs may have been sites of the earliest star formation (SF) activity in the Universe. However, to date, all dwarf irregular (dIrr) and blue compact dwarf (BCD) galaxies with star formation histories (SFHs) studied from *Hubble Space Telescope* (*HST*) imaging of their resolved stellar population show stars older than 10 Gyr (e.g. Aloisi, Tosi & Greggio 1999; Izotov & Thuan 2002; Aloisi et al. 2007; McQuinn et al. 2010; Weisz et al. 2011). Irrespective of such findings, these chemically unevolved systems, with young stellar populations superimposed upon older, underlying populations, are still used as nearby guides that provide essential information on early galaxy formation and stellar evolution which cannot be extracted from the faint systems now being detected at $z \sim 9$–11 (e.g. Ellis et al. 2013; Pirzkal et al. 2015; Oesch et al. 2016).

Based on the mass–metallicity relation (e.g. Berg et al. 2012) and the galaxy luminosity function, we know that low-mass, and hence low-metallicity, objects should be abundant. However, locating the most metal-poor galaxies [i.e. extremely metal poor with $<0.1\,\mathrm{Z}_\odot$ or $12 + \log(\mathrm{O/H}) < 7.69$, 'extremely metal-poor galaxies' (XMPs)][1] within this group is difficult and so far, only a small

[1] Within this paper, we refer to metallicity in terms of oxygen abundance, $12 + \log(\mathrm{O/H})$, and define solar metallicity, $\mathrm{Z}_\odot$, as $12 + \log(\mathrm{O/H}) = 8.69$ (Asplund et al. 2009).

★ E-mail: bjames@ast.cam.ac.uk

number have been detected (e.g. Izotov, Thuan & Guseva 2012; Sánchez Almeida et al. 2016). Their detection is hindered by their intrinsic faintness and the fact that previous magnitude-limited selection techniques relied on the presence of bright H II regions, which will only be the case if the galaxies are undergoing a rapid period of SF, i.e. a starburst. The cause of this intense star-forming activity still remains unclear – while many of these high-luminosity, low-mass XMP galaxies show signs of interaction, suggesting that both their SF activity and metal content may be influenced by their environment, a systematic study of the environment surrounding 20 XMP galaxies by Filho et al. (2015) found that only 25 per cent of their sample had undergone major mergers or interactions in the past.

In light of the low yield from spectroscopic searches, new methods for XMP detection have been explored – e.g. blind H I surveys. It was via this specific method that AGC 198691, the most metal-deficient galaxy now known ($Z \sim 1/50\,Z_{\odot}$; Hirschauer et al. 2016), was discovered, along with another XMP galaxy, Leo P ($Z \sim 1/34\,Z_{\odot}$; Giovanelli et al. 2013; Skillman et al. 2013). This latter XMP in particular has very low levels of SF (i.e. $<1 \times 10^{-4}$ $M_{\odot}$ yr^{-1}; Rhode et al. 2013; McQuinn et al. 2015a) and an unconventional morphology, with H II regions embedded within very low-surface-brightness (LSB) emission. Moreover, the low metal content of Leo P is thought to be a result of inefficient SF and a loss of metals through outflows (McQuinn et al. 2015b) – i.e. a result of secular evolution rather than interaction. Leo P's discovery and diffuse appearance led us to speculate how common is this structure amongst XMPs and can we use its morphological properties to uncover more XMPs?

This indeed turned out to be true and using this method, James et al. (2015, hereafter J15) brought to light a new sample of dwarf galaxies: 'blue diffuse dwarf (BDD) galaxies'. Using the morphological properties of Leo P as a basis, a search was conducted on Sloan Digital Sky Survey (SDSS) imaging data which uncovered ∼150 previously unstudied LSB star-forming galaxies. These galaxies are faint, blue systems, each with isolated H II regions randomly scattered within a diffuse continuum. The primary aim of this search was to find more XMPs like Leo P and early optical long-slit spectroscopy of 12 candidates confirmed that ∼25 per cent of our sample were indeed XMPs. Combined with SDSS imaging, our spectra reveal them to be nearby systems (5–120 Mpc) with regions of recent and ongoing SF (i.e. ages of ∼7 Myr and star formation rates (SFRs) of $\log(\mathrm{SFR}/M_{\odot}\ \mathrm{yr}^{-1}) \sim -3.5$ to -0.5) randomly distributed throughout their diffuse, chemically unevolved gas. As such, J15 concluded that BDDs may have properties that bridge the gap between quiescent dIrrs and starbursting BCDs, i.e. active SF in less structured systems.

However, since J15 covered only a small fraction of the full sample, many of the conclusions regarding the BDD population as a whole suffered from small number statistics. We have now obtained long-slit observations for 51 out of 150 BDD galaxies and take this opportunity to re-visit the topic of BDDs within the context of other dwarf galaxies with a more statistically sound sample. Dwarf galaxies appear to fall into groups/classifications depending on properties of SF, morphology, and also their chemical content. For example, BCDs are characterized by bright, compact starbursting regions, whereas dIrrs are quiescent, with multiple irregularly distributed H II regions. XMP galaxies themselves also appear to fall into two groups – active, cometary-shaped systems and quiescent, diffuse structures. However, as we discuss in this paper, the classification of such systems may not be as clear-cut and could instead be linked to the methodology used to detect them.

The paper is structured as follows: in Section 3, we present the sample of 51 BDD galaxies and describe observations and data reduction. Section 4 presents the chemical (i.e. direct-method oxygen abundances and nitrogen-to-oxygen ratios), physical (i.e. luminosities, SFRs, and ionization parameters), and photometric (i.e. magnitudes, colours, and stellar mass) properties of the galaxies. In Section 5, we discuss and explore these properties within the context of other dwarf galaxy samples via, e.g. emission-line diagnostics and the mass–metallicity relation, and in Section 6 we draw conclusions on our findings.

2 OVERVIEW OF SELECTION CRITERIA

A full description of the selection criteria used to create this sample can be found in J15. Here, we provide a brief overview of the criteria used to equip the reader with a better understanding of the sample's properties. As mentioned previously, the selection criteria were primarily motivated by the morphology of Leo P, a recently discovered XMP galaxy which, in SDSS images, appears as a very diffuse LSB object with several embedded H II regions. The main selection criteria adopted and applied to a local SQL (Structured Query Language) data base of the SDSS DR9 catalogue were the following:

(i) Presence of blue point sources $-0.5 < (g-r)_0 < 1$, $-2 < (r-i)_0 < 0$ consistent with H II regions. In order to avoid artefacts from bright stars, we required that the SDSS photometric flags for these objects would not have SUBTRACTED and SATURATED fields set.[2] The objects having higher density of such sources within 10, 20, and 30 arcsec were ranked higher.

(ii) Presence of one or several of faint extended sources ($\mathrm{modelmag}_g > 20$) within 10, 20, and 30 arcsec.

(iii) Absence of bright ($\mathrm{modelmag}_g < 18$) galaxy nearby.

(iv) Absence of known LEDA[3] source or bright UCAC[4] star nearby.

(v) High galactic latitude.

After deselecting all known sources within NASA/IPAC Extragalactic Database (NED) and inspecting the list for promising cases, we obtained a final list of ∼150 LSB star-forming dwarf galaxies. Overall, with respect to the properties of Leo P (our prototype for this search), the JKB objects are found to have similarly low luminosities and metallicities, but at the same time are more massive and with more active SF. We discuss each of these properties in detail in Sections 4 and 5.

3 OBSERVATIONS AND DATA PROCESSING

At present, our full sample consists of ∼150 BDD galaxies, of which we have obtained optical spectroscopy for 51 galaxies, as listed in Table 1. The sample considered here includes both the 12 galaxies originally presented in J15 and 39 new BDD candidates. The table is listed in order of their JKB number,[5] along with general properties

[2] https://www.sdss3.org/dr8/algorithms/flags_detail.php

[3] Lyon-Meudon Extragalactic Database: http://leda.univ-lyon1.fr/

[4] USNO CCD Astrograph Catalog: http://www.usno.navy.mil/USNO/astrometry/optical-IR-prod/ucac

[5] Due to cross-identification purposes within NED and SIMBAD, it was necessary to replace the 'KJ' acronym used in J15 with 'JKB'. We stress to the reader that all objects presented here (which includes those presented in J15) will be listed within NED and SIMBAD as 'JKB' *not* 'KJ', and will be referred to as 'JKB objects' hereafter.

Table 1. Blue diffuse dwarfs galaxies in the current observed sample. Identifications according to SDSS and AGC (Arecibo General Catalog; Haynes et al. 2011) are also given where available. Redshifts were derived from fitting all the emission lines seen within the spectrum and converted into distances using the Hubble flow with respect to the CMB. Distances in parenthesis denote those which are uncertain due to peculiar velocities – see the text for details. Distances noted with asterisk (⋆) are for objects that are within 20° of the Virgo cluster and will therefore have an additional uncertainty due to the Virgo flow. SDSS images of each target can be found in Fig. 1. PA and $T_{\rm exp}$ refer to the position angle of the spectroscopic slit and the exposure time of the MMT observations, respectively. The JKB object number reflects the history of catalogue creation.

Obj ID	SDSS ID	AGC ID	RA	Dec.	z	D (Mpc)	Slit PA (deg)	$T_{\rm exp}$ (s)	UT date of obs. (yyyy mm dd)
JKB 1	J160753.65+090703.7	–	16:07:54	9:07:04	0.027 860	122	135	2 × 600	2014 Jan 28
JKB 2	J140406.04+310055.8	–	14:04:06	31:00:56	0.013 988	60	42	3 × 900	2015 Jan 28
JKB 3	J141708.66+134105.5	242011	14:17:09	13:41:06	0.016 116	69	20	2 × 1200	2014 Jan 28
JKB 4	J142532.35+523515.2	–	14:25:32	52:35:15	0.002 019	(9)	133	3 × 900	2015 Jan 28
JKB 5	J085739.15+590256.4	–	8:57:39	59:02:56	0.003 739	(16)	45	2 × 1200	2014 Jan 28
JKB 7	J113453.11+110116.1	212838	11:34:53	11:01:16	0.002 491	(11)	137	2 × 1200	2014 Jan 28
JKB 8	J083908.76+242130.4	749391	8:39:09	24:21:31	0.027 810	122	110,67	2 × 900, 2 × 1200	2014 Oct 21, 22
JKB 10	J001445.99+104846.9	–	0:14:46	10:48:47	–	–	123	1 × 1200	2014 Oct 21
JKB 15	J000031.45+305209.3	102729	0:00:31	30:52:09	0.015 076	65	55	2 × 1200	2014 Oct 21
JKB 16	J112710.87+391515.6	–	11:27:11	39:15:15	0.006 797	29	74	3 × 800	2014 Dec 24
JKB 18	J092127.17+072152.7	193816	9:21:27	7:21:53	0.004 171	(18)	162	2 × 1200	2014 Jan 28
JKB 19	J211309.36+043853.9	–	21:13:09	4:38:54	–	–	42	2 × 1200	2014 Oct 22
JKB 21	J081246.92+043536.2	188949	8:12:47	4:35:36	0.033 467	146	140	2 × 1200	2014 Oct 22
JKB 22	J114109.10+244505.2	749439	11:41:09	24:45:05	0.011 464	49⋆	66	2 × 1200	2014 Dec 24
JKB 24	J002211.19+111757.3	–	0:22:11	11:17:57	0.017 668	76	51	2 × 1200	2014 Dec 23
JKB 25	J010730.97-040129.0	–	1:07:31	−4:01:29	0.019 589	85	175	3 × 1200	2014 Oct 22
JKB 26	J141814.44+432249.7	–	14:18:14	43:22:50	0.012 731	55	135	3 × 780	2015 Jan 28
JKB 28	J005757.32-094119.2	–	0:57:57	−9:41:19	0.014 728	63	30	2 × 1200	2014 Oct 22
JKB 29	J130110.39+365424.2	–	13:01:10	36:54:24	0.022 526	98	105	1 × 947	2014 Jan 28
JKB 32	J021111.29+281618.9	123128	2:11:11	28:16:19	–	–	175	2 × 1200	2014 Jan 27
JKB 33	J005912.57+113007.8	–	0:59:13	11:30:08	–	–	60	1 × 1200	2014 Dec 24
JKB 37	J062538.13+655228.0	–	6:25:38	65:52:28	0.013 856	60	20	3 × 1200	2014 Jan 27
JKB 40	J081459.45+451745.5	–	8:15:00	45:17:46	0.012 695	55	85	2 × 1200	2014 Oct 22
JKB 42	J092844.05+360100.3	–	9:28:44	36:01:00	0.030 807	134	55	2 × 600	2014 Dec 24
JKB 53	J115754.21+563816.7	–	11:57:54	56:38:17	0.001 066	(5)	45	2 × 1200	2014 Jan 28
JKB 62	J112331.57+571630.5	–	11:23:32	57:16:31	0.006 574	28	95	2 × 1200	2014 Dec 24
JKB 64	J133009.20+321715.9	–	13:30:09	32:17:16	0.002 048	(9)	90	3 × 900	2015 Jan 28
JKB 69	J100849.99+485351.1	–	10:08:50	48:53:51	0.014 390	62	98	2 × 1200	2014 Dec 24
JKB 74	J081407.17+360906.7	–	8:14:07	36:09:07	–	–	96	1 × 1200	2014 Oct 21
JKB 78	J092036.41+494031.3	–	9:20:36	49:40:31	0.001 587	(7)	73	3 × 1200	2014 Jan 28
JKB 80	J092603.64+560915.5	–	9:26:04	56:09:15	0.002 206	(11)	40	1 × 1200	2014 Jan28
JKB 83	J095549.64+691957.4	–	9:55:50	69:19:57	0.000 185	(1)	92	2 × 1200	2014 Dec24
JKB 85	J095921.87+390856.4	–	9:59:22	39:08:56	0.022 944	(10)	40	3 × 900	2015 Jan28
JKB 89	J101518.65+125934.1	205134	10:15:19	12:59:34	0.016 585	72	10	3 × 720	2014 Dec 24
JKB 91	J104701.47+273825.6	–	10:47:01	27:38:25	0.005 110	22	90	3 × 720	2014 Dec 24
JKB 97	J120920.02+242649.5	749452	12:09:20	24:26:50	0.008 217	35⋆	135	2 × 800	2014 Dec 24
JKB 102	J025139.17+334650.3	–	2:51:39	33:46:50	–	–	97	1 × 1200	2014 Jan 27
JKB 107	J033410.64+064218.0	–	3:34:11	6:42:18	–	–	25	1 × 1200	2014 Jan 27
JKB 114	J092423.79+402257.2	–	9:24:24	40:22:57	–	–	96	2 × 1200	2014 Oct 21, 22
JKB 119	J001722.78+174156.9	–	0:17:23	17:41:57	0.003 161	(13)	159	2 × 1200	2014 Oct 21
JKB 122	J122542.55+264834.5	749236	12:25:42	26:48:35	0.000 371	(2)	146	2 × 1200	2014 Dec 24
JKB 124	J014850.49+220641.6	–	1:48:50	22:06:42	–	–	150	1 × 1200	2014 Oct 21
JKB 129	J002041.45+083701.2	103419	0:20:41	8:37:01	–	–	56	3 × 1200	2014 Dec 24
JKB 131	J013813.59+105825.6	–	1:38:14	10:58:26	0.010 041	43	55	2 × 1200	2014 Oct 22
JKB 133	J023711.21+205238.5	–	2:37:11	20:52:39	0.013 318	57	57	2 × 1200	2014 Oct 21
JKB 136	J020521.94-054153.2	–	2:05:22	−5:41:53	0.017 456	75	40	2 × 1200	2014 Oct 21
JKB 137	J215817.93-025404.8	–	21:58:18	−2:54:05	0.016 668	72	4	2 × 1200	2014 Oct 22
JKB 138	J014610.53+284901.4	111473	1:46:11	28:49:02	0.012 198	52	45	2 × 1200	2014 Oct 22
JKB 141	J002004.10+083021.5	103622	0:20:04	8:30:22	0.018 561	80	145	2 × 1200	2014 Dec 24
JKB 142	J014548.23+162240.6	–	1:45:48	16:22:40	0.002 304	(10)	115	2 × 1200	2014 Dec 24
JKB 144	J233102.23+222644.3	332237	23:31:02	22:26:44	0.022 897	99	48	2 × 1200	2014 Dec 23

such as coordinates and redshift, and observational details such as the position angle of the spectrograph slit and exposure time. The JKB objects are not numbered with respect to their RA – instead the JKB number reflects the history of catalogue creation. Observations were made with the Multiple Mirror Telescope (MMT) blue channel spectrograph on the dates indicated in Table 1, using the 1 arcsec × 180 arcsec slit with medium resolution grating (300 grooves mm^{-1}). This gives a spatial scale along the slit of 0.6 arcsec pixel^{-1}, a spectral range of 3500–8000 Å, and a spectral resolution of ∼7 Å (full width at half-maximum (FWHM)).

As in J15, the processing of the spectra was performed using a custom pipeline that follows all the standard reduction steps. As

such, and in order to maintain a homogeneous sample of data, all observations have been reduced together using the same pipeline, i.e. including those presented in J15. Raw data were bias subtracted and flat-fielded, and wavelength calibration was performed using the lamp spectra recorded immediately after or before each science exposure. After subtracting the sky spectrum from each science frame, the spectra of science objects were extracted by summing the flux along the slit within an aperture. Extracted spectra from multiple

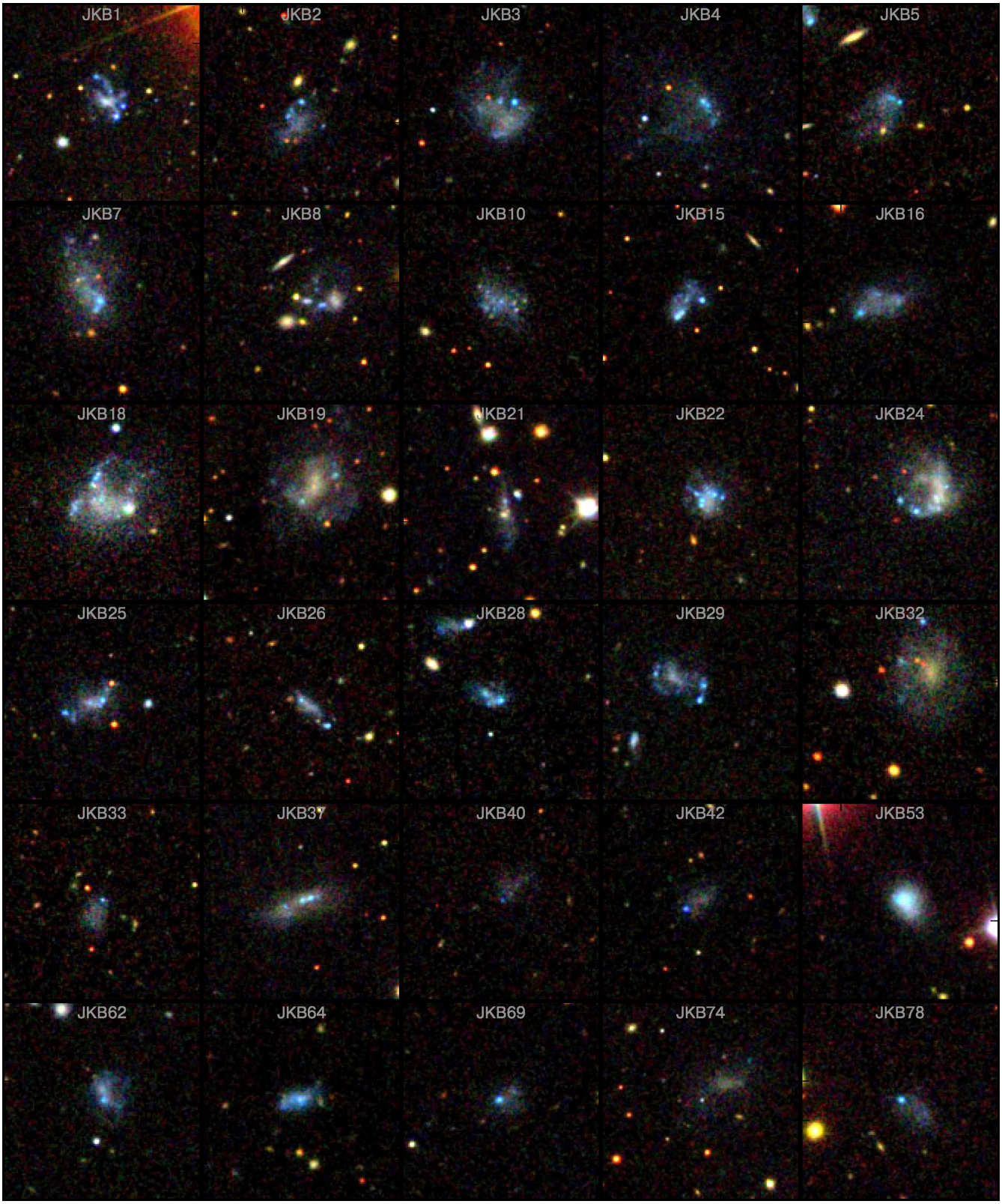

Figure 1. SDSS images of the BDD galaxies presented in this paper. Information on each object can be found in Table 1. Images were created from *gri*-band SDSS imaging and are ∼91 arcsec on each side. North is up and east is to the left.

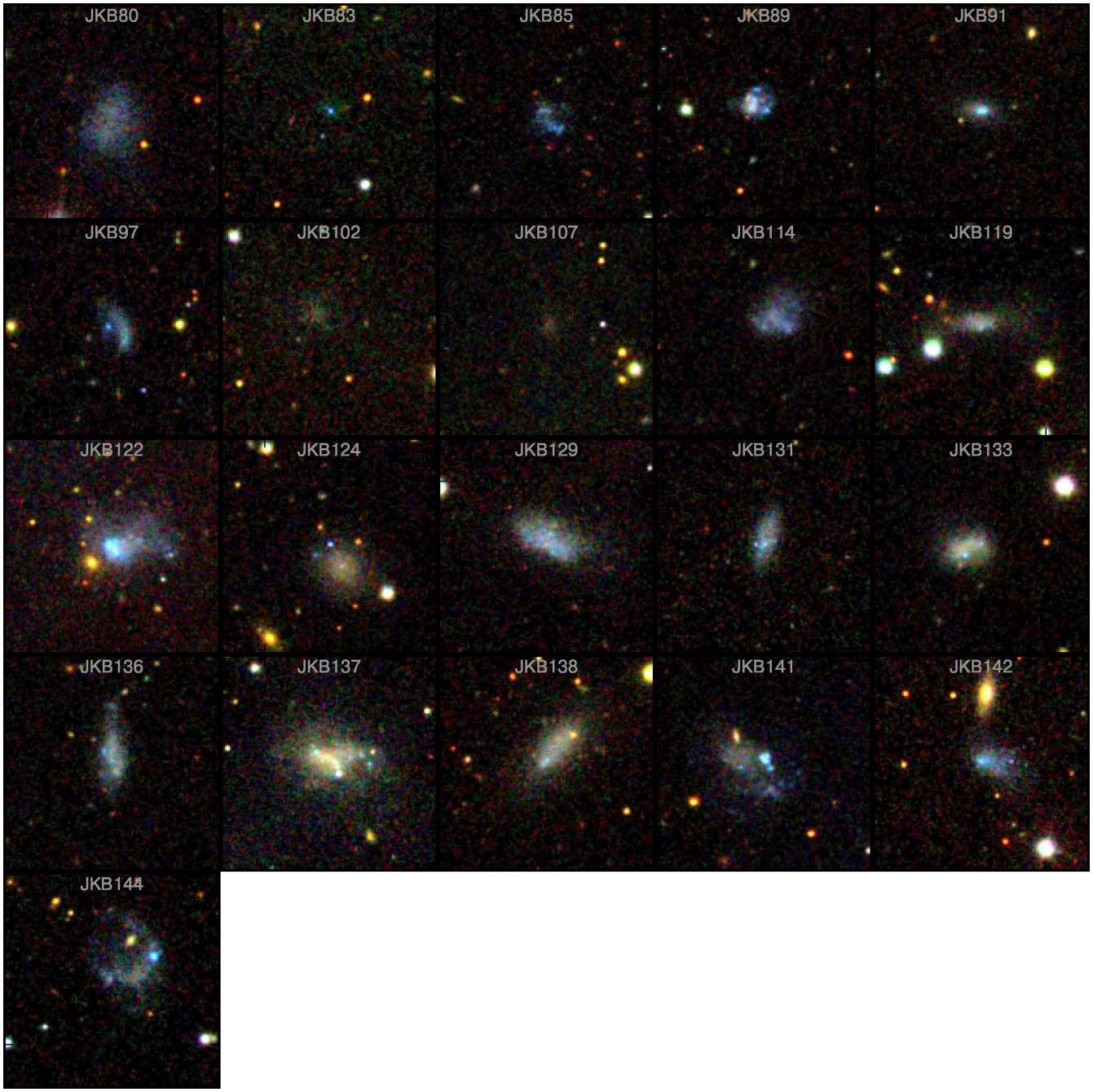

Figure 1 – *continued*

exposures were combined using weighted average together with σ-clipping to exclude residuals from cosmic rays. The flux calibration of the spectra was performed using spectrophotometric standard stars observed throughout each night with the instrument set-up described above. Uncertainties resulting from flux calibration were estimated to be ∼10 per cent and were incorporated into the error spectrum. We adopt this somewhat conservative error in order to account for the effects of systematic uncertainties, such as not fully photometric conditions, seeing variation throughout the night, possible slit losses, etc. We note that in order to avoid large systematic slit losses due to differential refraction (Filippenko 1982), all the objects below airmass of ∼1.1 were observed at the parallactic angle (which is listed as the position angle in Table 1). In the cases where multiple H II regions were clearly visible in the two-dimensional spectra, their spectra were separately extracted. Such cases are denoted has JKB X.1, JKB X.2, etc., where X denotes the JKB catalogue number.

The emission lines detected within each spectrum were fitted with a single Gaussian component (multiple Gaussian components were not necessary). The resultant redshifts are given in Table 1 whereas the integrated line fluxes for each emission line are given in Table A1. The distances have been derived assuming the Hubble flow ($H_0 = 70$ km s^{-1} Mpc^{-1}) with respect to the Cosmic Microwave Background (CMB; Hinshaw et al. 2009) and were found to range from ∼1 to 150 Mpc . Due to peculiar motions, we expect that distances and distance-dependent quantities will be unreliable for

D < 10–20 Mpc (see e.g. Tonry et al. 2000). For this paper, we decided to focus on the sample of objects with distances larger than 20 Mpc, as for those objects the uncertainty (90 per cent interval) on the distance modulus is $\lesssim$1 mag, as tested using the sample of nearby galaxies from the HyperLEDA catalogue (Makarov et al. 2014). This distance uncertainty for objects with $D \gtrsim 20$ Mpc should provide an additional 1 dex scatter of $\lesssim$0.5 mag on photometric quantities (i.e. absolute magnitudes and surface brightnesses) and $\lesssim$0.3 dex on parameters like SFR, stellar mass, etc. In tables presented in Section 4, we mark all the distance-dependent quantities for objects with D < 20 Mpc by '*', to signal the possibility of significant uncertainty and do not include such quantities in the plots or related discussions.

At this point of our analysis, objects for which no strong emission lines (e.g. Hα, Hβ, or [O III]) were detected were removed from our spectroscopic analysis (namely JKB 10, 19, 32, 33, 74, 80, 102, 107, 114, 124, and 129). They are, however, included in the photometric analysis described in Section 4.3. Any separately extracted spectra of different positions within the objects that showed no evidence of emission lines were also excluded from our spectroscopic analysis. Spectra of all objects, and their separately extracted H II region spectra, for those with both detected and undetected emission lines, are shown in Fig. B1.

We stress here that the non-emission-line JKB objects are still considered as an important part of our BDD sample. This is because we employ a photometric rather than emission-line-based selection technique and as such the JKB objects are expected to represent galaxies at different evolutionary phases. For example, the non-emission-line objects may represent BDD galaxies that are observed during quiescent periods between star-forming events.

A full spectroscopic analysis was undertaken on 40/51 objects and, if we account for spectra extracted from individual H II regions, this amounts to 57 individual spectra. As in J15, line fluxes and their uncertainties were obtained by sampling the likelihood function with a Markov chain Monte Carlo method, in order to simultaneously fit all of the observed lines within the spectrum, while requiring the redshifts and line widths to be the same for all the lines. If a line was found to be below a 3σ detection, we measure the upper limit on the line flux using the error spectrum and the expected line profile. In some cases, underlying stellar absorption was visible, i.e. when the Hα equivalent width (EW) was less than 100 Å. In these cases, Balmer line fluxes were corrected accordingly.

4 RESULTS

We list both the observed and dereddened line fluxes in Table A1. Reddening values were estimated from the observed F(Hα)/F(Hβ) and F(Hβ)/F(H γ) ratios (combined in a 3:1 ratio, respectively), adopting the case B recombination ratios (appropriate for gas with T = 10 000 K and N_e= 100 cm^{-3}) and the Large Magellanic Cloud extinction curve (Fitzpatrick 1999). In cases where H γ was not detected, only the F(Hα)/F(Hβ) ratio was employed.

4.1 Chemical properties

Chemical abundances were calculated using the 'direct method', where abundance measurements are based on the physical conditions of the gas (i.e. utilizing electron temperature, T_e, and electron density, N_e) and extinction corrected line fluxes. Our methodology differs slightly to that adopted by J15 in that we utilize the updated atomic data presented in Berg et al. (2015) and assume that the ions are well approximated by a five-level atom.[6] Each H II region is modelled by three separate ionization zones (low, medium, and high), and the abundance calculations for ions within each zone are made using the temperature within the respective zone. Here, we deal with species from only the medium- and low-ionization zones. For the medium-ionization zone, where O^{2+} resides, we use T_e([O III]) calculated from [O III] (λ4959 + λ5007)/[O III](λ4363). T_e([O III]) is derived using an iterative method alongside the calculation of electron densities N_e([S II]) (λ6716/λ6731) and N_e([O II]) (λ3729/λ3727).

Using this direct electron temperature, we then calculate T_e([O II]) for the low-ionization zone, where O^+ resides. We calculate T_e([O II]) using the relationship between T_e([O II]) and T_e([O III]) from Izotov et al. (2006) derived from metal-poor emission-line galaxies. While several similar relationships can be found in the literature (e.g. Garnett 1992; López-Sánchez et al. 2012; Croxall et al. 2016), not all are well constrained within the high T_e (i.e. low metallicity) regime, where many of our objects lie. As discussed by Croxall et al. (2016), systematic offsets can result from T_e([O II]) relations that utilize different atomic data, although such effects on our O^+/H^+ abundance determination are negligible since the uncertainty in T_e([O III]) is the dominant factor. Uncertainties in both values of T_e correspond to uncertainties in the relevant extinction-corrected fluxes, and are then propagated into the errors in the abundance values.

We compute both $O^+/H^+$and N^+/H^+ abundances using the low-ionization zone T_e and N_e. Total oxygen abundances are calculated from the sum of O^{2+} and O^+, and N/O abundance ratios are derived simply from N^+/O^+ (a valid assumption given that both ions reside in the same ionization zone and hence no ionization correction factors are needed).

Table 2 lists the resultant T_e([O III]), T_e([O II]), O^+/H^+, O^{2+}/H^+, 12+log(O/H), and log(N/O) for the sample. We also list the weighted mean N_e calculated from N_e([O II]) and N_e([S II]) and adopting T_e([O III]). Here we choose to use T_e([O III]) over T_e([O II]) because (i) T_e([O III]) is more robustly (i.e. directly) measured than T_e([O II]) and (ii) N_e measurements made using T_e([O II]) rather than T_e([O III]) were found to differ by <10 cm^{-3} due to the weak dependence of N_e on T_e.

Direct calculations of the oxygen abundance (i.e. from detections of the [O III]λ4363 line) were available for ~50 per cent of the sample (i.e. 26/51 objects). For those spectra where [O III]λ4363 was undetected, we list the oxygen abundances as lower limits. Since the [O III] emission lines in question are coolants in the H II regions, in the abundance range relevant here an upper limit on the flux ratio of [O III]λ4363/[O III] λ5007 (deduced from the noise level at the redshifted wavelength of λ4363) translates into an upper limit on the temperature and thereby a lower limit on the oxygen abundance (Stasińska et al. 2012). For those spectra where [N II]λ6584 was undetected, we list N/O ratios as upper limits (due to the upper limit on the flux detection). N/O abundance ratios are not listed for galaxies with lower limit oxygen abundances. Out of those for which direct-method abundances were obtainable, oxygen abundances were found to be in the range 7.43 < 12+log(O/H) < 8.01, with 11 out of 26 objects falling within the XMP classification (i.e. 0.1 < $Z_\odot$, 12+log(O/H) < 7.69). This accounts for approximately 20 per cent of the total sample presented here, which is in rough agreement with the fraction of XMP objects reported in J15

[6] We implement this via the IDL library IMPRO: https://github.com/moustakas/impro.

Table 2. Ionic and elemental abundances for the BDD galaxies presented in this paper, derived from the emission-line measurements given in Table A1. Electron density and temperatures are also listed.

JKB ID	N_e([O II],[S II]) (cm^{-3})	T_e([O III]) (K)	T_e([O II]) (K)	O^+/H^+ ($\times10^{-5}$)	O^{2+}/H^+ ($\times10^{-5}$)	12+log(O/H)	log(N/O)	[O/H]
1.0	330 ± 170	<16 100	<14 400	>3.66	>3.24	>7.84	–	>−0.85
1.1	790 ± 130	15 900 ± 1870	14 300 ± 743	1.41 ± 0.37	4.41 ± 1.58	7.76 ± 0.12	<−2.34	−0.93 ± 0.13
2.0	810 ± 150	<11600	<11 400	>3.44	>3.00	>7.81	–	>−0.88
2.1	730 ± 290	17 200 ± 2380	14 700 ± 573	0.48 ± 0.12	2.40 ± 0.94	7.46 ± 0.14	<−2.07	−1.23 ± 0.15
3.0	210 ± 65	13 200 ± 1820	12 800 ± 1330	2.34 ± 1.17	8.00 ± 4.19	8.01 ± 0.18	−1.59 ± 0.14	−0.68 ± 0.19
3.1	550 ± 130	<18 800	<15 000	>5.46	>1.27	>7.83	–	>−0.86
4.0	160 ± 47	14 100 ± 2040	13 400 ± 1260	2.67 ± 1.05	2.71 ± 1.26	7.73 ± 0.13	−1.59 ± 0.11	−0.96 ± 0.14
5.0	290 ± 110	<14 000	<13 300	>3.04	>1.67	>7.67	–	>−1.02
7.0	150 ± 48	13 400 ± 1440	12 900 ± 1010	3.25 ± 1.13	4.93 ± 1.83	7.91 ± 0.11	−1.46 ± 0.10	−0.78 ± 0.12
8.11	46 ± 27	14 800 ± 1710	13 800 ± 903	2.60 ± 0.78	4.06 ± 1.50	7.82 ± 0.11	−1.58 ± 0.10	−0.87 ± 0.12
8.12	$1.1^{+2.0}_{-1.1}$	<28 000	<10 200	>16.76	>0.77	>8.24	–	>−0.45
8.2	490 ± 370	<24 200	<13 400	>2.03	>0.87	>7.46	–	>−1.23
8.3	180 ± 120	13 300 ± 1710	12 900 ± 1220	2.19 ± 0.89	5.40 ± 2.34	7.88 ± 0.14	−1.45 ± 0.12	−0.81 ± 0.15
15.1	400 ± 120	17 100 ± 2190	14 700 ± 560	1.15 ± 0.28	3.26 ± 1.20	7.64 ± 0.12	−1.70 ± 0.13	−1.05 ± 0.13
15.2	570 ± 130	16 800 ± 3010	14 600 ± 858	2.40 ± 0.68	1.95 ± 0.99	7.64 ± 0.12	−1.78 ± 0.14	−1.05 ± 0.13
16.1	$1.7^{+6.8}_{-1.7}$	15 800 ± 1890	14 300 ± 784	1.51 ± 0.41	3.02 ± 1.11	7.66 ± 0.11	−1.47 ± 0.09	−1.03 ± 0.12
16.2	470^{+640}_{-470}	<23 600	<13 800	>4.70	>0.81	>7.74	–	>−0.95
16.3	$3.4^{+18}_{-3.4}$	<28 000	<10 200	>14.73	>0.34	>8.18	–	>−0.51
18.0	370 ± 110	19 600 ± 2860	14 900 ± 164	2.07 ± 0.44	1.63 ± 0.62	7.57 ± 0.09	−1.67 ± 0.09	−1.12 ± 0.10
18.1	$4.7^{+25}_{-4.7}$	<28 000	<10 200	>37.76	>0.54	>8.58	–	>−0.11
21.0	40^{+46}_{-40}	<13 000	<12 600	>5.76	>6.44	>8.09	–	>−0.60
22.0	$6.7^{+6.8}_{-6.7}$	13 400 ± 1240	13 000 ± 869	2.11 ± 0.66	7.35 ± 2.44	7.98 ± 0.12	−1.41 ± 0.09	−0.71 ± 0.13
22.1	140 ± 45	14 100 ± 1500	13 400 ± 934	2.04 ± 0.65	5.77 ± 2.07	7.89 ± 0.12	−1.60 ± 0.10	−0.80 ± 0.13
24.0	48 ± 38	<8970	<8630	>28.20	>22.12	>8.70	–	>0.01
24.1	29^{+32}_{-29}	13 500 ± 1620	13 000 ± 1120	3.63 ± 1.36	5.17 ± 2.09	7.94 ± 0.12	−1.57 ± 0.11	−0.75 ± 0.13
25.0	420 ± 33	13 600 ± 1370	13 100 ± 931	2.11 ± 0.69	6.63 ± 2.32	7.94 ± 0.12	−1.57 ± 0.09	−0.75 ± 0.13
26.0	640 ± 270	25 800 ± 2530	12 300 ± 2040	2.40 ± 1.81	1.08 ± 0.29	7.54 ± 0.23	>−2.12	−1.15 ± 0.23
26.1	320 ± 77	15 900 ± 2140	14 300 ± 856	1.60 ± 0.45	2.30 ± 0.92	7.59 ± 0.11	−1.86 ± 0.13	−1.10 ± 0.13
28.0	740 ± 190	19 100 ± 2890	15 000 ± 25.1	1.04 ± 0.22	1.65 ± 0.66	7.43 ± 0.11	<−2.26	−1.26 ± 0.12
29.0	360 ± 140	<13 800	<13 200	>2.74	>2.03	>7.68	–	>−1.01
29.2	840^{+930}_{-840}	<12 500	<12 300	>3.62	>3.09	>7.83	–	>−0.86
37.0	130 ± 45	15 200 ± 1790	14 000 ± 861	2.44 ± 0.72	4.33 ± 1.60	7.83 ± 0.11	−1.47 ± 0.09	−0.86 ± 0.12
40.0	180 ± 120	23 300 ± 2860	13 900 ± 1440	2.06 ± 0.88	1.12 ± 0.35	7.50 ± 0.13	−1.48 ± 0.16	−1.19 ± 0.14
42.0	650 ± 190	16 100 ± 1800	14 400 ± 681	0.71 ± 0.18	6.58 ± 2.27	7.86 ± 0.14	−1.54 ± 0.13	−0.83 ± 0.14
53.0	330 ± 42	17 400 ± 2250	14 800 ± 476	0.79 ± 0.18	2.55 ± 0.94	7.52 ± 0.12	−1.61 ± 0.08	−1.17 ± 0.13
62.0	680 ± 390	<12 800	<12 500	>2.83	>5.19	>7.90	–	>−0.79
64.0	650 ± 170	22 200 ± 2780	14 400 ± 1050	1.91 ± 0.61	0.83 ± 0.26	7.44 ± 0.11	−1.88 ± 0.15	−1.25 ± 0.12
69.0	380 ± 110	16 000 ± 2110	14 400 ± 813	1.34 ± 0.38	4.54 ± 1.79	7.77 ± 0.13	−1.40 ± 0.11	−0.92 ± 0.14
78.0	430 ± 110	15 500 ± 1840	14 200 ± 818	0.99 ± 0.28	3.53 ± 1.29	7.65 ± 0.13	−1.51 ± 0.10	−1.04 ± 0.14
83.0	220 ± 86	<13 500	<13 000	>3.82	>2.02	>7.77	–	>−-0.92
85.0	92 ± 60	<12 000	<11 800	>4.32	>5.85	>8.01	–	>−0.68
89.0	290 ± 74	15 100 ± 2030	14 000 ± 993	2.72 ± 0.86	4.20 ± 1.73	7.84 ± 0.12	<−2.29	−0.85 ± 0.13
91.0	130 ± 21	13 000 ± 1240	12 700 ± 928	3.96 ± 1.33	5.85 ± 2.01	7.99 ± 0.11	−1.40 ± 0.10	−0.70 ± 0.12
97.0	35 ± 29	14 800 ± 2270	13 800 ± 1200	2.08 ± 0.76	3.82 ± 1.82	7.77 ± 0.14	−1.58 ± 0.14	−0.92 ± 0.15
97.1	3500^{+5400}_{-3500}	<28 000	<10 200	>19.36	>0.50	>8.30	–	>−0.39
119.0	1300^{+1600}_{-1300}	<28 000	<10 200	>34.30	>0.27	>8.54	–	>−0.15
122.0	150 ± 27	15 200 ± 1750	14 000 ± 843	1.31 ± 0.37	3.37 ± 1.22	7.67 ± 0.12	−1.56 ± 0.08	−1.02 ± 0.13
131.0	340 ± 99	<14 100	<13 400	>4.64	>3.03	>7.88	–	>−0.81
133.0	290 ± 140	<13 500	<13 000	>5.24	>4.54	>7.99	–	>−0.70
133.1	80 ± 42	14 000 ± 2030	13 400 ± 1270	2.88 ± 1.16	4.99 ± 2.33	7.90 ± 0.14	−1.43 ± 0.12	−0.79 ± 0.15
136.0	720 ± 260	<12 700	<12 400	>2.90	>4.94	>7.89	–	>−0.80
137.0	15^{+42}_{-15}	<27 700	<10 600	>16.21	>0.87	>8.23	–	>−0.46
138.2	840 ± 380	<23 900	<13 600	>9.46	>0.81	>8.01	–	>−0.68
141.0	200 ± 47	17 500 ± 2410	14 800 ± 502	2.66 ± 0.62	2.51 ± 0.98	7.71 ± 0.10	−1.55 ± 0.08	−0.98 ± 0.11
142.0	84 ± 42	<10 500	<10 400	>5.36	>5.89	>8.05	–	>−0.64
144.0	600 ± 43	14 000 ± 1530	13 300 ± 961	2.20 ± 0.71	6.88 ± 2.51	7.96 ± 0.12	−1.53 ± 0.09	−0.73 ± 0.13
144.1	390 ± 370	<28 000	<10 200	>23.73	>1.28	>8.40	–	>−0.29

(25 per cent). We show the [O III]λ4363 profile for each object classified as an XMP in Fig. 2. Nitrogen-to-oxygen ratios were found to lie in the range $-1.88 < \log(\mathrm{N/O}) < -1.39$.

4.2 Physical properties

4.2.1 Star formation rates and L*(Hα)*

In Table 3, we list the Hα luminosity and SFRs for our sample of BDD galaxies. For the cases with multiple H II regions, we also list the total luminosities and SFRs. Luminosities are calculated using the extinction-corrected Hα line fluxes (Table A1) and the distances given in Table 1. For objects with $D > 20$ Mpc, total luminosities are in the range of $38.7 < \log(L_{\mathrm{H}\alpha}/\mathrm{erg\ s^{-1}}) < 40.6$, which lie in the intermediate range between quiescent dIrrs (van Zee 2000) and starbursting BCDs (Gil de Paz, Madore & Pevunova 2003). Hα luminosities are converted into SFRs using the Kennicutt (1998, hereafter K98) prescription, except for low-luminosity cases, i.e. when $L(\mathrm{H}\alpha) < 2.5 \times 10^{39}$ erg s^{-1}, where we follow the prescription detailed in Lee et al. (2009). This latter prescription is essentially a recalibration the K98 relation to account for the underprediction of SFRs by Hα compared to those from FUV fluxes within the low-luminosity regime, under the assumption that the FUV traces the SFR in dwarf galaxies more robustly. This recalibration is especially relevant for our sample as we lack FUV observations and are almost exclusively within the low SFR regime. Total SFRs are seen to be in the range 0.1–3.3 $\times$ 10^{-1} M$_\odot$ yr^{-1} with a median of 3.5 $\times$ 10^{-2} M$_\odot$ yr^{-1} (again excluding objects with $D < 20$ Mpc). SFRs for individual H II regions have a slightly lower median of 2.4 $\times$ 10^{-2} M$_\odot$ yr^{-1}. These values are somewhat higher than those quoted within J15 due to the fact that in J15 we did not use the Lee et al. (2009) prescription and thus underestimated the SFRs for the galaxies with the lowest luminosities. Uncertainties in SFR values due to distance uncertainties are expected to be $\lesssim$0.3 dex. We discuss the SF properties of the JKB objects in relation to other dwarf galaxy types in Section 5.

4.2.2 Age of the current ionizing population

Following the methodology given in J15, we investigate the current age of the star-forming population via the luminosities of hydrogen recombination lines, Hα and Hβ, which provide an estimate of the ionizing flux present, assuming a radiation bounded nebula (Schaerer & Vacca 1998). Using the Balmer line EW and its metallicity, we estimate the age of the latest star-forming episode in each object by comparing the EWs with those predicted by the spectral synthesis code, STARBURST99 (Leitherer et al. 2010). Details of the models can be found in J15. We interpolate between the models at the metallicity of each galaxy and assess the age of the current stellar population according to its EW(Hβ) and EW(Hα). The mean and half-difference between these two ages are given in Table 3.

The ages of the current ionizing stellar populations within the BDD galaxies were found to range between 4.2 and 11.5 Myr, with a mean age of 7.4 $\pm$ 1.9 Myr (this excludes galaxies for which lower limit oxygen abundances are available, as only upper limits can be calculated in these cases). These ages suggest that BDD galaxies have H II regions either experiencing their first cycle of SF or undergoing a recent burst of SF. With regards to Wolf-Rayet (WR) stars, which tend to exist between 3 and 6 Myr (Leitherer et al. 1999), the WR feature at ∼4690 Å is identified in only three objects; JKB 3, 7, and 119. Although this is somewhat surprising given the relatively young ages of the current ionizing stellar population within BDDs, WR features are not typically seen in young XMP galaxies (Shirazi & Brinchmann 2012). We do, however, detect the high-ionization line He IIλ4686 in five BDDs, a nebular line often seen in low-metallicity galaxies. The mechanism(s) behind the existence of this line in nearby systems is still under debate and includes WR stars, shocks, or X-ray binaries. In XMP galaxies such as IZw 18 and those observed here, Kehrig et al. (2015) suggest that either low-metallicity supermassive O stars or rotating metal-free stars are more likely culprits for such hard ionizing radiation. Since only one of the five BDD galaxies in which He IIλ4686 is detected (JKB 1, 7, 16, 22, and 29) is not an XMP galaxy, we cannot rule out that any of the proposed mechanisms for this line are at play within these objects.

4.3 Photometric properties

Table 4 lists the photometric SDSS *g*-band magnitudes for the BDD sample in Table 1, along with the $u-g$, $g-r$, $r-i$, and $i-z$ colours. Total magnitudes were measured within the R_{25} (the radius where the azimuthally averaged *r*-band surface brightness reaches 25 mag arcsec^{-2}), while the surface brightnesses were measured within the effective radii (radius with 50 per cent of the total flux). Also listed are the absolute *B*-band magnitudes computed using distances listed from Table 1[7] and the *V*-band surface brightness, μ_v. Uncertainties on all distance-dependent photometric properties resulting from distance uncertainties are expected to be $\lesssim$0.5 mag. For objects with $D > 20$ Mpc, total *g*-band apparent magnitudes lie between 21.0 and 16.3 mag, absolute magnitudes are between ∼−10 and −18 mag and surface brightnesses between 23 and 25 mag arcsec^{-2}. Each of these are somewhat typical values for dwarf galaxies although not as bright as many of the starbursting BCD galaxies.

4.3.1 Stellar masses

Stellar masses ($M_\star$) were estimated by modelling the BDDs stellar content via a flexible stellar population synthesis code (FSPS; Conroy, Gunn & White 2009) using the broad-band colours listed in Table 4. A grid of synthetic spectra was created assuming a constant SFH, a Chabrier IMF and the Milky Way extinction law from Cardelli, Clayton & Mathis (1989). Each spectrum was synthesized for a range of stellar metallicities ($0.01 < Z_*/Z_\odot < 1.5$) and *V*-band optical depths of τ_v =0–2 for a dust screen. Synthetic SDSS colours were computed from each spectrum at the correct redshift of each object as a function of Z_*, τ_v, and age. Because the FSPS models can be evaluated at arbitrary points within the bounds of the cube, we adopt the following priors on Z_*, τ_v, and age: $Z_* = Z_{\mathrm{H\,II}} \pm 0.3$ dex, $-4 < \log(\tau_v) < 0.3$, and age>1 Myr, respectively.

For each object, the likelihood of the colours given in Table 4 and metallicities given in Table 2 is sampled using a Markov chain Monte Carlo methodology, producing a posterior probability distribution for the parameters of the model. We do not correct the broad-band magnitudes for the contribution of emission lines because the effect is very minor (typically $\lesssim$0.1 mag) so can usually be ignored. Whilst we are aware that a constant SFH may offer an oversimplified description of our systems, without any additional

[7] In order to convert the magnitude from the Sloan photometric system to Johnsons we used the prescription of Lupton 2005 http://classic.sdss.org/dr7/algorithms/sdssUBVRITransform.html#Lupton2005.

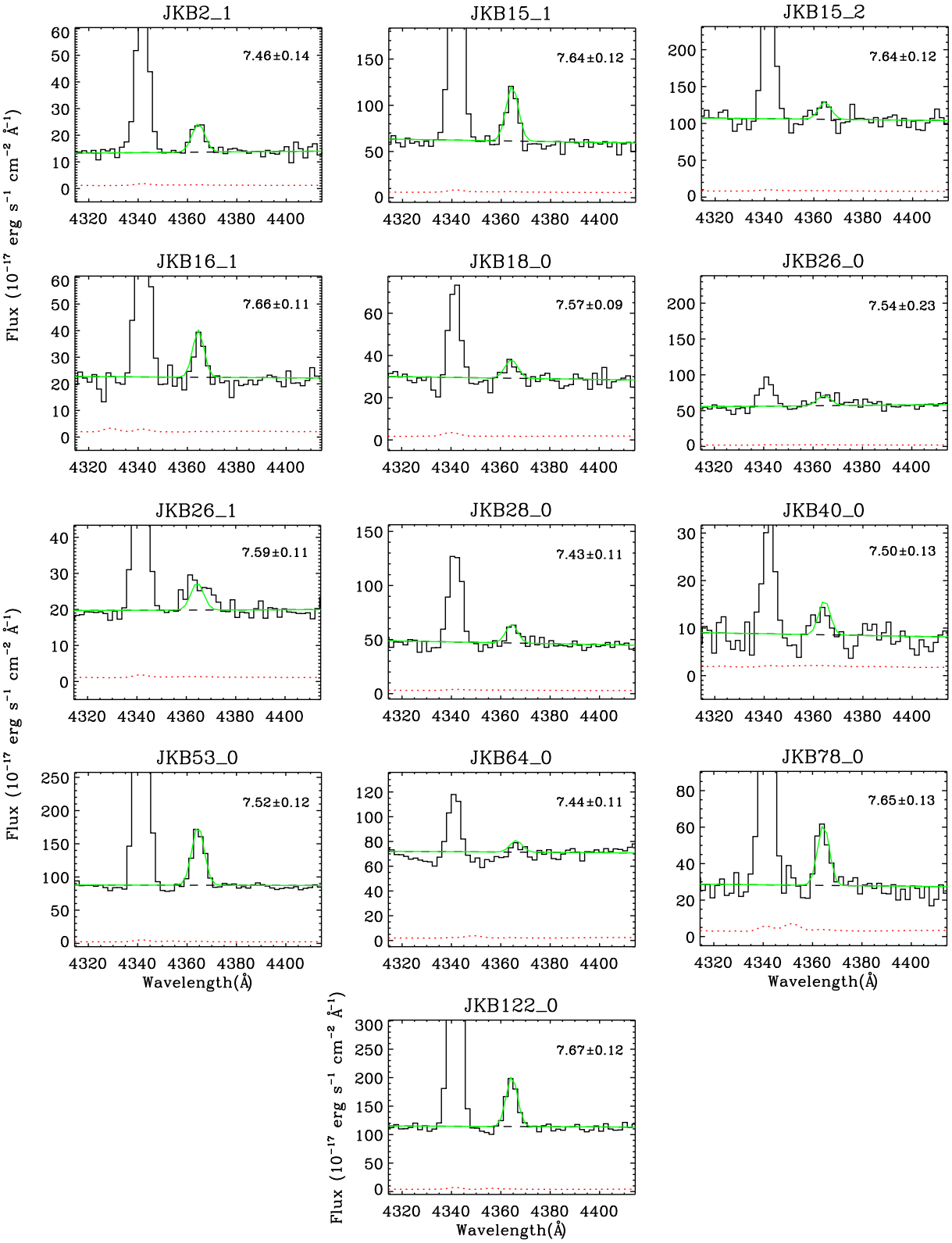

Figure 2. The auroral line, [O III]λ4363 profile for the confirmed extremely metal-poor (i.e. 12 + log(O/H) < 7.69) BDDs in our sample. Each zoom-in shows the observed spectrum (black histogram), error (red dashed), and fitted profile to the [O III]λ4363 line (green). Measured fluxes are listed in Table A1, while the resultant chemical abundances can be found in Table 2. The 12 + log(O/H) value of each object is inset within each panel.

Table 3. Physical properties of the new, extended sample of BDD galaxies: Hα luminosity and star formation rate (listed for both individual H II regions and for the entire galaxy), along with the age of the current star-forming population determined from the EW of Hα and Hβ. Objects noted with '$\star$' are those with uncertain distances, i.e. $D < 20$ Mpc.

ID	L(Hα) ($\times 10^{38}$ erg s^{-1})	SFR(Hα) ($\times 10^{-2}$ M$_\odot$ yr^{-1})	L(Hα)$_{total}$ ($\times 10^{38}$ erg s^{-1})	SFR(Hα)$_{total}$ ($\times 10^{-2}$ M$_\odot$ yr^{-1})	Age(EW(Hα,Hβ)) (Myr)
JKB 1.0	31.48 ± 3.58	2.49 ± 0.28	124.98 ± 10.12	9.88 ± 0.80	<11.25
JKB 1.1	93.50 ± 9.47	7.39 ± 0.75	–	–	6.36 ± 0.88
JKB 2.0	15.09 ± 1.65	2.17 ± 0.39	44.36 ± 3.91	4.48 ± 0.48	<8.51
JKB 2.1	29.27 ± 3.55	2.31 ± 0.28	–	–	8.33 ± 0.79
JKB 3.0	56.25 ± 8.91	4.44 ± 0.70	70.05 ± 9.27	6.50 ± 0.79	4.27 ± 0.48
JKB 3.1	13.80 ± 2.56	2.06 ± 0.36	–	–	<11.20
JKB 4.0$\star$	0.71 ± 0.08	0.33 ± 0.08	0.71 ± 0.08	0.33 ± 0.08	8.17 ± 0.72
JKB 5.0$\star$	1.09 ± 0.12	0.43 ± 0.10	1.09 ± 0.12	0.43 ± 0.10	<9.82
JKB 7.0$\star$	0.99 ± 0.10	0.40 ± 0.09	0.99 ± 0.10	0.40 ± 0.09	6.81 ± 1.00
JKB 8.1	109.12 ± 11.04	8.62 ± 0.87	258.99 ± 18.05	22.33 ± 1.51	7.18 ± 0.94
JKB 8.1	8.79 ± 1.00	1.56 ± 0.27	–	–	<10.10
JKB 8.2	18.89 ± 1.99	2.50 ± 0.46	–	–	<11.46
JKB 8.3	122.19 ± 14.10	9.65 ± 1.11	–	–	5.96 ± 1.06
JKB 15.1	75.44 ± 7.76	5.96 ± 0.61	149.94 ± 11.28	11.85 ± 0.89	6.54 ± 0.72
JKB 15.2	74.50 ± 8.18	5.89 ± 0.65	–	–	8.74 ± 0.52
JKB 16.1	4.35 ± 0.44	1.01 ± 0.20	5.44 ± 0.45	1.56 ± 0.22	7.60 ± 1.27
JKB 16.2	0.71 ± 0.08	0.33 ± 0.08	–	–	<12.95
JKB 16.3	0.38 ± 0.04	0.22 ± 0.05	–	–	<10.81
JKB 18.0$\star$	1.18 ± 0.13	0.45 ± 0.10	1.78 ± 0.18	0.74 ± 0.12	9.90 ± 0.65
JKB 18.1$\star$	0.60 ± 0.12	0.29 ± 0.07	–	–	<10.71
JKB 21.0	31.77 ± 3.60	2.51 ± 0.28	31.77 ± 3.60	2.51 ± 0.28	<8.47
JKB 22.0	32.19 ± 3.40	2.54 ± 0.27	52.22 ± 4.01	5.13 ± 0.55	5.01 ± 0.78
JKB 22.1	20.03 ± 2.12	2.59 ± 0.48	–	–	6.16 ± 1.04
JKB 24.0	167.10 ± 25.45	13.20 ± 2.01	248.98 ± 27.18	19.67 ± 2.15	<5.64
JKB 24.1	81.88 ± 9.53	6.47 ± 0.75	–	–	6.12 ± 0.85
JKB 25.0	67.62 ± 8.66	5.34 ± 0.68	67.62 ± 8.66	5.34 ± 0.68	4.78 ± 0.65
JKB 26.0	6.39 ± 0.64	1.28 ± 0.24	17.50 ± 1.30	3.08 ± 0.39	11.47 ± 0.78
JKB 26.1	11.11 ± 1.13	1.80 ± 0.31	–	–	8.60 ± 0.71
JKB 28.0	15.01 ± 1.55	2.17 ± 0.39	15.01 ± 1.55	2.17 ± 0.39	9.57 ± 0.61
JKB 29.0	19.92 ± 2.07	2.58 ± 0.48	39.73 ± 2.91	5.15 ± 0.68	<9.61
JKB 29.2	19.81 ± 2.04	2.57 ± 0.48	–	–	<8.88
JKB 37.0	28.83 ± 3.62	2.28 ± 0.29	28.83 ± 3.62	2.28 ± 0.29	7.70 ± 1.06
JKB 40.0	5.29 ± 0.56	1.14 ± 0.22	5.29 ± 0.56	1.14 ± 0.22	9.99 ± 0.99
JKB 42.0	226.73 ± 23.06	17.91 ± 1.82	226.73 ± 23.06	17.91 ± 1.82	5.51 ± 0.80
JKB 53.0$\star$	0.47 ± 0.05	0.25 ± 0.06	0.47 ± 0.05	0.25 ± 0.06	7.02 ± 1.06
JKB 62.0	4.94 ± 0.66	1.09 ± 0.21	4.94 ± 0.66	1.09 ± 0.21	<9.28
JKB 64.0$\star$	0.54 ± 0.07	0.28 ± 0.07	0.54 ± 0.07	0.28 ± 0.07	11.05 ± 0.49
JKB 69.0	40.09 ± 4.05	3.17 ± 0.32	40.09 ± 4.05	3.17 ± 0.32	7.73 ± 1.11
JKB 78.0$\star$	0.41 ± 0.04	0.23 ± 0.06	0.41 ± 0.04	0.23 ± 0.06	6.52 ± 1.18
JKB 83.0$\star$	0.01 ± 0.00	0.02 ± 0.01	0.01 ± 0.00	0.02 ± 0.01	<7.69
JKB 85.0$\star$	37.02 ± 4.20	2.92 ± 0.33	37.02 ± 4.20	2.92 ± 0.33	<8.70
JKB 89.0	29.46 ± 3.04	2.33 ± 0.24	29.46 ± 3.04	2.33 ± 0.24	9.45 ± 0.83
JKB 91.0	6.58 ± 0.66	1.30 ± 0.24	6.58 ± 0.66	1.30 ± 0.24	5.72 ± 1.36
JKB 97.0	5.97 ± 0.61	1.22 ± 0.23	7.46 ± 0.65	1.74 ± 0.25	7.70 ± 1.37
JKB 97.1	1.49 ± 0.21	0.52 ± 0.11	–	–	<9.69
JKB 119.0$\star$	0.60 ± 0.14	0.29 ± 0.07	0.60 ± 0.14	0.29 ± 0.07	<9.95
JKB 122.0$\star$	0.10 ± 0.01	0.10 ± 0.04	0.10 ± 0.01	0.10 ± 0.04	6.41 ± 1.01
JKB 131.0	8.29 ± 1.01	1.50 ± 0.27	8.29 ± 1.01	1.50 ± 0.27	<9.35
JKB 133.0	8.52 ± 0.89	1.53 ± 0.27	33.71 ± 2.79	3.52 ± 0.34	<8.57
JKB 133.1	25.19 ± 2.64	1.99 ± 0.21	–	–	7.18 ± 1.17
JKB 136.0	18.19 ± 1.84	2.44 ± 0.45	18.19 ± 1.84	2.44 ± 0.45	<9.15
JKB 137.0	100.14 ± 40.23	7.91 ± 3.18	100.14 ± 40.23	7.91 ± 3.18	<9.24
JKB 138.2	10.75 ± 4.62	1.76 ± 0.30	10.75 ± 4.62	1.76 ± 0.30	<11.17
JKB 141.0	190.59 ± 21.26	15.06 ± 1.68	190.59 ± 21.26	15.06 ± 1.68	8.02 ± 0.92
JKB 142.0$\star$	2.09 ± 0.23	0.64 ± 0.14	2.09 ± 0.23	0.64 ± 0.14	<7.33
JKB 144.0	392.82 ± 41.34	31.03 ± 3.27	410.35 ± 41.51	33.42 ± 3.30	4.18 ± 0.45
JKB 144.1	17.53 ± 3.72	2.39 ± 0.44	–	–	<10.60

Table 4. Photometric properties of the BDD sample calculated from SDSS images. Objects without M_b values are those for which spectroscopic redshifts could not be measured. Objects noted with '⋆' are those with uncertain distances, i.e. $D < 20$ Mpc, and consequential photometric uncertainties of >1 mag.

Obj ID	g	$u-g$	$g-r$	$r-i$	$i-z$	M_b	μ_v
JKB 1	17.32	0.92	0.08	−0.13	−0.42	−17.85	23.73
JKB 2	18.11	0.87	0.19	0.14	0.15	−15.49	24.23
JKB 3	17.05	0.80	0.23	0.07	0.25	−16.86	23.86
JKB 4⋆	18.00	0.64	0.18	−0.02	0.30	−11.39	23.89
JKB 5⋆	17.95	0.87	0.24	0.10	−0.76	−12.77	23.93
JKB 7⋆	16.93	0.76	0.27	0.11	0.28	−12.89	23.68
JKB 8	17.37	0.98	0.50	0.36	0.16	−17.67	23.92
JKB 10	17.75	0.67	0.23	0.07	0.18	–	23.76
JKB 15	18.14	1.19	−0.59	0.15	−0.71	−15.88	24.14
JKB 16	17.72	0.78	0.17	0.10	−0.01	−14.32	23.84
JKB 18⋆	15.57	0.99	0.35	0.13	0.02	−15.33	22.79
JKB 19	16.92	0.98	0.39	0.30	0.10	–	24.04
JKB 21	18.59	0.85	0.34	0.30	−0.02	−16.91	24.07
JKB 22	17.45	0.67	0.13	0.01	0.11	−15.74	23.05
JKB 24	16.51	0.88	0.36	0.17	0.07	−17.57	23.33
JKB 25	17.66	0.81	0.27	0.43	0.44	−16.66	23.59
JKB 26	18.78	1.22	0.26	0.15	0.10	−14.60	23.49
JKB 28	18.31	0.61	0.11	−0.26	0.31	−15.44	23.55
JKB 29	17.59	0.67	0.12	−0.06	0.47	−17.10	24.24
JKB 32	17.03	0.90	0.49	0.25	0.03	−16.55	24.07
JKB 33	18.87	0.54	0.29	0.08	0.23	–	24.09
JKB 37	17.72	0.99	0.34	0.14	0.15	−15.82	23.79
JKB 40	20.55	0.82	0.23	0.36	0.02	−12.84	24.71
JKB 42	19.24	0.86	0.26	0.20	−0.14	−16.09	24.50
JKB 53⋆	16.95	0.82	0.18	0.06	−0.06	−11.06	22.13
JKB 62	18.03	0.65	0.11	0.01	0.13	−13.96	23.84
JKB 64⋆	18.04	0.41	0.10	−0.24	0.02	−11.41	23.33
JKB 69	18.79	0.50	0.06	0.04	0.34	−14.92	23.37
JKB 74	19.12	0.96	0.39	0.24	0.13	–	24.28
JKB 78⋆	18.64	0.62	0.13	0.01	0.15	−10.25	24.25
JKB 80⋆	17.41	0.77	0.22	0.20	0.35	−12.44	24.05
JKB 83⋆,[a]	20.00	−0.22	0.50	−0.88	0.16	−4.10	23.26
JKB 85⋆	18.76	0.64	0.11	−0.11	−0.06	−15.96	24.11
JKB 89	18.02	0.79	0.14	0.08	0.19	−15.98	23.10
JKB 91	18.58	0.85	0.26	0.09	0.14	−12.81	22.75
JKB 97	18.34	0.73	0.10	−0.02	−0.00	−14.13	24.00
JKB 102	19.70	1.34	0.66	0.21	−0.39	–	24.52
JKB 107	20.99	–	0.69	0.45	0.61	–	24.75
JKB 114	17.79	0.74	0.14	0.16	−0.02	–	23.68
JKB 119⋆	18.34	0.96	0.44	0.24	0.15	−11.95	23.63
JKB 122⋆	16.32	0.81	0.27	0.33	−0.75	−9.37	23.07
JKB 124	17.78	0.87	0.51	0.31	0.22	–	24.04
JKB 129	17.03	0.85	0.33	0.18	0.01	–	23.32
JKB 131	18.06	0.79	0.32	0.10	0.24	−14.79	23.42
JKB 133	17.58	1.20	0.44	0.25	0.26	−15.85	23.27
JKB 136	17.86	0.90	0.31	0.09	0.18	−16.20	23.45
JKB 137	16.31	1.11	0.52	0.22	0.14	−17.58	22.90
JKB 138	17.28	1.09	0.53	0.30	0.04	−15.93	23.63
JKB 141	17.23	1.04	0.18	0.14	0.45	−17.01	24.09
JKB 142⋆	18.08	0.81	0.20	0.08	0.02	−11.60	23.41
JKB 144	17.41	1.17	0.21	0.08	0.36	−17.28	23.64

Note. [a]Known to be a single H II region within M 81.

information from their resolved stellar populations, we are not able to adopt a more physical model.

The resultant stellar masses for our sample of BDDs are listed in Table 5. Uncertainties on each mass are dominated by the uncertainties on the photometric measurements and possible offsets between Z_* and $Z_{\rm H\,II}$. We expect uncertainties on the stellar mass due to

Table 5. Stellar masses derived from stellar population synthesis and SDSS colours listed in Table 4. Also listed are SSFRs derived from $M_\star$ and total SFRs listed in Table 3. Details can be found in Section 4.3.1. Objects noted with '⋆' are those with uncertain distances, i.e. $D < 20$ Mpc.

Obj ID	$\log(M_\star)/M_\odot$	$\log(\mathrm{SSFR/yr^{-1}})$
JKB 1	8.10 ± 0.42	-9.10 ± 0.42
JKB 2	7.80 ± 0.32	-9.15 ± 0.33
JKB 3	8.34 ± 0.29	-9.52 ± 0.29
JKB 4⋆	5.91 ± 0.32	-8.39 ± 0.32
JKB 5⋆	6.30 ± 0.48	-8.67 ± 0.48
JKB 7⋆	6.82 ± 0.27	-9.22 ± 0.27
JKB 8	8.95 ± 0.25	-9.60 ± 0.25
JKB 15	6.65 ± 0.05	-7.58 ± 0.05
JKB 16	7.21 ± 0.32	-9.02 ± 0.32
JKB 18⋆	7.95 ± 0.19	-10.08 ± 0.19
JKB 22	7.60 ± 0.28	-8.89 ± 0.28
JKB 24	8.80 ± 0.24	-9.50 ± 0.24
JKB 25	8.29 ± 0.27	-9.57 ± 0.27
JKB 26	7.66 ± 0.18	-9.18 ± 0.18
JKB 28	7.24 ± 0.34	-8.91 ± 0.34
JKB 29	8.12 ± 0.29	-9.41 ± 0.29
JKB 37	8.15 ± 0.20	-9.79 ± 0.20
JKB 40	6.82 ± 0.27	-8.76 ± 0.27
JKB 42	8.10 ± 0.23	-8.84 ± 0.24
JKB 53⋆	6.03 ± 0.23	-8.63 ± 0.24
JKB 62	6.89 ± 0.28	-8.85 ± 0.28
JKB 64⋆	5.47 ± 0.27	-8.02 ± 0.27
JKB 69	7.04 ± 0.28	-8.53 ± 0.29
JKB 78⋆	5.34 ± 0.36	-7.97 ± 0.36
JKB 83⋆,[a]	2.78 ± 0.13	-6.48 ± 0.13
JKB 85⋆	7.51 ± 0.27	-9.05 ± 0.27
JKB 89	7.90 ± 0.26	-9.54 ± 0.26
JKB 91	6.84 ± 0.23	-8.73 ± 0.23
JKB 97	7.03 ± 0.25	-8.79 ± 0.25
JKB 119⋆	6.69 ± 0.25	-9.23 ± 0.25
JKB 122⋆	5.38 ± 0.23	-8.38 ± 0.23
JKB 131	7.59 ± 0.28	-9.41 ± 0.28
JKB 133	8.33 ± 0.21	-9.79 ± 0.21
JKB 136	8.19 ± 0.25	-9.81 ± 0.25
JKB 137	9.02 ± 0.21	-10.12 ± 0.21
JKB 138	8.31 ± 0.25	-10.06 ± 0.25
JKB 141	8.52 ± 0.23	-9.35 ± 0.23
JKB 142⋆	6.23 ± 0.25	-8.42 ± 0.25
JKB 144	8.69 ± 0.20	-9.17 ± 0.20

Note. [a]Known to be a single H II region within M 81.

distance uncertainties to be $\lesssim$0.3 dex. Stellar masses are in the range $\log(M_\star/M_\odot) \sim 5$–9, with an average of $\log(M_\star/M_\odot) = 7.3 \pm 1.0$ (these numbers exclude JKB 83 which is known to be a single H II region in M81). Such masses are typical of BCD and irregular dwarf galaxies, albeit towards the low-mass end. It should be noted here that there are several caveats hindering our stellar mass calculations. First, we are relying on SDSS photometry and only computing total fluxes where the surface brightness of galaxies is above ($\langle\mu_v\rangle \sim 25$ mag arcsec^{-2}), which may lead us to lose some stellar mass in the very diffuse stellar component. Secondly, significant uncertainties in stellar mass estimates can exist due the assumed constant SFH. Finally, we lack infrared imaging (e.g. Zhao, Gao & Gu 2013), which would make our stellar mast estimates more robust. However, in the absence of deeper optical or infrared imaging, we adopt the values calculated here and restrict our mass-related analysis to the mass–metallicity relation described in the subsequent section, for the sake of comparison with other samples. In the future, we hope

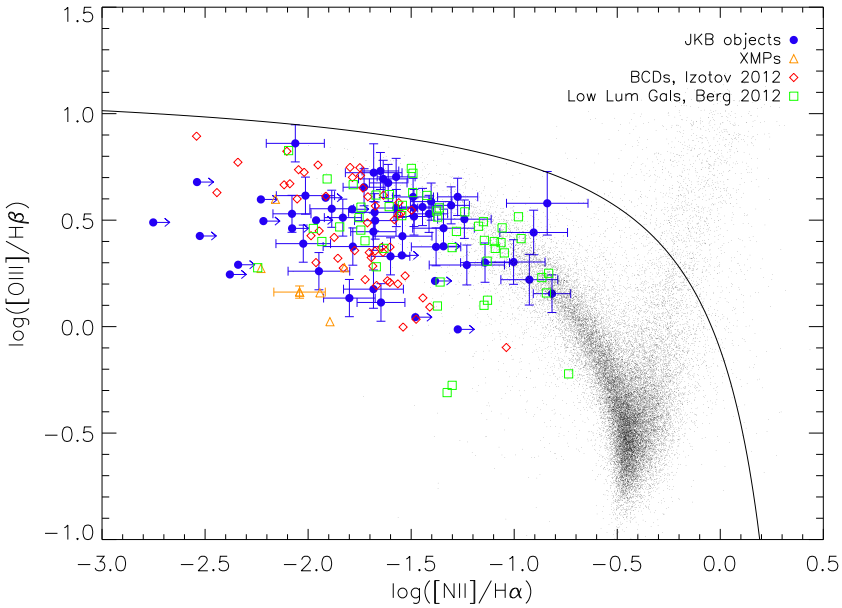

Figure 3. The 'BPT' emission-line diagnostic diagram, showing [O III](λ5007)/Hβ versus [N II](λ6584)/Hα, traditionally used to separate galaxies according to their metallicity, and strength and hardness of their ionizing radiation. In black we show the SDSS emission-line galaxies (selected according to the criteria of Brinchmann, Kunth & Durret 2008), which form a branch of star-forming galaxies on the left, and Seyferts/LINERs on the right. The BDD galaxies (i.e. JKB objects listed in Table 1) are distributed throughout the top-left region of the star-forming branch where galaxies of low metallicity and high-ionization fall. For comparison, we also plot a selection of XMPs, BCDs, and low-luminosity dwarf galaxies (see the text for details). The black solid line represents the 'maximum starburst line' of (Kewley et al. 2001).

to obtain deep broad-band optical and infrared imaging of the entire sample and undertake a detailed and accurate photometric analysis of these low-luminosity objects.

Table 5 also lists the specific star formation rates (SSFR = SFR/$M_\star$) for each galaxy, calculated from the total SFR values (Table 3) and stellar masses. SSFRs are in the range $-10.0 < \log(\mathrm{SSFR/yr^{-1}}) < -6.5$, with a mean $\log(\mathrm{SSFR/yr^{-1}}) = -9.0 \pm 0.7$. Such SSFRs are typical of low-mass dwarf galaxies (e.g. Lee et al. 2009; Huang et al. 2012) and, with respect to their stellar masses, fit nicely within the narrow SSFR range seen within the low-mass range of the 'star-forming sequence' (Schiminovich et al. 2007).

5 DISCUSSION

The conclusion of J15, which considered a sample of only 12 JKB objects, was that BDDs have properties reminiscent of both dwarf irregular galaxies and BCD galaxies. In fact, in consideration of their SFRs and surface brightness fluxes, they appear to lie directly in between these two populations. In this section, we assess whether these conclusions still hold now that we have increased our spectroscopic sample of JKB objects by a factor of 4.

In each of the following sections, we compare the JKB objects against a variety of dwarf galaxy samples. We use the comparison sample adopted in J15 along with some additional dIrr and BCD galaxy samples. Overall this includes: XMP galaxies [Leo P (Skillman et al. 2013), LeoA (van Zee & Haynes 2006), UGCA292 (van Zee 2000), DDO68 (Pustilnik, Kniazev & Pramskij 2005), SBS1129+576 (Guseva et al. 2003; Ekta, Chengalur & Pustilnik 2006), SBS1129+577 (Ekta et al. 2006), J2104-0035 and UGC772 (Ekta, Chengalur & Pustilnik 2008), UM133 and SDSSJ011914 (Ekta & Chengalur 2010), HS2134 (Pustilnik et al. 2006)] and the sample of Morales-Luis et al. (2011); low-luminosity and dwarf irregular galaxies of Berg et al. (2012), Haurberg, Rosenberg & Salzer (2013) and the SHIELD galaxies from Haurberg et al. (2013); and BCDs from Izotov, Thuan & Guseva (2007), Izotov et al. (2012), and Berg et al. (2016). Within each of the figures, the three groups of dwarf galaxies (XMP galaxies, low-luminosity dwarf irregulars, and BCDs) are colour-coded orange, green, and red, respectively. In order to avoid discrepancies between metallicity measurements, we only include galaxies for which a direct measurement of the metallicity has been reported. To ensure a fair comparison with our JKB objects, all SFRs for the comparison samples have been calculated according to the method described above, i.e. utilizing the K98 relation for all galaxies with $L(\mathrm{H}\alpha) > 3.5 \times 10^{39}$ erg s^{-1} and the Lee et al. (2009) recalibration for those with luminosities below this cut-off.

5.1 Emission-line diagnostics

If we first look to Fig. 3, we place our new, larger sample of BDDs on to the traditional emission-line diagnostic plot, log[O III]/Hβ versus log([N II]/Hα) (i.e. the traditional 'BPT' diagram introduced by Baldwin, Phillips & Terlevich 1981). The BDDs are distributed within the low-metallicity, high-ionization parameter (i.e. U-parameter, defined as the number density ratio of ionizing photons to particles) region of the diagram, alongside the comparison sample of BCDs, XMPs and low-luminosity galaxies. Whilst we do not list the U-parameter for individual galaxies, they were calculated following the method outlined in J15 and found to have the range $-3.59 < \log(U) < -2.19$. Such properties are to be expected, given the low-metallicity, highly ionized gas surrounding their young photoionizing stellar populations.

A distinct offset can be seen in Fig. 3 between SDSS galaxies and low-metallicity dwarf galaxies. This is due to low-metallicity systems having smaller [O III]/Hβ and [N II]/Hα ratios than high-metallicity systems, as noted in Izotov et al. (2012). Also, SDSS

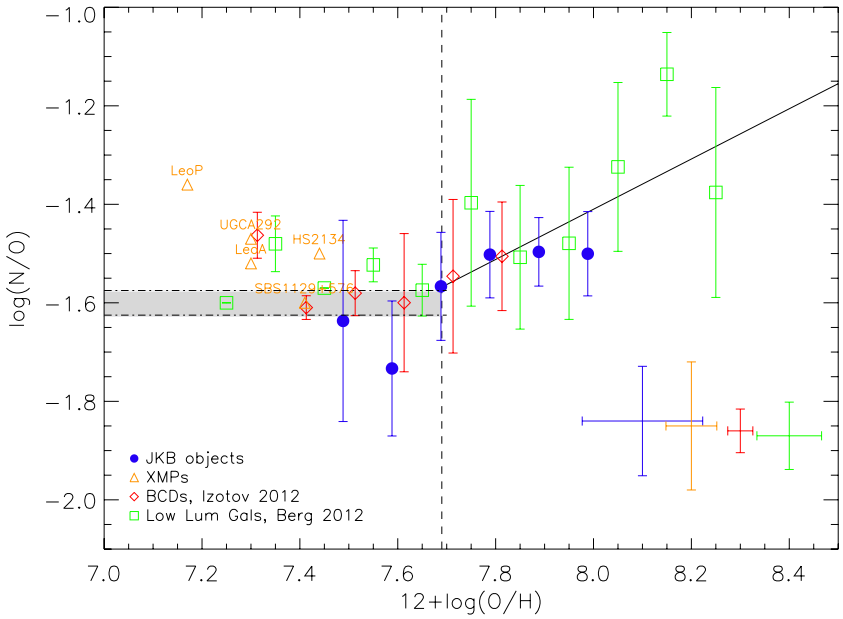

Figure 4. The relationship between oxygen abundance and nitrogen-to-oxygen ratio in the low-metallicity regime. We show the results from our sample of BDD galaxies (i.e. JKB objects listed in Table 1, blue circles), where metallicity and N/O values correspond to the average measured for that system. For comparison, we plot the recently compiled sample of BCDs by Izotov et al. (2012) and the low-luminosity dwarf galaxies of Berg et al. (2012). Each sample has been binned by $\Delta \log(\mathrm{O/H}) = 0.1$ and error bars on each point represent the standard deviation within that bin. We additionally show the individual values from a selection of XMP galaxies (see the text for details). Error bars at the bottom right of the plot represent the typical uncertainty on a single measurement within that sample. The black solid line shows the relationship between log(N/O) and log(O/H) in the metallicity range $12 + \log(\mathrm{O/H}) > 7.7$ derived by Berg et al. (2012) for low-luminosity galaxies, while the grey-shaded region is the narrow N/O plateau proposed for XMPs by Izotov & Thuan (1999). The vertical dashed line represents the XMP cut-off ($12 + \log(\mathrm{O/H}) < 7.69$).

galaxies do not typically occupy this region due to the rarity of low-metallicity galaxies.

5.2 Nitrogen-to-oxygen ratio

With regards to their chemical properties, JKB objects have metallicities in the range $7.43 < 12 + \log(\mathrm{O/H}) < 8.01$, i.e. 0.05–0.21 $(\mathrm{O/H})_{\odot}$. Nitrogen-to-oxygen ratios were found to lie in the range $-1.88 < \log(\mathrm{N/O}) < -1.39$ and are typical values for the metallicity range of the sample. This is evident in Fig. 4, where we show the distribution of log (N/O) as a function of metallicity for our sample (excluding those with N/O limits) alongside other low-metallicity galaxies such as BCDs (Izotov et al. 2012), low-luminosity galaxies from Berg et al. (2012), and other known XMP galaxies. In J15, we were unable to make any firm conclusions on the reality of the scatter in N/O values at low metallicity due to our limited sample size and limited accuracy of abundance determinations. Here, with the N/O values from 26 spectra, we can see that while a plateau may exist in N/O for XMP objects, the relatively large scatter in N/O for galaxies within this metallicity regime suggests that the plateau may not be as narrow as proposed by Izotov & Thuan (1999). For example, the galaxies in Fig. 4 with $12 + \log(\mathrm{O/H}) < 7.69$ have a mean N/O value of $\langle \log(\mathrm{N/O}) \rangle = -1.55 \pm 0.02$ with an intrinsic 1 dex scatter of 0.10.

In contrast to the BDD galaxies and other typical low-mass dwarf galaxies, some XMPs and BCDs have been found to have high N/O values for their metallicity. For example, Sánchez Almeida et al. (2016) find that 10 per cent of the 332 XMPs within their sample have $\log(\mathrm{N/O}) \gtrsim -1.2$.[8] Such large N/O values at low O/H can be attributed to the accretion of metal-poor gas – i.e. mixing which lowers the abundance of O whilst maintaining the original N/O ratio (see e.g. Amorín, Pérez-Montero & Vílchez 2010, and references therein). If this is indeed the case, the relatively normal N/O ratio in our BDD sample suggests that the accretion of significant amounts of metal-poor gas does not appear to be at play within BDDs, as we will see in subsequent sections. However, given our small sample size (i.e. chemical abundance measurements for only 26 JKB objects) and a probable uncertainty on the expected 10 per cent fraction showing high N/O values from Sánchez Almeida et al. (2016), we cannot rule out that high N/O values would indeed be seen in larger sample. In support of this conclusion, it should also be noted that the large scatter in N/O at intermediate metallicities is not solely restricted to XMP and BCD galaxies. van Zee & Haynes (2006) found that a large scatter in N/O also exists for isolated dwarf irregular galaxies with $12 + \log(\mathrm{O/H}) < 8.2$, which they attribute to either varied SFHs or an increased production of secondary nitrogen at intermediate metallicities.

[8] We do not include this sample in Fig. 4 because chemical abundances were not calculated using the direct method.

5.3 Combined properties

The most efficient way of assessing the placement of BDDs within the context of other dwarf galaxy populations is by combining their physical (e.g. SFR), chemical (e.g. metallicity), and photometric properties (e.g. magnitudes and masses).

First in Fig. 5 we plot SFR versus *B*-band absolute magnitude. Despite the SFR recalibration towards higher SFRs for low-luminosity galaxies (which was not implemented in J15), we can see that JKB objects still appear to lie mid-range in SFR between dwarf irregulars and BCDs, i.e. with the majority of JKB objects lying between $-12 < M_B < -18$ and occupying the upper range of the dIrr SFR and the lower range of the BCD SFR distributions. Interestingly,

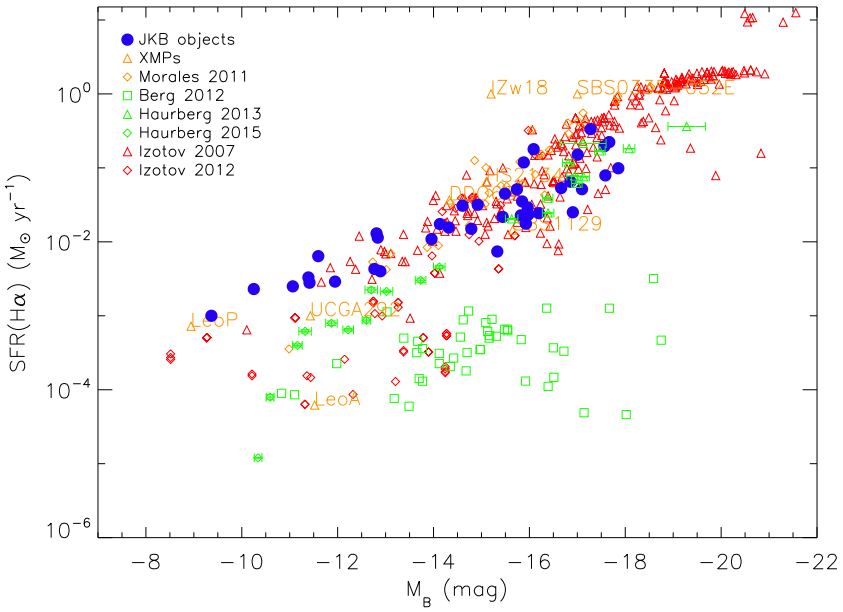

Figure 5. The relationship between absolute *B*-band magnitude (M_B) and total star formation rates for our sample of blue diffuse dwarf galaxies (i.e. JKB objects listed in Table 1). We also overplot the comparison sample described in Section 5.

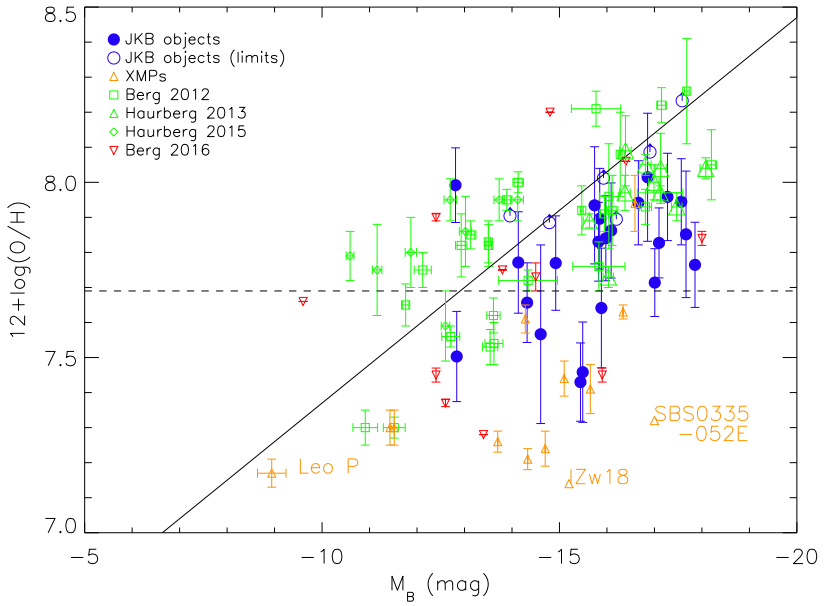

Figure 6. The relationship between oxygen abundance and absolute *B*-band magnitude (M_B) for our sample of blue diffuse dwarf galaxies (i.e. JKB objects listed in Table 1). In cases where multiple H II regions exist, we plot the average O/H abundance measured within that system. We also overplot the comparison sample described in Section 5 and the *L*–*Z* relationship of Berg et al. (2012).

the emission-line-selected samples of XMP galaxies from Morales-Luis et al. (2011) have SFRs that are similar to those of JKB objects, despite the fact that the JKB object's H II regions were not bright enough to be selected for the SDSS spectroscopic sample. By design, Morales-Luis et al. (2011) XMP samples are bursty or 'active' XMPs, with mostly cometary morphologies, and therefore do not include the diffuse XMPs like Leo P or those seen within our sample. Secondly, in Fig. 6, we plot metallicity as a function of *B*-band magnitude, commonly known as the *L*–*Z* relation. JKB objects show a significant amount of scatter around and slightly below the *L*–*Z* relation defined from the low-luminosity sample of Berg et al. (2012) but generally are in agreement with low-luminosity dwarf irregular galaxies. They do not, however, show the same overall trend of XMP galaxies, who typically fall well below the relation. This is thought to be due to the inflow of pristine gas which both depletes the metals within the interstellar medium (ISM) and fuels SF within their H II regions .

A similar trend can be seen in Fig. 7, where we place the BDD galaxies into context with other dIrrs and BCDs within the mass–metallicity diagram. Since values of mass and metallicity are more easily available in the literature than individual emission line fluxes, here we can make several additions to our comparison sample: dIrrs from Lee et al. (2006) and van Zee & Haynes (2006), BCD galaxies from Zhao et al. (2013), and a sample of XMP galaxies from

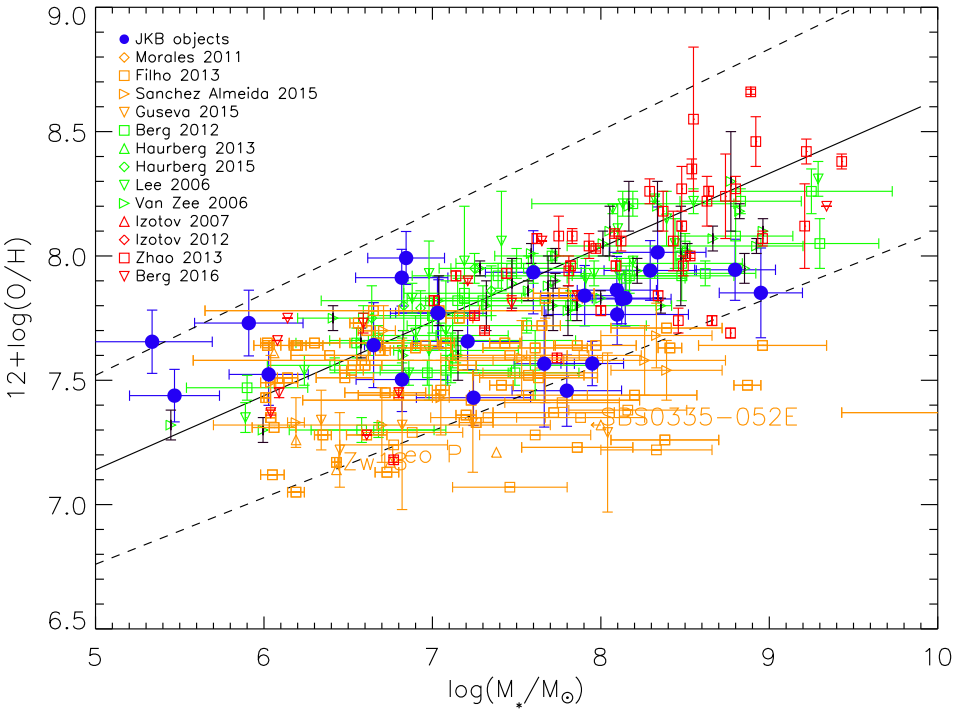

Figure 7. The relationship between oxygen abundance and stellar mass for our sample of blue diffuse dwarf galaxies (i.e. JKB objects listed in Table 1). In cases where multiple H II regions exist, we plot the average O/H abundance measured within that system. We overplot *M–Z* relation for low-mass galaxies derived by Lee et al. (2006) and the comparison sample described in Sections 5 and 5.3. It should be noted that stellar masses have additional, unquantified uncertainties owing to a presumed constant SFR model.

Filho et al. (2015), Sánchez Almeida et al. (2015), and Guseva et al. (2015). Again, the XMPs tend to fall below the *M–Z* relation, whose studies attribute to two possible scenarios: (i) the infall of metal-poor gas (diluting the metal content of the ISM and increasing the mass; e.g. Peeples, Pogge & Stanek 2009); or (ii) they are genuinely young systems that are currently chemically unevolved (Guseva et al. 2015). Since all XMP galaxies whose stellar populations are resolvable by the *HST* have been found to have underlying populations >1 Gyr old (Aloisi et al. 1999, 2007; Izotov & Thuan 2002), we consider the latter scenario unlikely. With regards to the former, given that the mass–metallicity relationship itself may result from gas accretion (e.g. Mannucci et al. 2010; Yates, Kauffmann & Guo 2012), we cannot rule out the inflow of metal-poor gas completely. Instead, the fact that BDDs appear to lie within the low-mass *M–Z* relation perhaps suggests that they do not sustain excessive inflows of metal-poor gas for their stellar mass.

5.4 Classifying blue diffuse dwarf galaxies

Overall it can be seen that several properties of BDD galaxies overlap with those of other dwarf galaxy classes. With regards to their chemical properties, they are certainly low-metallicity objects. They have blue optical colours, owing to the fact that they host young photoionizing stellar populations within their H II regions. Whilst both these properties are typical of BCD galaxies and other XMP galaxies, their morphologies are not. The large majority of XMP galaxies are cometary in shape (Papaderos et al. 2008; Filho et al. 2013; Sánchez Almeida et al. 2016), with $\lesssim$10 per cent showing multiple knots of SF. Skillman et al. (2013) classify these cometary XMP-types as *bursty*-XMPs, unlike Leo P which is a *quiescent*-XMP. Within this classification scheme, 'quiescent' is associated with 'diffuse' and 'bursty' with 'compact'. BCD galaxies are very similar to *bursty+compact* XMPs in this respect, with a large and luminous concentration of SF at their centre (e.g. Gil de Paz et al. 2003, and references therein). While the 'diffuse' aspect of BDDs aligns them closely with dIrrs in a morphological context, as we have seen from Fig. 5 their star-forming regions are more active than dIrrs. In this sense, the XMP galaxies within our sample of BDDs would be exceptions to the Skillman et al. (2013) classification, as they are *active+diffuse*-XMPs.

In general, the larger population of BDDs appears to be a population of *active* dwarf irregular galaxies that can extend down to extremely low metallicity, suggesting that the placement of BDDs within the grand scheme of dwarf galaxy evolution is not clear-cut. In light of this 'active dIrr' scenario, a question exists as to whether BDDs could offer an evolutionary link between dwarf irregular galaxies and BCDs. The existence of such a link between these two sub-classes of dwarf galaxies has long been a subject of debate. Originally, it was thought that dIrrs were post-starburst BCDs (Thuan 1985; Davies & Phillipps 1988); however, in-depth studies of their surface brightness profiles suggest otherwise. For example, Janowiecki & Salzer (2014) show that the underlying hosts of BCDs have significantly more concentrated light distributions, with properties that are so distinct from dIrrs that major structural changes would be required in order transform the two populations into one another. However, even if BDDs may not have been BCD galaxies in the past, they may represent a different phase of dIrr evolution when SF is more prevalent. In order to determine the possible role of BDDs with respect to their neighbouring dwarf galaxy classifications (dIrrs and BCDs), we would require deep imaging of our sample – a definite future goal of this study.

However, what we *can* say is that BDDs belong within the class of LSB dwarf galaxies, a broad classification that encompasses both irregular and spheroidal dwarf galaxies with a central *B*-band surface-brightness $\mu_{B,0} \gtrsim 23$ mag arcsec^{-1} (Kunth & Östlin 2000). In particular, they would be classed as LSB dIrr galaxies. In this respect, we may have uncovered a sample of LSB dIrr galaxies that bridge the BCD and dIrr populations with regards to physical and morphological properties – a population of actively star-forming galaxies where the H II regions are not centrally clustered.

The method by which SF occurs in BDDs could be the element that separates them from the accretion-induced SF witnessed in BCDs and XMPs (as demonstrated by the mass–metallicity relation) and the lack of SF seen in dIrrs. Despite the apparent absence of significant amounts of gas flowing into central star-forming complexes, they continue to host H II regions embedded within low-luminosity, metal-poor gas. Whilst the SF could be linked to past/ongoing interactions, these galaxies were selected on the basis of being isolated, implying that only past interactions can be relevant. Alternatively, stars may be forming from previously ejected and reprocessed gas that has now cooled and fallen back on to the H II regions.

The chemically young nature of the gas within the H II regions suggests very low levels of SF in the past. This could be verified by resolving their stellar populations (for the closest BDDs) and mapping their SFHs. We know that dwarf galaxies appear to have SFHs that suggest 'gasping' and not bursting SF – i.e. long, moderate activity and short quiescent phases (Annibali et al. 2003) and dIrrs and BCDs have similar SFHs despite having very different current SFRs. As such, it would be interesting to determine whether BDDs have SFHs that are intermediate between these two classes, as their physical and chemical properties suggest. As such, the SFHs of BDDs would not only provide significant insight into their chemical evolutionary history but also their relation to other dwarf galaxy populations. On the other hand, integral-field-unit observations would enable us to assess the kinematic stability of the gas and assess the possible role of past interactions/mergers in their star-forming activity. Consolidating SFHs and kinematical maps will provide additional insight into whether the low metal content of BDDs is environmentally driven or a natural consequence of evolution – for example, McQuinn et al. (2015b) use SFHs and chemical evolution models to suggest that Leo P's extremely low metal content is due to the combined effects of inefficient SF and it losing 95 per cent of its oxygen via stellar feedback (e.g. outflows) . It would be interesting to explore whether BDDs fall into the class of XMP galaxies that show signs of interaction (e.g. the higher luminosity, low-mass XMPs of Izotov et al. 2012) or the secularly evolving, low-mass, low-luminosity XMPs like Leo P. Such observations will form part of a future study using VLT-MUSE observations of a sub-sample of the BDD population (James et al., in preparation).

6 CONCLUSIONS

In order to unveil more XMP objects, J15 utilized the morphological properties of Leo P to conduct a search within the SDSS imaging data base. This resulted in ∼150 previously unstudied blue, diffuse galaxies with H II regions scattered throughout LSB gas, which we called BDD galaxies. J15 concentrated on 12 BDD galaxies (or JKB objects) for which we had MMT optical spectroscopic data at the time. Here, we have extended this sample to 51 BDD galaxies in order to obtain a fuller picture of this population of dwarf galaxies.

The 51 galaxies in our sample are at distances of 1–150 Mpc (although we expect distance measurements below 20 Mpc to be highly affected by peculiar motions) and are 20–50 arcsec across. All of the spectra showed bright emission lines typical of star-forming galaxies, with the exception of 11 objects, which were not included in the spectroscopic analysis. These non-emission-line objects may represent BDD galaxies observed during quiescent periods between SF episodes. A full spectroscopic analysis was undertaken on 40/51 objects, amounting to 57 individual spectra once accounting for extractions from multiple H II regions within the same system. Using SDSS *ugriz* images, a photometric analysis was undertaken on the complete sample of 51 galaxies. The main results from this study are as follows:

(i) Direct-method oxygen abundances were obtained via electron temperature measurements for 29/51 objects and were found to range from $7.43 < 12 + \log(\mathrm{O/H}) < 8.01$. Eleven of these 29 objects have O/H values below 0.1 $Z_\odot$ and are therefore classified as being extremely metal poor.

(ii) Using the same 'direct method', nitrogen-to-oxygen ratios were calculated and found to lie between $-1.88 < \log(\mathrm{N/O}) < -1.39$, which are typical values for the metallicity range described above.

(iii) Total luminosities were found to be in the range $39 < \log(L_{\mathrm{H}\alpha/\mathrm{erg\,s^{-1}}}) < 41$, which translate to current SFRs between 1.1 × 10^{-2} and 33.4 × 10^{-2} $\mathrm{M_\odot\ yr^{-1}}$ and a median of 3.5 × 10^{-2} $\mathrm{M_\odot\ yr^{-1}}$. In consideration of their faintness, SFRs were calculated using the low-luminosity regime recalibration of the K98 relation by Lee et al. (2009).

(iv) Absolute *B*-band luminosities are between ∼−10 and −18 mag and *V*-band surface brightnesses are between 23 and 25 mag arcsec^{-1}.

(v) Using SED modelling, stellar masses were found to range from $\log(M_*/\mathrm{M_\odot}) \sim 5$ to 9, with an average of $\log(M_*/\mathrm{M_\odot}) \sim 7$. Specific SFRs were found to lie in the range $-10.0 < \log(\mathrm{SSFR/yr^{-1}}) < -6.5$, with a mean of $\log(\mathrm{SSFR})/\mathrm{yr^{-1}} \sim -9$, which fit within the star-forming sequence for low-mass galaxies. However, without deep optical and infrared imaging, such mass estimates are thought to have significant uncertainties.

From the photometric and spectroscopic analysis of our significantly larger sample of BDD galaxies, we confirm the findings of Paper I in that BDDs appear to be a population of dwarf galaxies that lie in between quiescent dIrrs and active starbursting BCD galaxies. By assessing the location of the BDD sample within the mass–metallicity relation we find that, unlike bright emission-line XMP galaxies, BDDs do not appear to be experiencing an excessive amount of metal-poor gas accretion relative to their stellar mass. As such, the triggering mechanism behind their ongoing SF may instead be due to past interactions or previously ejected gas that has now cooled. Their diffuse and irregular morphology separates them from the compact BCD structure, or the typically cometary *bursty*-XMP galaxies. With regards to this latter class, the XMP-BDD galaxies instead belong to a 'diffuse yet active' XMP category. Overall, BDDs appear to be a sample of dwarf galaxies that bridge the dIrr+BCD galaxy populations with regards to physical and morphological properties – a population of actively star-forming galaxies where the H II regions are not centrally clustered, i.e. dIrrs experiencing an *active* stage of SF. In the broader scheme of dwarf galaxy classification, they fit within the class of LSB dIrr galaxies.

In order to fully assess the role that BDDs may play within dwarf galaxy evolution, three major pieces of the puzzle are still required. First, deep optical and infrared imaging would enable accurate photometric profiling of their underlying host component and allow us to compare their light distributions with those of dIrrs

and BCDs. Secondly, SFHs obtained from resolved stellar population studies of the closest BDDs could provide significant insight into their past, and present mode of SF, alongside their chemical evolutionary history. Finally, kinematical information from integral field unit observations would enable us to explore how it is that SF can be actively ongoing in such random hap-hazard structures. In the future, we hope to extend our BDD sample by applying our search algorithms to data from Southern hemisphere surveys, such as dark energy survey and visible and infrared survey telescope for astronomy.

ACKNOWLEDGEMENTS

The observations reported here were obtained at the MMT Observatory, a joint facility of the University of Arizona and the Smithsonian Institution. The authors are sincerely grateful to Danielle Berg for discussions regarding chemical abundance calculations, Janice Lee for advice on calculating SFRs in the low-luminosity regime, and Matt Auger for assistance with SED modelling. We are grateful to the University of Arizona Observatory time assignment committee who awarded time to this programme, and thank the MMT telescope operators and staff for technical support. BLJ thanks support from the Science & Technology Facilities Council (STFC). The research leading to these results has received funding from the European Research Council under the European Union's Seventh Framework Programme (FP/2007-2013)/ERC Grant Agreement no. 308024. SK acknowledges financial support from the ERC. DPS acknowledges support from the National Science Foundation through the grant AST-1410155. EWO is partially supported by NSF grant AST1313006. This research has made use of the NASA/IPAC Extragalactic Database (NED) which is operated by the Jet Propulsion Laboratory, California Institute of Technology, under contract with the National Aeronautics and Space Administration.

REFERENCES

Aloisi A., Tosi M., Greggio L., 1999, AJ, 118, 302
Aloisi A. et al., 2007, ApJ, 667, L151
Amorín R. O., Pérez-Montero E., Vílchez J. M., 2010, ApJ, 715, L128
Annibali F., Greggio L., Tosi M., Aloisi A., Leitherer C., 2003, AJ, 126, 2752
Asplund M., Grevesse N., Sauval A. J., Scott P., 2009, ArA&A, 47, 481
Baldwin J. A., Phillips M. M., Terlevich R., 1981, PASP, 93, 5
Berg D. A. et al., 2012, ApJ, 754, 98
Berg D. A., Skillman E. D., Croxall K. V., Pogge R. W., Moustakas J., Johnson-Groh M., 2015, ApJ, 806, 16
Berg D. A., Skillman E. D., Henry R. B. C., Erb D. K., Carigi L., 2016, ApJ, 827, 126
Brinchmann J., Kunth D., Durret F., 2008, A&A, 485, 657
Cardelli J. A., Clayton G. C., Mathis J. S., 1989, ApJ, 345, 245
Conroy C., Gunn J. E., White M., 2009, ApJ, 699, 486
Croxall K., Pogge R. W., Berg D. A., Skillman E. D., Moustakas J., 2016, ApJ, 830, 4
Davies J. I., Phillipps S., 1988, MNRAS, 233, 553
Ekta B., Chengalur J. N., 2010, MNRAS, 406, 1238
Ekta, Chengalur J. N., Pustilnik S. A., 2006, MNRAS, 372, 853
Ekta, Chengalur J. N., Pustilnik S. A., 2008, MNRAS, 391, 881
Ellis R. S. et al., 2013, ApJ, 763, L7
Filho M. E. et al., 2013, A&A, 558, A18
Filho M. E., Sánchez Almeida J., Muñoz-Tuñón C., Nuza S. E., Kitaura F., Heß S., 2015, ApJ, 802, 82
Filippenko A. V., 1982, PASP, 94, 715
Fitzpatrick E. L., 1999, PASP, 111, 63
Garnett D. R., 1992, AJ, 103, 1330
Gil de Paz A., Madore B. F., Pevunova O., 2003, ApJS, 147, 29
Giovanelli R. et al., 2013, AJ, 146, 15
Guseva N. G., Papaderos P., Izotov Y. I., Green R. F., Fricke K. J., Thuan T. X., Noeske K. G., 2003, A&A, 407, 75
Guseva N. G., Izotov Y. I., Fricke K. J., Henkel C., 2015, A&A, 579, A11
Haurberg N. C., Rosenberg J., Salzer J. J., 2013, ApJ, 765, 66
Haynes M. P. et al., 2011, AJ, 142, 170
Hinshaw G. et al., 2009, ApJS, 180, 225
Hirschauer A. S. et al., 2016, ApJ, 822, 108
Huang S., Haynes M. P., Giovanelli R., Brinchmann J., Stierwalt S., Neff S. G., 2012, AJ, 143, 133
Izotov Y. I., Thuan T. X., 1999, ApJ, 511, 639
Izotov Y. I., Thuan T. X., 2002, ApJ, 567, 875
Izotov Y. I., Stasińska G., Meynet G., Guseva N. G., Thuan T. X., 2006, A&A, 448, 955
Izotov Y. I., Thuan T. X., Guseva N. G., 2007, ApJ, 671, 1297
Izotov Y. I., Thuan T. X., Guseva N. G., 2012, A&A, 546, A122
James B. L., Koposov S., Stark D. P., Belokurov V., Pettini M., Olszewski E. W., 2015, MNRAS, 448, 2687 (J15)
Janowiecki S., Salzer J. J., 2014, ApJ, 793, 109
Kehrig C., Vílchez J. M., Pérez-Montero E., Iglesias-Páramo J., Brinchmann J., Kunth D., Durret F., Bayo F. M., 2015, ApJ, 801, L28
Kennicutt R. C., Jr, 1998, ArA&A, 36, 189 (K98)
Kewley L. J., Dopita M. A., Sutherland R. S., Heisler C. A., Trevena J., 2001, ApJ, 556, 121
Kunth D., Östlin G., 2000, A&AR, 10, 1
Lee H., Skillman E. D., Cannon J. M., Jackson D. C., Gehrz R. D., Polomski E. F., Woodward C. E., 2006, ApJ, 647, 970
Lee J. C. et al., 2009, ApJ, 706, 599
Leitherer C. et al., 1999, ApJS, 123, 3
Leitherer C., Ortiz Otálvaro P. A., Bresolin F., Kudritzki R.-P., Lo Faro B., Pauldrach A. W. A., Pettini M., Rix S. A., 2010, ApJS, 189, 309
López-Sánchez Á. R., Dopita M. A., Kewley L. J., Zahid H. J., Nicholls D. C., Scharwächter J., 2012, MNRAS, 426, 2630
McQuinn K. B. W. et al., 2010, ApJ, 721, 297
McQuinn K. B. W. et al., 2015a, ApJ, 812, 158
McQuinn K. B. W. et al., 2015b, ApJ, 815, L17
Makarov D., Prugniel P., Terekhova N., Courtois H., Vauglin I., 2014, A&A, 570, A13
Mannucci F., Cresci G., Maiolino R., Marconi A., Gnerucci A., 2010, MNRAS, 408, 2115
Morales-Luis A. B., Sánchez Almeida J., Aguerri J. A. L., Muñoz-Tuñón C., 2011, ApJ, 743, 77
Oesch P. A. et al., 2016, ApJ, 819, 129
Papaderos P., Guseva N. G., Izotov Y. I., Fricke K. J., 2008, A&A, 491, 113
Peeples M. S., Pogge R. W., Stanek K. Z., 2009, ApJ, 695, 259
Pirzkal N. et al., 2015, ApJ, 804, 11
Pustilnik S. A., Kniazev A. Y., Pramskij A. G., 2005, A&A, 443, 91
Pustilnik S. A., Engels D., Kniazev A. Y., Pramskij A. G., Ugryumov A. V., Hagen H.-J., 2006, Astron. Lett., 32, 228
Rhode K. L. et al., 2013, AJ, 145, 149
Sánchez Almeida J. et al., 2015, ApJ, 810, L15
Sánchez Almeida J., Pérez-Montero E., Morales-Luis A. B., Muñoz-Tuñón C., García-Benito R., Nuza S. E., Kitaura F. S., 2016, ApJ, 819, 110
Schaerer D., Vacca W. D., 1998, ApJ, 497, 618
Schiminovich D. et al., 2007, ApJS, 173, 315
Shirazi M., Brinchmann J., 2012, MNRAS, 421, 1043
Skillman E. D. et al., 2013, AJ, 146, 3
Stasińska G. et al., 2012, EAS Publ. Ser., 3, 54
Thuan T. X., 1985, ApJ, 299, 881
Tonry J. L., Blakeslee J. P., Ajhar E. A., Dressler A., 2000, ApJ, 530, 625
van Zee L., 2000, ApJ, 543, L31
van Zee L., Haynes M. P., 2006, ApJ, 636, 214
Weisz D. R. et al., 2011, ApJ, 739, 5
Yates R. M., Kauffmann G., Guo Q., 2012, MNRAS, 422, 215
Zhao Y., Gao Y., Gu Q., 2013, ApJ, 764, 44

APPENDIX A: OBSERVED FLUXES AND LINE INTENSITIES

Table A1. Spectroscopic line fluxes and de-reddened line intensities (both relative to Hβ = 100) as measured from the spectra shown in Fig. B1.

	JKB 1.0		JKB 1.1		JKB 2.0		JKB 2.1	
[O II] 3727.10	170 ± 27	199 ± 33	69.9 ± 10.2	69.9 ± 10.2	65.3 ± 9.6	77.1 ± 11.4	18.6 ± 3.0	24.4 ± 3.9
[O II] 3729.86	140 ± 23	163 ± 27	57.3 ± 8.3	57.3 ± 8.3	54.2 ± 8.0	64.0 ± 9.6	17.6 ± 2.8	23.1 ± 3.8
He I 3820.84	–	–	–	–	–	–	–	–
[Ne III] 3870.16	41.8 ± 8.5	47.8 ± 9.7	33.5 ± 4.8	33.5 ± 4.8	6.11 ± 1.36	7.04 ± 1.57	15.9 ± 2.4	20.1 ± 3.0
He I+H8 3889.75	–	–	19.1 ± 2.8	19.1 ± 2.8	14.3 ± 2.3	16.4 ± 2.7	13.7 ± 2.1	17.2 ± 2.7
He II 3969.55	–	–	24.7 ± 3.6	24.7 ± 3.6	10.6 ± 1.9	12.0 ± 2.2	16.4 ± 2.4	20.2 ± 3.1
He I 4027.49	–	–	2.31 ± 0.74	2.31 ± 0.74	–	–	–	–
[S II] 4069.75	–	–	–	–	–	–	–	–
Hδ 4102.89	–	–	24.3 ± 3.5	24.3 ± 3.5	20.7 ± 3.2	23.1 ± 3.5	20.5 ± 3.0	24.3 ± 3.6
Hγ 4341.68	–	–	43.9 ± 6.3	43.9 ± 6.3	36.0 ± 5.2	38.7 ± 5.6	38.7 ± 5.5	43.5 ± 6.3
[O III] 4364.44	<7.47	<7.97	10.4 ± 1.6	10.4 ± 1.6	<1.28	<1.37	7.10 ± 1.23	7.94 ± 1.38
He I 4472.93	–	–	4.69 ± 0.90	4.69 ± 0.90	–	–	3.17 ± 0.76	3.46 ± 0.82
Fe III 4659.35	–	–	–	–	–	–	–	–
He II 4687.02	–	–	2.12 ± 0.64	2.12 ± 0.64	–	–	–	–
Ar IV 4741.49	–	–	–	–	–	–	–	–
Hβ 4862.72	100 ± 15	100 ± 15	100 ± 14	100 ± 14	100 ± 14	100 ± 14	100 ± 14	100 ± 14
[O III] 4960.29	118 ± 18	117 ± 18	154 ± 21	154 ± 21	45.1 ± 6.5	44.5 ± 6.4	105 ± 14	103 ± 14
[O III] 5008.24	361 ± 54	355 ± 53	477 ± 67	477 ± 67	138 ± 19	136 ± 19	317 ± 45	308 ± 43
[N II] 5756.24	–	–	–	–	–	–	–	–
He I 5877.59	–	–	8.46 ± 1.35	8.46 ± 1.35	10.0 ± 1.9	9.0 ± 1.7	11.6 ± 1.8	9.7 ± 1.6
[O I] 6302.05	–	–	2.04 ± 0.61	2.04 ± 0.61	3.81 ± 1.10	3.29 ± 0.95	–	–
[S III] 6313.80	–	–	–	–	–	–	–	–
[O I] 6365.54	–	–	–	–	–	–	–	–
Hα 6564.61	335 ± 50	285 ± 43	252 ± 35	252 ± 35	292 ± 41	247 ± 35	355 ± 50	270 ± 39
[N II] 6585.20	<5.49	<4.68	<0.73	<0.73	4.65 ± 1.15	3.92 ± 0.98	<0.63	<0.48
He I 6679.99	40.1 ± 8.9	33.9 ± 7.5	7.85 ± 1.41	7.85 ± 1.41	–	–	3.59 ± 0.73	2.70 ± 0.55
[S II] 6718.29	49.3 ± 9.1	41.6 ± 7.7	10.3 ± 1.6	10.3 ± 1.6	13.5 ± 2.1	11.3 ± 1.8	4.48 ± 0.84	3.35 ± 0.64
[S II] 6732.67	29.1 ± 7.3	24.5 ± 6.1	8.97 ± 1.44	8.97 ± 1.44	13.2 ± 2.3	11.1 ± 1.9	4.76 ± 1.06	3.55 ± 0.80
[Ne III] 6870.16	–	–	–	–	–	–	–	–
[Ar III] 7137.80	–	–	2.23 ± 0.71	2.23 ± 0.71	6.42 ± 1.74	5.21 ± 1.42	4.90 ± 1.21	3.49 ± 0.87
[O II] 7321.47	52.5 ± 10.4	42.6 ± 8.6	6.66 ± 1.28	6.66 ± 1.28	–	–	–	–
[O II] 7332.25	–	–	–	–	5.26 ± 1.25	4.21 ± 1.01	2.84 ± 0.74	1.99 ± 0.53
$F(H\beta) \times 10^{-16}$ *erg s*$^{-1}$ *cm*$^{-2}$	3.63 ± 0.41		20.5 ± 2.1		7.91 ± 0.80		9.93 ± 1.00	
I(Hβ) $\times 10^{-16}$ erg s^{-1} cm^{-2}	6.02 ± 0.81		20.5 ± 2.1		13.5 ± 1.6		23.6 ± 3.3	
$E(B-V)$	0.15 ± 0.02		0.00 ± 0.01		0.16 ± 0.02		0.26 ± 0.03	

Table A1 – *continued*

	JKB 3.0		JKB 3.1		JKB 4.0		JKB 5.0	
[O II] 3727.10	58.3 ± 12.9	58.3 ± 12.9	212 ± 32	308 ± 51	99.6 ± 14.3	126.7 ± 18.5	91.3 ± 13.8	110.1 ± 16.9
[O II] 3729.86	101 ± 22	101 ± 22	193 ± 29	280 ± 47	71.4 ± 10.3	90.9 ± 13.4	105 ± 15	127 ± 19
He I 3820.84	–	–	–	–	–	–	12.1 ± 2.6	14.3 ± 3.1
[Ne III] 3870.16	33.1 ± 7.3	33.1 ± 7.3	–	–	11.8 ± 1.9	14.5 ± 2.3	8.41 ± 1.91	9.88 ± 2.25
He I+H8 3889.75	18.1 ± 4.0	18.1 ± 4.0	–	–	9.86 ± 1.67	12.10 ± 2.07	7.61 ± 2.29	8.92 ± 2.70
He II 3969.55	24.5 ± 5.4	24.5 ± 5.4	–	–	12.8 ± 1.9	15.5 ± 2.4	7.41 ± 1.94	8.57 ± 2.25
He I 4027.49	1.51 ± 0.42	1.51 ± 0.42	–	–	–	–	–	–
[S II] 4069.75	–	–	–	–	4.80 ± 1.00	5.66 ± 1.18	–	–
H δ 4102.89	24.9 ± 5.5	24.9 ± 5.5	–	–	19.8 ± 2.9	23.2 ± 3.4	16.9 ± 2.9	19.1 ± 3.3
H γ 4341.68	45.0 ± 10.0	45.0 ± 10.0	31.2 ± 6.3	36.7 ± 7.4	38.6 ± 5.5	42.9 ± 6.2	37.3 ± 6.1	40.4 ± 6.6
[O III] 4364.44	7.60 ± 1.70	7.60 ± 1.70	<5.19	<6.06	3.30 ± 0.83	3.65 ± 0.92	<2.00	<2.16
He I 4472.93	3.81 ± 0.88	3.81 ± 0.88	–	–	3.14 ± 0.76	3.40 ± 0.82	5.33 ± 1.68	5.66 ± 1.78
Fe III 4659.35	–	–	–	–	–	–	–	–
He II 4687.02	–	–	–	–	–	–	–	–
Ar IV 4741.49	–	–	–	–	–	–	–	–
Hβ 4862.72	100 ± 22	100 ± 22	100 ± 15	100 ± 15	100 ± 14	100 ± 14	100 ± 14	100 ± 14
[O III] 4960.29	174 ± 38	174 ± 38	68.9 ± 10.8	67.0 ± 10.5	73.8 ± 10.5	72.4 ± 10.3	43.7 ± 6.5	43.0 ± 6.4
[O III] 5008.24	528 ± 116	528 ± 116	208 ± 30	199 ± 29	219 ± 31	213 ± 30	132 ± 19	129 ± 18
[N II] 5756.24	–	–	–	–	–	–	–	–
He I 5877.59	10.0 ± 2.2	10.0 ± 2.2	–	–	10.4 ± 2.1	8.9 ± 1.8	10.5 ± 2.5	9.2 ± 2.2
[O I] 6302.05	2.77 ± 0.65	2.77 ± 0.65	–	–	4.72 ± 0.91	3.81 ± 0.74	–	–
[S III] 6313.80	1.51 ± 0.39	1.51 ± 0.39	–	–	2.29 ± 0.77	1.85 ± 0.62	–	–
[O I] 6365.54	–	–	–	–	2.07 ± 0.64	1.66 ± 0.51	–	–
Hα 6564.61	256 ± 56	256 ± 56	346 ± 51	237 ± 38	342 ± 48	267 ± 38	309 ± 44	256 ± 37
[N II] 6585.20	5.34 ± 1.20	5.34 ± 1.21	25.1 ± 5.2	17.1 ± 3.8	8.61 ± 1.37	6.73 ± 1.08	7.01 ± 1.56	5.78 ± 1.30
He I 6679.99	2.61 ± 0.61	2.61 ± 0.61	–	–	2.41 ± 0.59	1.87 ± 0.46	–	–
[S II] 6718.29	12.6 ± 2.8	12.6 ± 2.8	55.1 ± 9.8	36.8 ± 7.1	24.7 ± 3.6	19.0 ± 2.8	21.1 ± 3.3	17.2 ± 2.7
[S II] 6732.67	10.0 ± 2.2	10.0 ± 2.2	40.3 ± 7.1	26.9 ± 5.2	17.8 ± 2.6	13.6 ± 2.0	11.1 ± 1.9	9.0 ± 1.6
[Ne III] 6870.16	–	–	–	–	–	–	–	–
[Ar III] 7137.80	6.21 ± 1.40	6.21 ± 1.40	14.3 ± 5.2	9.0 ± 3.3	4.39 ± 0.79	3.24 ± 0.59	5.74 ± 1.32	4.53 ± 1.05
[O II] 7321.47	2.41 ± 0.59	2.41 ± 0.59	19.5 ± 4.8	11.8 ± 3.1	4.56 ± 0.96	3.30 ± 0.70	–	–
[O II] 7332.25	0.82 ± 0.25	0.82 ± 0.25	–	–	–	–	6.54 ± 1.83	5.08 ± 1.43
F(Hβ) × 10^{-16} erg s^{-1} cm^{-2}	36.1 ± 5.6		2.81 ± 0.30		12.8 ± 1.3		7.06 ± 0.72	
I(Hβ) × 10^{-16} erg s^{-1} cm^{-2}	36.1 ± 5.8		9.36 ± 2.35		27.9 ± 3.8		13.0 ± 1.7	
$E(B-V)$	0.00 ± 0.01		0.36 ± 0.07		0.24 ± 0.03		0.18 ± 0.02	

Table A1 *– continued*

	JKB 7.0		JKB 8.11		JKB 8.12		JKB 8.2	
[O II] 3727.10	136 ± 19	148 ± 21	91.0 ± 13.2	96.3 ± 14.0	126 ± 34	126 ± 34	71.3 ± 15.3	71.3 ± 15.3
[O II] 3729.86	78.1 ± 11.3	85.2 ± 12.4	135 ± 19	143 ± 20	376 ± 70	376 ± 70	84.2 ± 16.9	84.2 ± 17.0
He I 3820.84	–	–	–	–	–	–	–	–
[Ne III] 3870.16	26.7 ± 3.9	28.8 ± 4.2	29.7 ± 4.5	31.1 ± 4.7	–	–	–	–
He I+H8 3889.75	14.5 ± 2.2	15.6 ± 2.4	12.3 ± 2.3	12.9 ± 2.4	–	–	–	–
He II 3969.55	19.5 ± 2.9	20.9 ± 3.1	16.9 ± 2.8	17.6 ± 2.9	–	–	–	–
He I 4027.49	–	–	–	–	–	–	–	–
[S II] 4069.75	2.90 ± 0.88	3.07 ± 0.93	–	–	–	–	–	–
H δ 4102.89	22.7 ± 3.3	24.0 ± 3.5	23.8 ± 3.6	24.7 ± 3.7	–	–	–	–
H γ 4341.68	41.1 ± 5.9	42.7 ± 6.1	42.4 ± 6.1	43.5 ± 6.3	–	–	28.8 ± 7.8	28.8 ± 7.8
[O III] 4364.44	4.87 ± 0.99	5.05 ± 1.02	6.75 ± 1.46	6.91 ± 1.49	<15.7	<15.7	<9.87	<9.87
He I 4472.93	3.33 ± 0.76	3.43 ± 0.78	4.04 ± 1.17	4.11 ± 1.19	–	–	–	–
Fe III 4659.35	–	–	2.85 ± 0.99	2.88 ± 1.00	–	–	–	–
He II 4687.02	2.09 ± 0.63	2.12 ± 0.64	–	–	–	–	–	–
Ar IV 4741.49	–	–	–	–	–	–	–	–
Hβ 4862.72	100 ± 14	100 ± 14	100 ± 14	100 ± 14	100 ± 19	100 ± 19	100 ± 16	100 ± 16
[O III] 4960.29	112 ± 16	112 ± 15	125 ± 17	124 ± 17	96.9 ± 18.9	96.9 ± 18.9	80.2 ± 13.7	80.2 ± 13.7
[O III] 5008.24	341 ± 48	338 ± 47	362 ± 51	360 ± 51	238 ± 42	238 ± 42	216 ± 34	216 ± 34
[N II] 5756.24	–	–	–	–	–	–	–	–
He I 5877.59	9.33 ± 1.62	8.80 ± 1.53	10.9 ± 1.8	10.5 ± 1.7	–	–	–	–
[O I] 6302.05	3.19 ± 0.68	2.95 ± 0.63	3.58 ± 0.99	3.40 ± 0.94	30.5 ± 10.7	30.5 ± 10.7	–	–
[S III] 6313.80	1.73 ± 0.61	1.60 ± 0.57	–	–	–	–	–	–
[O I] 6365.54	2.42 ± 0.60	2.23 ± 0.55	–	–	–	–	–	–
Hα 6564.61	292 ± 41	267 ± 37	286 ± 40	270 ± 38	260 ± 45	260 ± 46	190 ± 29	190 ± 30
[N II] 6585.20	11.3 ± 1.7	10.3 ± 1.6	7.69 ± 1.47	7.26 ± 1.39	<11.8	<11.8	<5.42	<5.42
He I 6679.99	3.67 ± 0.68	3.35 ± 0.62	9.08 ± 1.73	8.55 ± 1.63	60.1 ± 16.3	60.1 ± 16.4	–	–
[S II] 6718.29	28.1 ± 4.0	25.6 ± 3.7	28.7 ± 4.2	27.0 ± 4.0	71.2 ± 15.9	71.2 ± 15.9	26.0 ± 6.1	26.0 ± 6.2
[S II] 6732.67	20.7 ± 3.0	18.8 ± 2.7	16.0 ± 2.5	15.0 ± 2.4	<13.8	<13.8	14.3 ± 5.0	14.3 ± 5.0
[Ne III] 6870.16	1.35 ± 0.47	1.22 ± 0.43	–	–	99.2 ± 20.4	99.2 ± 20.5	–	–
[Ar III] 7137.80	6.52 ± 1.03	5.84 ± 0.92	–	–	–	–	–	–
[O II] 7321.47	–	–	18.5 ± 3.0	17.2 ± 2.8	76.8 ± 21.0	76.8 ± 21.1	24.4 ± 7.4	24.4 ± 7.4
[O II] 7332.25	–	–	–	–	–	–	22.8 ± 6.3	22.8 ± 6.4
F(Hβ) × 10^{-16} erg s^{-1} cm^{-2}	19.2 ± 1.9		18.6 ± 1.9		1.88 ± 0.26		5.66 ± 0.67	
I(Hβ) × 10^{-16} erg s^{-1} cm^{-2}	25.5 ± 2.7		22.3 ± 2.3		1.88 ± 0.28		5.66 ± 0.68	
$E(B-V)$	0.09 ± 0.01		0.06 ± 0.01		0.00 ± 0.02		0.00 ± 0.01	

Table A1 – *continued*

	JKB 8.3		JKB 15.1		JKB 15.2		JKB 16.1	
[O II] 3727.10	55.1 ± 8.1	55.1 ± 8.3	52.3 ± 7.8	57.4 ± 8.6	100 ± 14	120 ± 18	57.6 ± 8.4	57.6 ± 8.4
[O II] 3729.86	100 ± 14	100 ± 14	57.2 ± 8.5	62.9 ± 9.3	101 ± 15	121 ± 18	98.9 ± 14.2	98.9 ± 14.2
He I 3820.84	–	–	–	–	—	–	–	–
[Ne III] 3870.16	25.3 ± 3.8	25.3 ± 3.9	27.8 ± 4.1	30.1 ± 4.4	20.6 ± 3.5	23.9 ± 4.0	25.1 ± 3.7	25.1 ± 3.7
He I+H8 3889.75	13.7 ± 2.4	13.7 ± 2.4	15.0 ± 2.4	16.2 ± 2.6	13.0 ± 2.7	15.1 ± 3.2	18.6 ± 2.8	18.6 ± 2.8
He II 3969.55	18.7 ± 3.0	18.7 ± 3.0	23.1 ± 3.4	24.8 ± 3.7	10.4 ± 2.3	11.9 ± 2.6	19.4 ± 2.9	19.4 ± 2.9
He I 4027.49	–	–	–	–	–	–	–	–
[S II] 4069.75	–	–	–	–	–	–	2.08 ± 0.74	2.08 ± 0.74
H δ 4102.89	22.0 ± 3.4	22.0 ± 3.4	23.3 ± 3.4	24.8 ± 3.7	17.3 ± 3.0	19.4 ± 3.4	23.3 ± 3.4	23.3 ± 3.4
H γ 4341.68	42.6 ± 6.2	42.6 ± 6.2	43.8 ± 6.3	45.6 ± 6.5	43.1 ± 6.3	46.5 ± 6.8	47.3 ± 6.8	47.3 ± 6.8
[O III] 4364.44	5.41 ± 1.43	5.41 ± 1.43	10.0 ± 1.7	10.5 ± 1.7	5.48 ± 1.73	5.90 ± 1.87	6.84 ± 1.17	6.84 ± 1.17
He I 4472.93	–	–	2.71 ± 0.82	2.79 ± 0.85	–	–	3.19 ± 0.73	3.19 ± 0.73
Fe III 4659.35	–	–	–	–	–	–	–	–
He II 4687.02	–	–	–	–	–	–	–	–
Ar IV 4741.49	–	–	–	–	–	–	–	–
Hβ 4862.72	100 ± 14	100 ± 14	100 ± 14	100 ± 14	100 ± 14	100 ± 14	100 ± 14	100 ± 14
[O III] 4960.29	123 ± 17	123 ± 17	138 ± 19	137 ± 19	82.1 ± 11.7	80.9 ± 11.6	106 ± 15	106 ± 15
[O III] 5008.24	364 ± 51	364 ± 51	416 ± 59	412 ± 58	242 ± 34	237 ± 33	314 ± 44	314 ± 44
[N II] 5756.24	–	–	–	–	–	–	–	–
He I 5877.59	9.92 ± 1.62	9.92 ± 1.63	11.7 ± 1.9	10.9 ± 1.8	10.5 ± 2.2	9.4 ± 2.0	8.84 ± 1.49	8.84 ± 1.50
[O I] 6302.05	–	–	–	–	6.58 ± 1.61	5.63 ± 1.38	–	–
[S III] 6313.80	–	–	–	–	–	–	–	–
[O I] 6365.54	–	–	–	–	–	–	2.08 ± 0.65	2.08 ± 0.65
Hα 6564.61	196 ± 28	196 ± 28	309 ± 43	281 ± 39	341 ± 48	285 ± 41	271 ± 38	271 ± 38
[N II] 6585.20	7.07 ± 1.29	7.07 ± 1.30	3.01 ± 0.88	2.73 ± 0.80	5.63 ± 1.68	4.71 ± 1.41	5.75 ± 1.05	5.75 ± 1.05
He I 6679.99	4.74 ± 1.08	4.74 ± 1.08	3.99 ± 0.91	3.60 ± 0.83	–	–	2.85 ± 0.70	2.85 ± 0.70
[S II] 6718.29	16.5 ± 2.5	16.5 ± 2.5	10.8 ± 1.7	9.7 ± 1.6	26.4 ± 4.0	21.8 ± 3.4	15.2 ± 2.2	15.2 ± 2.3
[S II] 6732.67	12.7 ± 2.0	12.7 ± 2.0	9.38 ± 1.72	8.46 ± 1.55	25.7 ± 4.2	21.3 ± 3.5	9.06 ± 1.42	9.06 ± 1.42
[Ne III] 6870.16	–	–	–	–	–	–	–	–
[Ar III] 7137.80	5.31 ± 1.20	5.31 ± 1.21	14.6 ± 2.6	13.0 ± 2.3	27.9 ± 4.8	22.4 ± 3.9	4.92 ± 0.90	4.92 ± 0.90
[O II] 7321.47	5.84 ± 1.28	5.84 ± 1.30	–	–	–	–	–	–
[O II] 7332.25	6.32 ± 1.25	6.32 ± 1.27	4.16 ± 1.03	3.66 ± 0.91	–	–	–	–
F(Hβ) $\times 10^{-16}$ erg s^{-1} cm^{-2}	34.3 ± 3.5		37.2 ± 3.7		27.3 ± 2.8		14.8 ± 1.5	
I(Hβ) $\times 10^{-16}$ erg s^{-1} cm^{-2}	34.3 ± 4.5		50.5 ± 5.4		48.1 ± 5.8		14.8 ± 1.5	
$E(B-V)$	0.00 ± 0.03		0.09 ± 0.01		0.17 ± 0.02		0.00 ± 0.01	

Table A1 – *continued*

	JKB 16.2		JKB 16.3		JKB 18.0		JKB 18.1	
[O II] 3727.10	60.1 ± 20.2	69.3 ± 23.4	120 ± 28	137 ± 32	110 ± 16	128 ± 19	500 ± 91	788 ± 157
[O II] 3729.86	281 ± 48	325 ± 56	266 ± 48	304 ± 56	86.6 ± 12.9	101.3 ± 15.2	218 ± 45	344 ± 76
He I 3820.84	43.8 ± 12.8	49.9 ± 14.6	–	–	5.78 ± 1.71	6.66 ± 1.98	136 ± 27	205 ± 43
[Ne III] 3870.16	31.9 ± 10.4	36.0 ± 11.8	33.1 ± 12.1	37.1 ± 13.6	23.3 ± 3.6	26.6 ± 4.1	47.3 ± 12.6	69.9 ± 19.2
He I+H8 3889.75	–	–	–	–	15.9 ± 2.9	18.1 ± 3.3	–	–
He II 3969.55	–	–	–	–	12.0 ± 2.2	13.5 ± 2.5	–	–
He I 4027.49	–	–	–	–	–	–	–	–
[S II] 4069.75	–	–	–	–	–	–	–	–
H δ 4102.89	–	–	–	–	20.2 ± 3.2	22.3 ± 3.6	–	–
H γ 4341.68	–	–	–	–	39.3 ± 5.9	42.0 ± 6.3	–	–
[O III] 4364.44	<8.02	<8.51	<13.5	<14.3	8.52 ± 1.79	9.09 ± 1.91	<14.7	<17.8
He I 4472.93	–	–	–	–	–	–	–	–
Fe III 4659.35	–	–	–	–	–	–	–	–
He II 4687.02	37.7 ± 9.6	38.5 ± 9.8	–	–	–	–	–	–
Ar IV 4741.49	–	–	–	–	–	–	–	–
Hβ 4862.72	100 ± 17	100 ± 17	100 ± 18	100 ± 18	100.0 ± 14.3	100.0 ± 14.3	100 ± 20	100 ± 20
[O III] 4960.29	64.3 ± 12.8	63.5 ± 12.7	38.6 ± 10.9	38.2 ± 10.8	94.0 ± 13.5	92.8 ± 13.3	70.4 ± 16.9	67.9 ± 16.3
[O III] 5008.24	204 ± 33	201 ± 33	112 ± 20	110 ± 20	283 ± 40	279 ± 39	174 ± 32	166 ± 30
[N II] 5756.24	–	–	–	–	–	–	–	–
He I 5877.59	–	–	–	–	11.0 ± 2.0	9.9 ± 1.8	–	–
[O I] 6302.05	–	–	–	–	6.91 ± 1.47	6.01 ± 1.29	–	–
[S III] 6313.80	–	–	–	–	–	–	–	–
[O I] 6365.54	–	–	–	–	–	–	–	–
Hα 6564.61	330 ± 53	286 ± 46	327 ± 55	286 ± 49	309 ± 44	263 ± 37	453 ± 80	286 ± 55
[N II] 6585.20	32.9 ± 10.2	28.4 ± 8.8	<10.9	<9.5	6.41 ± 1.33	5.47 ± 1.14	54.0 ± 12.9	33.9 ± 8.6
He I 6679.99	–	–	–	–	3.70 ± 0.99	3.14 ± 0.84	30.0 ± 9.4	18.5 ± 6.0
[S II] 6718.29	45.2 ± 10.6	38.7 ± 9.1	56.5 ± 13.1	48.9 ± 11.4	24.2 ± 3.6	20.4 ± 3.1	116 ± 21	70 ± 14
[S II] 6732.67	29.6 ± 9.0	25.3 ± 7.8	50.5 ± 12.3	43.7 ± 10.7	18.7 ± 2.8	15.8 ± 2.4	66.6 ± 14.0	40.5 ± 9.2
[Ne III] 6870.16	–	–	–	–	–	–	–	–
[Ar III] 7137.80	–	–	–	–	6.58 ± 1.22	5.41 ± 1.01	27.0 ± 8.7	15.2 ± 5.1
[O II] 7321.47	–	–	–	–	–	–	–	–
[O II] 7332.25	–	–	–	–	4.11 ± 1.11	3.34 ± 0.90	33.9 ± 10.9	18.4 ± 6.2
F(Hβ) × 10^{-16} erg s^{-1} cm^{-2}	1.46 ± 0.18		0.82 ± 0.11		6.74 ± 0.68		1.17 ± 0.17	
I(Hβ) × 10^{-16} erg s^{-1} cm^{-2}	2.32 ± 0.34		1.26 ± 0.19		11.2 ± 1.3		5.09 ± 1.47	
$E(B-V)$	0.14 ± 0.02		0.13 ± 0.02		0.15 ± 0.02		0.44 ± 0.08	

Table A1 – *continued*

	JKB 21.0		JKB 22.0		JKB 22.1		JKB 24.0	
[O II] 3727.10	136 ± 22	160 ± 26	66.4 ± 9.5	76.1 ± 11.0	64.2 ± 9.3	73.6 ± 10.7	178 ± 25	276 ± 42
[O II] 3729.86	197 ± 30	231 ± 36	71.6 ± 10.3	82.0 ± 11.8	80.2 ± 11.5	91.9 ± 13.3	73.4 ± 10.9	113.6 ± 17.8
He I 3820.84	–	–	–	–	–	–	6.57 ± 1.76	9.75 ± 2.66
[Ne III] 3870.16	40.0 ± 7.8	45.9 ± 9.0	32.3 ± 4.6	36.3 ± 5.2	31.1 ± 4.5	35.0 ± 5.1	30.7 ± 4.6	44.7 ± 6.9
He I+H8 3889.75	–	–	13.9 ± 2.1	15.6 ± 2.3	13.4 ± 2.0	15.0 ± 2.3	8.42 ± 1.87	12.21 ± 2.76
He II 3969.55	22.4 ± 5.7	25.4 ± 6.5	21.2 ± 3.1	23.6 ± 3.4	20.5 ± 3.0	22.8 ± 3.4	–	–
He I 4027.49	–	–	2.15 ± 0.62	2.37 ± 0.68	–	–	–	–
[S II] 4069.75	–	–	–	–	–	–	–	–
H δ 4102.89	21.9 ± 5.5	24.3 ± 6.1	21.7 ± 3.1	23.7 ± 3.4	22.3 ± 3.3	24.4 ± 3.6	16.8 ± 2.8	22.3 ± 3.8
H γ 4341.68	41.4 ± 7.3	44.4 ± 7.8	43.0 ± 6.1	45.6 ± 6.5	41.3 ± 5.9	43.8 ± 6.3	38.3 ± 5.6	46.3 ± 6.9
[O III] 4364.44	<5.22	<5.58	7.19 ± 1.16	7.61 ± 1.22	7.17 ± 1.25	7.59 ± 1.32	<1.55	<1.85
He I 4472.93	–	–	3.76 ± 0.70	3.92 ± 0.73	4.50 ± 0.89	4.70 ± 0.93	–	–
Fe III 4659.35	–	–	–	–	–	–	–	–
He II 4687.02	–	–	2.11 ± 0.55	2.16 ± 0.56	–	–	–	–
Ar IV 4741.49	–	–	–	–	–	–	–	–
Hβ 4862.72	100 ± 15	100 ± 15	100 ± 14	100 ± 14	100 ± 14	100 ± 14	100 ± 14	100 ± 14
[O III] 4960.29	137 ± 20	135 ± 20	171 ± 24	169 ± 24	153 ± 21	151 ± 21	150 ± 21	145 ± 20
[O III] 5008.24	410 ± 60	403 ± 59	512 ± 72	504 ± 71	458 ± 64	451 ± 64	426 ± 60	406 ± 57
[N II] 5756.24	–	–	–	–	–	–	7.07 ± 1.99	5.43 ± 1.54
He I 5877.59	–	–	11.1 ± 1.7	10.1 ± 1.5	12.6 ± 2.0	11.5 ± 1.8	14.8 ± 2.6	11.0 ± 2.0
[O I] 6302.05	–	–	3.60 ± 0.69	3.19 ± 0.62	2.10 ± 0.68	1.86 ± 0.60	10.4 ± 2.0	7.1 ± 1.4
[S III] 6313.80	–	–	2.00 ± 0.57	1.77 ± 0.50	–	–	–	–
[O I] 6365.54	–	–	1.49 ± 0.49	1.31 ± 0.43	–	–	5.90 ± 1.62	3.95 ± 1.10
Hα 6564.61	324 ± 47	275 ± 41	322 ± 45	281 ± 40	312 ± 44	272 ± 38	443 ± 63	284 ± 43
[N II] 6585.20	<3.96	<3.35	8.64 ± 1.34	7.52 ± 1.18	5.85 ± 1.09	5.09 ± 0.95	23.6 ± 3.7	15.1 ± 2.5
He I 6679.99	–	–	4.35 ± 0.77	3.76 ± 0.67	3.91 ± 0.82	3.38 ± 0.71	–	–
[S II] 6718.29	35.5 ± 7.1	29.8 ± 6.0	21.6 ± 3.1	18.7 ± 2.7	19.0 ± 2.8	16.4 ± 2.4	45.7 ± 6.7	28.5 ± 4.5
[S II] 6732.67	15.7 ± 4.8	13.2 ± 4.0	13.9 ± 2.0	12.0 ± 1.8	13.6 ± 2.0	11.7 ± 1.8	30.6 ± 4.6	19.0 ± 3.1
[Ne III] 6870.16	–	–	–	–	–	–	–	–
[Ar III] 7137.80	–	–	7.11 ± 1.11	5.99 ± 0.94	6.76 ± 1.13	5.69 ± 0.95	7.48 ± 1.77	4.31 ± 1.06
[O II] 7321.47	36.3 ± 8.8	29.3 ± 7.2	2.62 ± 0.67	2.19 ± 0.56	–	–	4.49 ± 1.45	2.51 ± 0.83
[O II] 7332.25	–	–	3.52 ± 0.67	2.93 ± 0.56	2.79 ± 0.70	2.32 ± 0.58	–	–
F(Hβ) × 10^{-16} erg s^{-1} cm^{-2}	2.61 ± 0.28		24.0 ± 2.4		15.4 ± 1.5		19.6 ± 2.0	
I(Hβ) × 10^{-16} erg s^{-1} cm^{-2}	4.40 ± 0.57		37.2 ± 4.2		24.0 ± 2.7		80.4 ± 15.7	
$E(B-V)$	0.16 ± 0.02		0.13 ± 0.01		0.13 ± 0.02		0.43 ± 0.05	

Table A1 *– continued*

	JKB 24.1		JKB 25.0		JKB 26.0		JKB 26.1	
[O II] 3727.10	156 ± 22	197 ± 28	75.3 ± 10.7	75.3 ± 11.0	80.8 ± 12.0	81.5 ± 12.1	85.6 ± 12.3	90.7 ± 13.1
[O II] 3729.86	61.4 ± 9.0	77.5 ± 11.6	74.8 ± 10.6	74.8 ± 11.0	50.8 ± 8.0	51.3 ± 8.0	61.9 ± 9.0	65.6 ± 9.6
He I 3820.84	4.50 ± 1.17	5.56 ± 1.45	–	–	–	–	–	–
[Ne III] 3870.16	25.6 ± 3.8	31.2 ± 4.6	26.6 ± 3.8	26.6 ± 3.9	30.4 ± 4.6	30.6 ± 4.7	18.9 ± 2.8	19.8 ± 2.9
He I+H8 3889.75	18.2 ± 2.8	22.1 ± 3.4	14.0 ± 2.0	14.0 ± 2.1	9.74 ± 2.22	9.81 ± 2.24	14.9 ± 2.3	15.7 ± 2.4
He II 3969.55	18.6 ± 2.9	22.3 ± 3.4	21.7 ± 3.1	21.7 ± 3.2	–	–	14.5 ± 2.2	15.1 ± 2.3
He I 4027.49	–	–	1.44 ± 0.38	1.44 ± 0.38	–	–	–	–
[S II] 4069.75	3.30 ± 0.99	3.86 ± 1.16	1.14 ± 0.35	1.14 ± 0.35	–	–	2.70 ± 0.73	2.81 ± 0.76
H δ 4102.89	21.1 ± 3.1	24.5 ± 3.7	24.2 ± 3.5	24.2 ± 3.5	17.3 ± 2.9	17.4 ± 2.9	21.2 ± 3.1	22.0 ± 3.2
H γ 4341.68	40.7 ± 5.9	45.0 ± 6.5	46.9 ± 6.6	46.9 ± 6.7	37.5 ± 5.6	37.7 ± 5.6	40.6 ± 5.8	41.6 ± 6.0
[O III] 4364.44	5.03 ± 1.16	5.54 ± 1.27	7.40 ± 1.10	7.40 ± 1.10	14.8 ± 2.7	14.9 ± 2.7	5.27 ± 1.04	5.40 ± 1.06
He I 4472.93	3.37 ± 0.93	3.63 ± 1.00	3.91 ± 0.62	3.91 ± 0.62	9.76 ± 2.03	9.78 ± 2.03	–	–
Fe III 4659.35	–	–	–	–	–	–	–	–
He II 4687.02	–	–	–	–	–	–	–	–
Ar IV 4741.49	–	–	–	–	–	–	–	–
Hβ 4862.72	100 ± 14	100 ± 14	100 ± 14	100 ± 14	100 ± 14	100 ± 14	100 ± 14	100 ± 14
[O III] 4960.29	125 ± 17	122 ± 17	162 ± 22	162 ± 22	99.5 ± 14.2	99.4 ± 14.2	82.5 ± 11.7	82.1 ± 11.7
[O III] 5008.24	369 ± 52	360 ± 51	473 ± 66	473 ± 66	313 ± 44	313 ± 44	246 ± 35	245 ± 34
[N II] 5756.24	–	–	–	–	–	–	–	–
He I 5877.59	10.8 ± 1.8	9.2 ± 1.6	8.72 ± 1.26	8.72 ± 1.28	9.95 ± 2.61	9.89 ± 2.59	7.86 ± 1.44	7.56 ± 1.38
[O I] 6302.05	6.83 ± 1.27	5.55 ± 1.04	1.97 ± 0.33	1.97 ± 0.34	10.4 ± 2.1	10.3 ± 2.1	5.31 ± 0.97	5.04 ± 0.92
[S III] 6313.80	–	–	1.27 ± 0.25	1.27 ± 0.26	–	–	–	–
[O I] 6365.54	–	–	0.60 ± 0.19	0.60 ± 0.20	–	–	–	–
Hα 6564.61	352 ± 50	278 ± 40	218 ± 30	218 ± 31	244 ± 34	242 ± 34	277 ± 39	261 ± 37
[N II] 6585.20	11.5 ± 1.9	9.1 ± 1.5	5.35 ± 0.79	5.35 ± 0.81	<1.49	<1.47	2.63 ± 0.71	2.48 ± 0.67
He I 6679.99	3.15 ± 0.90	2.46 ± 0.71	2.57 ± 0.41	2.57 ± 0.42	–	–	3.58 ± 0.72	3.37 ± 0.68
[S II] 6718.29	36.3 ± 5.3	28.2 ± 4.2	14.0 ± 2.0	14.0 ± 2.1	9.60 ± 1.90	9.51 ± 1.88	15.5 ± 2.3	14.5 ± 2.1
[S II] 6732.67	24.2 ± 3.6	18.8 ± 2.8	11.1 ± 1.6	11.1 ± 1.7	5.37 ± 1.58	5.32 ± 1.56	11.3 ± 1.7	10.6 ± 1.6
[Ne III] 6870.16	–	–	–	–	–	–	–	–
[Ar III] 7137.80	5.59 ± 1.16	4.17 ± 0.88	9.34 ± 1.38	9.34 ± 1.45	–	–	3.29 ± 0.74	3.06 ± 0.68
[O II] 7321.47	3.98 ± 0.97	2.91 ± 0.72	–	–	–	–	–	–
[O II] 7332.25	2.85 ± 0.94	2.09 ± 0.69	1.71 ± 0.35	1.71 ± 0.36	4.88 ± 1.58	4.82 ± 1.56	3.58 ± 0.77	3.31 ± 0.71
F(Hβ) × 10^{-16} erg s^{-1} cm^{-2}	19.1 ± 1.9		34.5 ± 3.4		6.64 ± 0.67		9.28 ± 0.93	
I(Hβ) × 10^{-16} erg s^{-1} cm^{-2}	40.5 ± 5.4		34.5 ± 5.3		6.83 ± 0.69		11.2 ± 1.2	
$E(B-V)$	0.23 ± 0.03		0.00 ± 0.04		0.01 ± 0.00		0.06 ± 0.01	

Table A1 – *continued*

	JKB 28.0		JKB 29.0		JKB 29.2		JKB 37.0	
[O II] 3727.10	57.4 ± 8.5	57.4 ± 8.6	87.8 ± 13.7	96.0 ± 15.0	61.7 ± 9.7	66.3 ± 10.4	97.1 ± 14.0	130.0 ± 19.2
[O II] 3729.86	51.9 ± 7.8	51.9 ± 7.8	97.5 ± 15.0	106.6 ± 16.4	116 ± 17	125 ± 18	75.6 ± 11.0	101.3 ± 15.1
He I 3820.84	–	–	–	–	–	–	–	–
[Ne III] 3870.16	13.8 ± 2.2	13.8 ± 2.2	10.4 ± 2.5	11.3 ± 2.7	68.2 ± 10.2	72.6 ± 10.8	26.5 ± 3.9	34.0 ± 5.1
He I+H8 3889.75	10.7 ± 1.9	10.7 ± 1.9	12.4 ± 2.8	13.4 ± 3.0	6.20 ± 2.10	6.60 ± 2.23	12.0 ± 2.1	15.4 ± 2.7
He II 3969.55	9.02 ± 1.73	9.02 ± 1.73	–	–	10.1 ± 2.4	10.7 ± 2.5	14.4 ± 2.4	18.0 ± 3.1
He I 4027.49	–	–	–	–	–	–	–	–
[S II] 4069.75	–	–	6.38 ± 2.31	6.78 ± 2.46	–	–	–	–
H δ 4102.89	19.6 ± 3.1	19.6 ± 3.1	12.0 ± 2.6	12.7 ± 2.8	18.5 ± 3.2	19.4 ± 3.4	13.8 ± 2.3	16.7 ± 2.8
H γ 4341.68	42.5 ± 6.2	42.5 ± 6.2	44.2 ± 6.8	45.9 ± 7.1	43.1 ± 6.6	44.5 ± 6.8	38.8 ± 5.6	44.1 ± 6.4
[O III] 4364.44	8.30 ± 1.71	8.30 ± 1.71	<2.32	<2.41	<2.16	<2.22	7.37 ± 1.53	8.33 ± 1.74
He I 4472.93	–	–	–	–	–	–	–	–
Fe III 4659.35	–	–	–	–	–	–	–	–
He II 4687.02	–	–	6.37 ± 1.94	6.45 ± 1.97	–	–	–	–
Ar IV 4741.49	–	–	–	–	–	–	–	–
Hβ 4862.72	100 ± 14	100 ± 14	100 ± 14	100 ± 14	100 ± 14	100 ± 14	100 ± 14	100 ± 14
[O III] 4960.29	89.6 ± 12.8	89.6 ± 12.8	51.2 ± 7.7	50.9 ± 7.7	60.2 ± 8.9	59.9 ± 8.8	150 ± 21	146 ± 20
[O III] 5008.24	266 ± 37	266 ± 37	151 ± 22	149 ± 21	177 ± 25	175 ± 25	419 ± 59	406 ± 57
[N II] 5756.24	–	–	–	–	–	–	–	–
He I 5877.59	6.46 ± 1.30	6.46 ± 1.30	8.81 ± 2.50	8.29 ± 2.36	11.8 ± 2.6	11.3 ± 2.4	10.9 ± 2.2	8.9 ± 1.8
[O I] 6302.05	–	–	–	–	786 ± 113	737 ± 106	6.69 ± 1.42	5.16 ± 1.10
[S III] 6313.80	–	–	–	–	–	–	5.70 ± 1.34	4.39 ± 1.04
[O I] 6365.54	–	–	–	–	4.66 ± 1.54	4.36 ± 1.44	–	–
Hα 6564.61	234 ± 33	234 ± 33	309 ± 44	282 ± 41	296 ± 42	275 ± 39	368 ± 52	273 ± 40
[N II] 6585.20	<0.70	<0.70	6.43 ± 1.94	5.87 ± 1.77	<1.24	<1.15	11.9 ± 2.1	8.8 ± 1.6
He I 6679.99	2.27 ± 0.76	2.27 ± 0.76	11.8 ± 3.3	10.7 ± 3.0	8.74 ± 2.83	8.09 ± 2.62	–	–
[S II] 6718.29	7.48 ± 1.30	7.48 ± 1.30	13.6 ± 2.8	12.3 ± 2.5	11.7 ± 2.5	10.8 ± 2.3	34.0 ± 5.0	24.8 ± 3.7
[S II] 6732.67	6.01 ± 1.46	6.01 ± 1.46	11.4 ± 2.5	10.3 ± 2.3	11.1 ± 2.3	10.3 ± 2.1	22.8 ± 3.5	16.6 ± 2.6
[Ne III] 6870.16	–	–	–	–	–	–	–	–
[Ar III] 7137.80	12.0 ± 2.5	12.0 ± 2.5	–	–	–	–	10.8 ± 2.0	7.5 ± 1.4
[O II] 7321.47	–	–	5.39 ± 1.95	4.78 ± 1.73	7.55 ± 2.03	6.86 ± 1.85	–	–
[O II] 7332.25	3.51 ± 1.09	3.51 ± 1.09	–	–	–	–	3.89 ± 1.18	2.63 ± 0.81
$F(\mathrm{H}\beta) \times 10^{-16}$ erg s^{-1} cm^{-2}	12.6 ± 1.3		4.44 ± 0.46		4.84 ± 0.50		9.11 ± 0.92	
$I(\mathrm{H}\beta) \times 10^{-16}$ erg s^{-1} cm^{-2}	12.6 ± 1.3		5.94 ± 0.65		6.10 ± 0.65		23.4 ± 3.5	
$E(B-V)$	0.00 ± 0.01		0.09 ± 0.01		0.07 ± 0.01		0.29 ± 0.03	

Table A1 *– continued*

	JKB 40.0		JKB 42.0		JKB 53.0		JKB 62.0	
[O II] 3727.10	71.7 ± 11.8	79.9 ± 13.2	31.8 ± 4.8	34.0 ± 5.1	41.8 ± 6.0	42.0 ± 6.0	63.5 ± 11.1	84.7 ± 15.1
[O II] 3729.86	98.5 ± 15.3	109.8 ± 17.1	30.0 ± 4.5	32.1 ± 4.8	42.9 ± 6.1	43.0 ± 6.1	59.3 ± 10.5	79.1 ± 14.3
He I 3820.84	–	–	–	–	–	–	–	–
[Ne III] 3870.16	23.1 ± 5.1	25.4 ± 5.6	48.9 ± 7.0	51.9 ± 7.5	26.0 ± 3.7	26.1 ± 3.7	24.5 ± 4.7	31.4 ± 6.1
He I+H8 3889.75	17.3 ± 4.8	19.0 ± 5.3	17.9 ± 2.7	18.9 ± 2.9	17.9 ± 2.6	18.0 ± 2.6	–	–
He II 3969.55	13.9 ± 3.3	15.2 ± 3.6	29.9 ± 4.3	31.5 ± 4.6	20.0 ± 2.8	20.1 ± 2.9	–	–
He I 4027.49	–	–	2.02 ± 0.72	2.12 ± 0.76	1.24 ± 0.27	1.25 ± 0.27	–	–
[S II] 4069.75	–	–	–	–	0.80 ± 0.23	0.80 ± 0.23	–	–
H δ 4102.89	25.1 ± 4.4	27.0 ± 4.7	25.8 ± 3.7	27.0 ± 3.9	24.1 ± 3.4	24.1 ± 3.4	–	–
H γ 4341.68	37.9 ± 5.9	39.7 ± 6.2	41.8 ± 6.0	43.0 ± 6.2	45.1 ± 6.4	45.1 ± 6.4	35.2 ± 5.9	39.9 ± 6.7
[O III] 4364.44	10.8 ± 2.9	11.3 ± 3.0	15.8 ± 2.4	16.3 ± 2.4	8.93 ± 1.28	8.95 ± 1.29	<3.73	<4.21
He I 4472.93	–	–	4.04 ± 0.86	4.13 ± 0.87	3.18 ± 0.48	3.19 ± 0.48	–	–
Fe III 4659.35	–	–	1.73 ± 0.62	1.75 ± 0.62	–	–	–	–
He II 4687.02	–	–	–	–	–	–	–	–
Ar IV 4741.49	–	–	–	–	–	–	–	–
Hβ 4862.72	100 ± 14	100 ± 14	100 ± 14	100 ± 14	100 ± 14	99 ± 14	100 ± 14	100 ± 14
[O III] 4960.29	91.9 ± 13.3	91.1 ± 13.2	241 ± 34	240 ± 34	113 ± 15	113 ± 15	107 ± 15	105 ± 15
[O III] 5008.24	269 ± 38	265 ± 38	730 ± 103	725 ± 102	338 ± 47	338 ± 47	325 ± 47	315 ± 45
[N II] 5756.24	–	–	–	–	–	–	–	–
He I 5877.59	–	–	10.9 ± 1.7	10.4 ± 1.6	10.00 ± 1.43	9.98 ± 1.43	16.7 ± 4.6	13.8 ± 3.8
[O I] 6302.05	–	–	–	–	0.85 ± 0.22	0.84 ± 0.22	–	–
[S III] 6313.80	–	–	–	–	1.30 ± 0.25	1.30 ± 0.25	–	–
[O I] 6365.54	–	–	–	–	–	–	–	–
Hα 6564.61	281 ± 40	252 ± 36	288 ± 40	268 ± 38	280 ± 39	279 ± 39	339 ± 49	253 ± 38
[N II] 6585.20	8.09 ± 2.40	7.24 ± 2.15	2.50 ± 0.73	2.33 ± 0.68	2.34 ± 0.38	2.33 ± 0.37	<3.73	<2.77
He I 6679.99	8.45 ± 2.46	7.53 ± 2.19	5.02 ± 1.01	4.67 ± 0.94	3.02 ± 0.46	3.01 ± 0.45	–	–
[S II] 6718.29	11.7 ± 2.6	10.4 ± 2.3	10.4 ± 1.7	9.6 ± 1.6	6.83 ± 0.98	6.80 ± 0.98	10.9 ± 3.1	7.9 ± 2.3
[S II] 6732.67	8.03 ± 2.33	7.13 ± 2.07	4.78 ± 0.98	4.44 ± 0.91	5.04 ± 0.73	5.02 ± 0.73	8.18 ± 2.87	5.97 ± 2.11
[Ne III] 6870.16	–	–	–	–	–	–	–	–
[Ar III] 7137.80	–	–	4.97 ± 1.10	4.56 ± 1.01	4.03 ± 0.59	4.02 ± 0.59	13.2 ± 3.1	9.1 ± 2.2
[O II] 7321.47	–	–	–	–	1.21 ± 0.26	1.20 ± 0.25	–	–
[O II] 7332.25	–	–	–	–	1.60 ± 0.34	1.59 ± 0.34	–	–
F(Hβ) × 10^{-16} erg s^{-1} cm^{-2}	3.92 ± 0.40		30.4 ± 3.1		62.3 ± 6.2		7.58 ± 0.79	
I(Hβ) × 10^{-16} erg s^{-1} cm^{-2}	5.56 ± 0.62		38.0 ± 3.9		63.1 ± 6.3		19.3 ± 3.2	
$E(B-V)$	0.11 ± 0.01		0.07 ± 0.01		0.00 ± 0.00		0.28 ± 0.04	

Table A1 – *continued*

	JKB 64.0		JKB 69.0		JKB 78.0		JKB 83.0	
[O II] 3727.10	76.2 ± 11.2	100.5 ± 15.1	61.5 ± 9.2	64.6 ± 9.6	44.8 ± 6.6	44.8 ± 6.6	113 ± 16	124 ± 18
[O II] 3729.86	59.8 ± 8.9	78.8 ± 12.1	63.4 ± 9.4	66.6 ± 9.9	46.9 ± 6.9	46.9 ± 6.9	138 ± 20	152 ± 22
He I 3820.84	12.4 ± 2.3	15.9 ± 3.0	–	–	–	–	–	–
[Ne III] 3870.16	15.3 ± 2.5	19.5 ± 3.2	35.2 ± 5.2	36.6 ± 5.4	22.4 ± 3.3	22.4 ± 3.3	–	–
He I+H8 3889.75	4.89 ± 1.52	6.18 ± 1.92	12.8 ± 2.4	13.3 ± 2.5	16.8 ± 2.5	16.8 ± 2.5	23.5 ± 4.2	25.5 ± 4.6
He II 3969.55	–	–	20.4 ± 3.3	21.1 ± 3.4	20.7 ± 3.0	20.7 ± 3.0	21.2 ± 3.8	22.8 ± 4.0
He I 4027.49	–	–	–	–	2.49 ± 0.70	2.49 ± 0.70	–	–
[S II] 4069.75	–	–	9.42 ± 1.90	9.73 ± 1.97	2.23 ± 0.73	2.23 ± 0.73	–	–
H δ 4102.89	10.8 ± 1.9	12.9 ± 2.3	22.7 ± 3.5	23.4 ± 3.7	23.3 ± 3.4	23.3 ± 3.4	25.5 ± 4.2	27.1 ± 4.5
H γ 4341.68	35.3 ± 5.1	39.7 ± 5.8	41.4 ± 6.0	42.2 ± 6.2	41.8 ± 6.0	41.8 ± 6.0	41.3 ± 6.3	43.0 ± 6.6
[O III] 4364.44	6.44 ± 1.56	7.22 ± 1.75	10.8 ± 2.1	11.1 ± 2.1	7.46 ± 1.27	7.46 ± 1.27	<2.08	<2.16
He I 4472.93	–	–	–	–	3.16 ± 0.68	3.16 ± 0.68	–	–
Fe III 4659.35	–	–	–	–	–	–	–	–
He II 4687.02	–	–	–	–	–	–	–	–
Ar IV 4741.49	–	–	–	–	–	–	–	–
Hβ 4862.72	100 ± 14	100 ± 14	100 ± 14	100 ± 14	100 ± 14	100 ± 14	100 ± 14	100 ± 14
[O III] 4960.29	62.9 ± 9.0	61.5 ± 8.8	166 ± 23	165 ± 23	117 ± 16	117 ± 16	46.7 ± 6.9	46.3 ± 6.8
[O III] 5008.24	187 ± 26	182 ± 25	496 ± 70	494 ± 70	357 ± 50	357 ± 50	144 ± 20	142 ± 20
[N II] 5756.24	–	–	–	–	–	–	–	–
He I 5877.59	8.17 ± 2.74	6.79 ± 2.28	12.1 ± 2.3	11.7 ± 2.2	9.76 ± 1.60	9.76 ± 1.60	9.33 ± 2.67	8.75 ± 2.50
[O I] 6302.05	–	–	–	–	–	–	–	–
[S III] 6313.80	–	–	–	–	–	–	–	–
[O I] 6365.54	–	–	–	–	–	–	–	–
Hα 6564.61	334 ± 47	252 ± 36	278 ± 39	264 ± 37	261 ± 37	261 ± 37	296 ± 42	268 ± 38
[N II] 6585.20	3.78 ± 1.17	2.85 ± 0.89	6.44 ± 1.53	6.13 ± 1.45	3.41 ± 0.68	3.41 ± 0.68	45.2 ± 6.8	41.0 ± 6.2
He I 6679.99	3.06 ± 0.97	2.28 ± 0.73	–	–	2.54 ± 0.53	2.54 ± 0.53	–	–
[S II] 6718.29	11.2 ± 1.8	8.3 ± 1.4	13.4 ± 2.2	12.7 ± 2.1	6.31 ± 1.00	6.31 ± 1.00	13.5 ± 2.5	12.2 ± 2.3
[S II] 6732.67	8.41 ± 1.50	6.22 ± 1.13	8.42 ± 2.09	7.99 ± 1.98	5.34 ± 0.87	5.34 ± 0.87	10.9 ± 2.2	9.8 ± 2.0
[Ne III] 6870.16	–	–	4.54 ± 1.43	4.29 ± 1.36	–	–	6.68 ± 2.14	5.98 ± 1.92
[Ar III] 7137.80	–	–	–	–	5.00 ± 0.83	5.00 ± 0.83	6.99 ± 1.90	6.20 ± 1.69
[O II] 7321.47	–	–	–	–	–	–	–	–
[O II] 7332.25	–	–	–	–	2.94 ± 0.85	2.94 ± 0.85	–	–
$F(\mathrm{H}\beta) \times 10^{-16}$ erg s^{-1} cm^{-2}	9.00 ± 0.91		26.7 ± 2.7		26.7 ± 2.7		18.5 ± 1.9	
$I(\mathrm{H}\beta) \times 10^{-16}$ erg s^{-1} cm^{-2}	22.0 ± 3.2		31.3 ± 3.2		26.7 ± 2.7		25.3 ± 2.7	
$E(B-V)$	0.27 ± 0.03		0.05 ± 0.01		0.00 ± 0.00		0.09 ± 0.01	

Table A1 *– continued*

	JKB 85.0		JKB 89.0		JKB 91.0		JKB 97.0	
[O II] 3727.10	77.7 ± 12.1	93.6 ± 14.7	106 ± 15	116 ± 17	129 ± 18	133 ± 19	92.9 ± 13.7	99.7 ± 14.7
[O II] 3729.86	112 ± 16	135 ± 20	120 ± 17	132 ± 19	129 ± 18	133 ± 19	87.2 ± 12.9	93.5 ± 13.8
He I 3820.84	21.6 ± 4.2	25.6 ± 5.1	8.57 ± 2.14	9.30 ± 2.32	–	–	–	–
[Ne III] 3870.16	22.9 ± 4.1	26.9 ± 4.8	33.8 ± 5.2	36.6 ± 5.6	31.9 ± 4.6	32.8 ± 4.7	23.2 ± 3.9	24.6 ± 4.1
He I+H8 3889.75	17.0 ± 3.6	19.9 ± 4.2	12.2 ± 2.6	13.2 ± 2.9	17.5 ± 2.6	18.0 ± 2.7	14.7 ± 2.7	15.6 ± 2.9
He II 3969.55	–	–	6.62 ± 2.07	7.10 ± 2.22	19.8 ± 2.9	20.2 ± 2.9	15.5 ± 2.7	16.4 ± 2.8
He I 4027.49	–	–	–	–	2.94 ± 0.78	3.00 ± 0.80	–	–
[S II] 4069.75	–	–	–	–	3.90 ± 0.77	3.98 ± 0.79	–	–
H δ 4102.89	16.4 ± 3.4	18.5 ± 3.8	16.7 ± 3.0	17.7 ± 3.2	23.4 ± 3.4	23.9 ± 3.4	22.0 ± 3.5	23.0 ± 3.6
H γ 4341.68	38.9 ± 6.2	42.1 ± 6.7	38.2 ± 5.7	39.7 ± 5.9	44.8 ± 6.4	45.4 ± 6.5	42.9 ± 6.3	44.2 ± 6.5
[O III] 4364.44	<3.04	<3.29	7.65 ± 2.04	7.94 ± 2.12	5.12 ± 0.88	5.19 ± 0.89	6.35 ± 1.60	6.54 ± 1.65
He I 4472.93	–	–	–	–	2.78 ± 0.60	2.81 ± 0.61	5.06 ± 1.40	5.17 ± 1.43
Fe III 4659.35	–	–	–	–	–	–	3.46 ± 1.25	3.50 ± 1.26
He II 4687.02	–	–	–	–	–	–	–	–
Ar IV 4741.49	26.2 ± 4.4	26.7 ± 4.5	–	–	–	–	–	–
Hβ 4862.72	100 ± 14	100 ± 14	100 ± 14	100 ± 14	100 ± 14	100 ± 14	100 ± 14	100 ± 14
[O III] 4960.29	102 ± 14	100 ± 14	137 ± 19	136 ± 19	124 ± 17	124 ± 17	115 ± 16	114 ± 16
[O III] 5008.24	295 ± 42	289 ± 41	399 ± 56	395 ± 56	372 ± 52	371 ± 52	346 ± 49	344 ± 49
[N II] 5756.24	–	–	–	–	–	–	3.68 ± 1.31	3.53 ± 1.26
He I 5877.59	12.3 ± 3.2	10.8 ± 2.8	12.0 ± 2.6	11.3 ± 2.4	11.4 ± 1.7	11.2 ± 1.7	9.69 ± 2.01	9.24 ± 1.92
[O I] 6302.05	–	–	–	–	6.40 ± 1.03	6.23 ± 1.00	–	–
[S III] 6313.80	–	–	–	–	1.49 ± 0.53	1.45 ± 0.51	–	–
[O I] 6365.54	–	–	–	–	2.38 ± 0.55	2.32 ± 0.54	–	–
Hα 6564.61	319 ± 46	264 ± 38	276 ± 39	252 ± 36	288 ± 40	280 ± 39	294 ± 42	274 ± 39
[N II] 6585.20	<2.67	<2.21	<1.64	<1.49	14.3 ± 2.1	13.8 ± 2.0	6.20 ± 1.57	5.77 ± 1.46
He I 6679.99	10.7 ± 3.8	8.8 ± 3.2	4.43 ± 1.58	4.02 ± 1.44	3.17 ± 0.63	3.07 ± 0.61	–	–
[S II] 6718.29	8.69 ± 2.58	7.10 ± 2.12	19.1 ± 3.5	17.3 ± 3.2	37.5 ± 5.3	36.4 ± 5.2	18.0 ± 2.9	16.7 ± 2.7
[S II] 6732.67	24.5 ± 4.4	20.0 ± 3.7	11.8 ± 2.3	10.7 ± 2.1	26.2 ± 3.7	25.4 ± 3.6	10.3 ± 1.9	9.5 ± 1.8
[Ne III] 6870.16	–	–	–	–	–	–	–	–
[Ar III] 7137.80	14.8 ± 3.4	11.7 ± 2.7	–	–	8.46 ± 1.28	8.15 ± 1.23	4.38 ± 1.30	4.01 ± 1.19
[O II] 7321.47	7.85 ± 2.38	6.13 ± 1.87	–	–	4.44 ± 0.87	4.27 ± 0.84	–	–
[O II] 7332.25	–	–	–	–	–	–	6.74 ± 1.89	6.13 ± 1.72
$F(\mathrm{H}\beta) \times 10^{-16}$ erg s^{-1} cm^{-2}	6.24 ± 0.65		13.5 ± 1.4		35.0 ± 3.5		11.0 ± 1.1	
$I(\mathrm{H}\beta) \times 10^{-16}$ erg s^{-1} cm^{-2}	11.4 ± 1.5		18.1 ± 1.9		38.5 ± 3.9		13.8 ± 1.4	
$E(B-V)$	0.18 ± 0.02		0.09 ± 0.01		0.03 ± 0.00		0.07 ± 0.01	

Table A1 – *continued*

	JKB 97.1		JKB 119.0		JKB 122.0		JKB 131.0	
[O II] 3727.10	174 ± 40	222 ± 52	477 ± 125	731 ± 203	49.3 ± 7.0	55.1 ± 7.9	143 ± 21	181 ± 27
[O II] 3729.86	112 ± 31	143 ± 40	<59.1	<90.7	61.4 ± 8.7	68.5 ± 9.8	145 ± 21	183 ± 28
He I 3820.84	–	–	–	–	–	–	–	–
[Ne III] 3870.16	–	–	–	–	21.4 ± 3.0	23.5 ± 3.4	36.7 ± 7.2	45.0 ± 8.9
He I+H8 3889.75	–	–	–	–	15.5 ± 2.2	17.0 ± 2.4	–	–
He II 3969.55	–	–	–	–	16.4 ± 2.3	17.8 ± 2.6	–	–
He I 4027.49	–	–	–	–	1.04 ± 0.29	1.12 ± 0.32	–	–
[S II] 4069.75	–	–	–	–	–	–	–	–
H δ 4102.89	–	–	–	–	20.6 ± 2.9	22.2 ± 3.2	15.1 ± 3.5	17.6 ± 4.1
H γ 4341.68	237 ± 45	264 ± 50	–	–	39.7 ± 5.6	41.6 ± 5.9	36.0 ± 5.7	39.8 ± 6.4
[O III] 4364.44	<16.4	<18.1	<24.5	<29.2	6.21 ± 0.91	6.50 ± 0.96	<3.70	<4.08
He I 4472.93	–	–	–	–	3.14 ± 0.49	3.25 ± 0.51	–	–
Fe III 4659.35	–	–	–	–	1.03 ± 0.25	1.05 ± 0.26	–	–
He II 4687.02	–	–	–	–	–	–	–	–
Ar IV 4741.49	–	–	–	–	–	–	–	–
Hβ 4862.72	100 ± 21	100 ± 21	100 ± 27	100 ± 27	100 ± 14	100 ± 14	100 ± 14	100 ± 14
[O III] 4960.29	56.4 ± 14.7	55.3 ± 14.4	<20.8	<20.1	107 ± 15	106 ± 15	85.2 ± 12.4	83.6 ± 12.2
[O III] 5008.24	168 ± 32	163 ± 31	101 ± 26	97 ± 25	328 ± 46	325 ± 45	243 ± 34	236 ± 34
[N II] 5756.24	–	–	–	–	–	–	–	–
He I 5877.59	–	–	128 ± 48	96 ± 36	9.83 ± 1.42	9.13 ± 1.32	11.9 ± 3.4	10.1 ± 2.9
[O I] 6302.05	–	–	–	–	2.22 ± 0.45	2.02 ± 0.40	9.16 ± 3.04	7.42 ± 2.47
[S III] 6313.80	–	–	–	–	1.08 ± 0.26	0.97 ± 0.24	–	–
[O I] 6365.54	–	–	–	–	–	–	–	–
Hα 6564.61	365 ± 67	285 ± 53	441 ± 98	285 ± 69	292 ± 41	261 ± 37	321 ± 46	253 ± 37
[N II] 6585.20	<15.1	<11.8	<23.6	<15.2	4.32 ± 0.65	3.86 ± 0.58	13.5 ± 3.1	10.6 ± 2.5
He I 6679.99	–	–	–	–	2.96 ± 0.46	2.63 ± 0.41	–	–
[S II] 6718.29	66.3 ± 16.9	51.0 ± 13.2	113 ± 31	71 ± 21	11.2 ± 1.6	10.0 ± 1.4	35.4 ± 5.6	27.4 ± 4.5
[S II] 6732.67	<15.7	<12.1	109 ± 31	68 ± 20	8.12 ± 1.17	7.20 ± 1.04	26.4 ± 4.5	20.4 ± 3.5
[Ne III] 6870.16	–	–	–	–	–	–	10.0 ± 3.3	7.6 ± 2.5
[Ar III] 7137.80	–	–	84.5 ± 29.6	49.3 ± 18.2	4.65 ± 0.69	4.05 ± 0.61	–	–
[O II] 7321.47	–	–	–	–	1.26 ± 0.30	1.09 ± 0.26	15.7 ± 3.9	11.5 ± 2.8
[O II] 7332.25	–	–	86.0 ± 33.7	48.5 ± 19.9	–	–	18.2 ± 3.9	13.3 ± 2.9
F(Hβ) × 10^{-16} erg s^{-1} cm^{-2}	1.46 ± 0.22		2.24 ± 0.43		81.9 ± 8.2		6.46 ± 0.67	
I(Hβ) × 10^{-16} erg s^{-1} cm^{-2}	3.20 ± 0.65		8.91 ± 3.15		117 ± 12		13.9 ± 2.0	
$E(B-V)$	0.24 ± 0.04		0.42 ± 0.09		0.11 ± 0.01		0.23 ± 0.03	

Table A1 *– continued*

	JKB 133.0		JKB 133.1		JKB 136.0		JKB 137.0	
[O II] 3727.10	156 ± 25	170 ± 27	83.4 ± 12.6	94.1 ± 14.2	91.0 ± 14.2	91.0 ± 14.2	111 ± 25	186 ± 53
[O II] 3729.86	189 ± 29	206 ± 32	125 ± 18	141 ± 20	72.4 ± 11.7	72.4 ± 11.7	223 ± 40	373 ± 93
He I 3820.84	–	–	–	–	–	–	–	–
[Ne III] 3870.16	15.7 ± 4.6	16.8 ± 5.0	21.8 ± 3.4	24.1 ± 3.8	16.0 ± 3.9	16.0 ± 3.9	–	–
He I+H8 3889.75	–	–	9.40 ± 2.02	10.41 ± 2.24	–	–	–	–
He II 3969.55	–	–	12.6 ± 2.3	13.8 ± 2.5	–	–	–	–
He I 4027.49	–	–	–	–	–	–	–	–
[S II] 4069.75	–	–	–	–	–	–	–	–
H δ 4102.89	21.6 ± 5.3	22.8 ± 5.6	21.3 ± 3.4	23.0 ± 3.7	–	–	–	–
H γ 4341.68	46.2 ± 7.8	48.0 ± 8.1	40.0 ± 5.9	42.2 ± 6.2	32.1 ± 5.6	32.1 ± 5.6	36.0 ± 11.0	44.9 ± 14.1
[O III] 4364.44	<4.76	<4.93	6.17 ± 1.70	6.48 ± 1.79	<3.84	<3.84	<11.8	<14.6
He I 4472.93	–	–	4.24 ± 1.33	4.40 ± 1.38	–	–	–	–
Fe III 4659.35	–	–	–	–	–	–	–	–
He II 4687.02	–	–	–	–	–	–	–	–
Ar IV 4741.49	–	–	–	–	–	–	–	–
Hβ 4862.72	100 ± 14	100 ± 14	100 ± 14	100 ± 14	100 ± 14	100 ± 14	100 ± 17	100 ± 17
[O III] 4960.29	109 ± 16	108 ± 16	131 ± 18	130 ± 18	102 ± 15	102 ± 15	98.7 ± 17.4	94.9 ± 16.7
[O III] 5008.24	322 ± 46	319 ± 46	391 ± 55	386 ± 54	289 ± 42	289 ± 42	292 ± 47	276 ± 45
[N II] 5756.24	–	–	–	–	–	–	–	–
He I 5877.59	15.3 ± 4.9	14.4 ± 4.6	12.7 ± 2.3	11.7 ± 2.2	14.0 ± 3.7	14.0 ± 3.7	–	–
[O I] 6302.05	–	–	–	–	12.5 ± 3.0	12.5 ± 3.0	–	–
[S III] 6313.80	–	–	–	–	–	–	–	–
[O I] 6365.54	–	–	–	–	–	–	36.9 ± 11.4	23.1 ± 8.0
Hα 6564.61	318 ± 46	292 ± 42	298 ± 42	264 ± 37	207 ± 30	207 ± 30	467 ± 75	277 ± 66
[N II] 6585.20	18.3 ± 4.8	16.8 ± 4.4	11.8 ± 2.2	10.5 ± 1.9	9.44 ± 2.95	9.44 ± 2.95	58.3 ± 13.5	34.5 ± 10.1
He I 6679.99	–	–	6.22 ± 1.51	5.47 ± 1.33	–	–	–	–
[S II] 6718.29	37.9 ± 6.7	34.5 ± 6.1	20.4 ± 3.2	17.9 ± 2.8	25.5 ± 5.0	25.5 ± 5.0	97.0 ± 20.3	55.7 ± 15.7
[S II] 6732.67	32.7 ± 6.3	29.8 ± 5.7	17.2 ± 2.8	15.0 ± 2.5	20.7 ± 4.0	20.7 ± 4.0	52.5 ± 12.8	30.0 ± 9.3
[Ne III] 6870.16	–	–	–	–	–	–	–	–
[Ar III] 7137.80	–	–	–	–	8.63 ± 3.04	8.63 ± 3.04	–	–
[O II] 7321.47	–	–	6.59 ± 1.75	5.61 ± 1.49	–	–	46.7 ± 12.7	23.6 ± 8.4
[O II] 7332.25	–	–	–	–	–	–	–	–
F(Hβ) × 10^{-16} erg s^{-1} cm^{-2}	5.33 ± 0.56		15.5 ± 1.6		12.3 ± 1.3		10.6 ± 1.3	
I(Hβ) × 10^{-16} erg s^{-1} cm^{-2}	7.02 ± 0.78		23.0 ± 2.5		12.3 ± 1.3		55.4 ± 32.1	
$E(B-V)$	0.08 ± 0.01		0.12 ± 0.01		0.00 ± 0.00		0.50 ± 0.17	

Table A1 – *continued*

	JKB 138.2		JKB 141.0		JKB 142.0		JKB 144.0	
[O II] 3727.10	325 ± 49	493 ± 119	108 ± 15	131 ± 19	58.8 ± 8.9	70.2 ± 10.7	79.9 ± 11.3	91.1 ± 13.0
[O II] 3729.86	147 ± 24	223 ± 55	135 ± 19	163 ± 23	83.8 ± 12.3	100.1 ± 14.8	62.7 ± 8.9	71.5 ± 10.2
He I 3820.84	33.1 ± 7.3	48.2 ± 13.4	–	–	8.64 ± 2.04	10.15 ± 2.40	–	–
[Ne III] 3870.16	43.6 ± 8.2	62.3 ± 15.5	26.8 ± 4.0	31.6 ± 4.7	15.0 ± 2.6	17.5 ± 3.0	36.0 ± 5.1	40.3 ± 5.7
He I+H8 3889.75	–	–	18.6 ± 2.9	21.9 ± 3.4	12.9 ± 2.5	15.0 ± 2.9	17.0 ± 2.4	19.0 ± 2.7
He II 3969.55	–	–	15.7 ± 2.6	18.2 ± 3.0	4.06 ± 1.47	4.66 ± 1.69	23.9 ± 3.4	26.4 ± 3.8
He I 4027.49	–	–	–	–	–	–	1.97 ± 0.38	2.17 ± 0.42
[S II] 4069.75	25.2 ± 7.0	33.5 ± 10.2	3.22 ± 1.13	3.67 ± 1.29	–	–	1.12 ± 0.31	1.22 ± 0.34
H δ 4102.89	–	–	22.2 ± 3.3	25.2 ± 3.8	13.4 ± 2.3	15.0 ± 2.6	24.1 ± 3.4	26.3 ± 3.7
H γ 4341.68	21.5 ± 6.1	25.7 ± 7.6	41.6 ± 6.0	45.3 ± 6.5	36.6 ± 5.4	39.5 ± 5.8	42.8 ± 6.1	45.3 ± 6.4
[O III] 4364.44	<7.49	<8.91	8.16 ± 1.56	8.84 ± 1.70	<1.37	<1.47	8.50 ± 1.24	8.98 ± 1.31
He I 4472.93	–	–	3.06 ± 1.03	3.25 ± 1.10	–	–	4.37 ± 0.66	4.56 ± 0.69
Fe III 4659.35	–	–	–	–	–	–	–	–
He II 4687.02	–	–	–	–	–	–	–	–
Ar IV 4741.49	–	–	–	–	–	–	0.72 ± 0.24	0.73 ± 0.24
Hβ 4862.72	100 ± 15	100 ± 15	100 ± 14	100 ± 14	100 ± 14	99 ± 14	100 ± 14	100 ± 14
[O III] 4960.29	79.6 ± 12.5	77.1 ± 12.2	117 ± 16	116 ± 16	63.5 ± 9.1	62.6 ± 9.0	180 ± 25	178 ± 25
[O III] 5008.24	203 ± 30	194 ± 29	335 ± 47	328 ± 46	199 ± 28	195 ± 27	545 ± 77	538 ± 76
[N II] 5756.24	–	–	–	–	–	–	–	–
He I 5877.59	–	–	12.0 ± 2.0	10.5 ± 1.8	22.1 ± 4.0	19.6 ± 3.6	12.0 ± 1.7	11.0 ± 1.6
[O I] 6302.05	–	–	4.39 ± 1.12	3.70 ± 0.95	–	–	4.02 ± 0.62	3.58 ± 0.55
[S III] 6313.80	–	–	–	–	–	–	1.18 ± 0.29	1.05 ± 0.26
[O I] 6365.54	–	–	–	–	–	–	1.09 ± 0.28	0.97 ± 0.25
Hα 6564.61	274 ± 40	179 ± 43	340 ± 48	279 ± 40	301 ± 42	251 ± 36	319 ± 45	279 ± 39
[N II] 6585.20	16.2 ± 4.6	10.6 ± 3.6	11.1 ± 1.9	9.1 ± 1.6	<1.38	<1.15	7.18 ± 1.06	6.27 ± 0.93
He I 6679.99	–	–	–	–	–	–	5.22 ± 0.82	4.54 ± 0.71
[S II] 6718.29	46.8 ± 7.8	29.8 ± 7.9	28.5 ± 4.2	23.1 ± 3.5	19.9 ± 3.1	16.4 ± 2.6	16.0 ± 2.3	13.9 ± 2.0
[S II] 6732.67	43.9 ± 7.5	27.9 ± 7.5	17.4 ± 2.7	14.1 ± 2.2	13.1 ± 2.2	10.8 ± 1.8	12.8 ± 1.8	11.1 ± 1.6
[Ne III] 6870.16	–	–	–	–	–	–	–	–
[Ar III] 7137.80	–	–	–	–	4.75 ± 1.34	3.79 ± 1.07	8.46 ± 1.24	7.17 ± 1.06
[O II] 7321.47	–	–	2.86 ± 1.02	2.21 ± 0.79	–	–	2.55 ± 0.44	2.14 ± 0.38
[O II] 7332.25	–	–	6.93 ± 1.50	5.35 ± 1.17	6.71 ± 1.65	5.28 ± 1.31	2.12 ± 0.39	1.78 ± 0.33
$F(\mathrm{H}\beta) \times 10^{-16}$ erg s^{-1} cm^{-2}	4.48 ± 0.49		45.3 ± 4.6		37.6 ± 3.8		74.9 ± 7.5	
$I(\mathrm{H}\beta) \times 10^{-16}$ erg s^{-1} cm^{-2}	17.2 ± 10.6		84.6 ± 10.4		66.9 ± 8.2		114 ± 12	
$E(B-V)$	0.41 ± 0.18		0.19 ± 0.02		0.17 ± 0.02		0.13 ± 0.01	

Table A1 – *continued*

	JKB 144.1	
[O II] 3727.10	188 ± 50	277 ± 78
[O II] 3729.86	256 ± 62	378 ± 97
He I 3820.84	–	–
[Ne III] 3870.16	129 ± 32	181 ± 46
He I+H8 3889.75	–	–
He II 3969.55	–	–
He I 4027.49	–	–
[S II] 4069.75	–	–
H δ 4102.89	–	–
H γ 4341.68	–	–
[O III] 4364.44	<21.0	<24.7
He I 4472.93	–	–
Fe III 4659.35	–	–
He II 4687.02	–	–
Ar IV 4741.49	–	–
Hβ 4862.72	100 ± 26	100 ± 26
[O III] 4960.29	181 ± 41	175 ± 40
[O III] 5008.24	396 ± 86	379 ± 82
[N II] 5756.24	91.2 ± 33.6	72.1 ± 26.8
He I 5877.59	74.6 ± 24.6	57.5 ± 19.2
[O I] 6302.05	–	–
[S III] 6313.80	–	–
[O I] 6365.54	–	–
Hα 6564.61	424 ± 92	285 ± 66
[N II] 6585.20	61.7 ± 23.6	41.4 ± 16.2
He I 6679.99	119 ± 35	79 ± 24
[S II] 6718.29	108 ± 30	71 ± 21
[S II] 6732.67	<29.8	<19.5
[Ne III] 6870.16	–	–
[Ar III] 7137.80	91.3 ± 29.9	55.9 ± 19.2
[O II] 7321.47	–	–
[O II] 7332.25	–	–
F(Hβ) $\times 10^{-16}$ erg s^{-1} cm^{-2}	1.40 ± 0.26	
I(Hβ) $\times 10^{-16}$ erg s^{-1} cm^{-2}	4.95 ± 1.61	
$E(B-V)$	0.38 ± 0.08	

APPENDIX B: OBSERVED SPECTRA

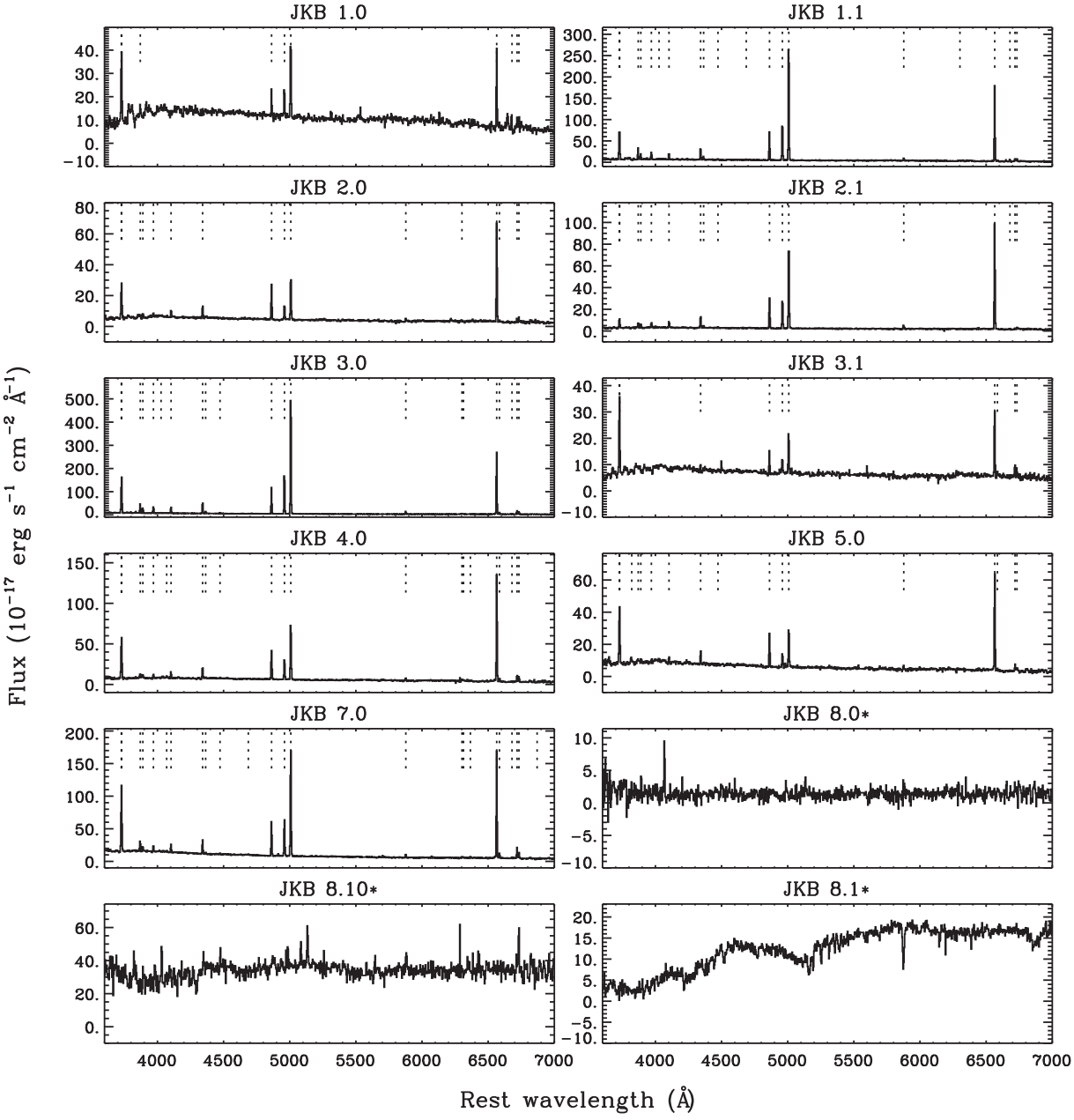

Figure B1. MMT spectra of the sample of BDD galaxies detailed in Table 1 and shown in Fig. 1. Wavelengths are given in the rest frame of each galaxy. Each spectrum has been smoothed with a 5-pixel boxcar for presentation purposes. Dashed lines indicate emission lines detected in each spectrum, as listed in Table A1. Object titles listed with '*' highlight those for which no strong emission lines were detected and are hence shown at the observed wavelength.

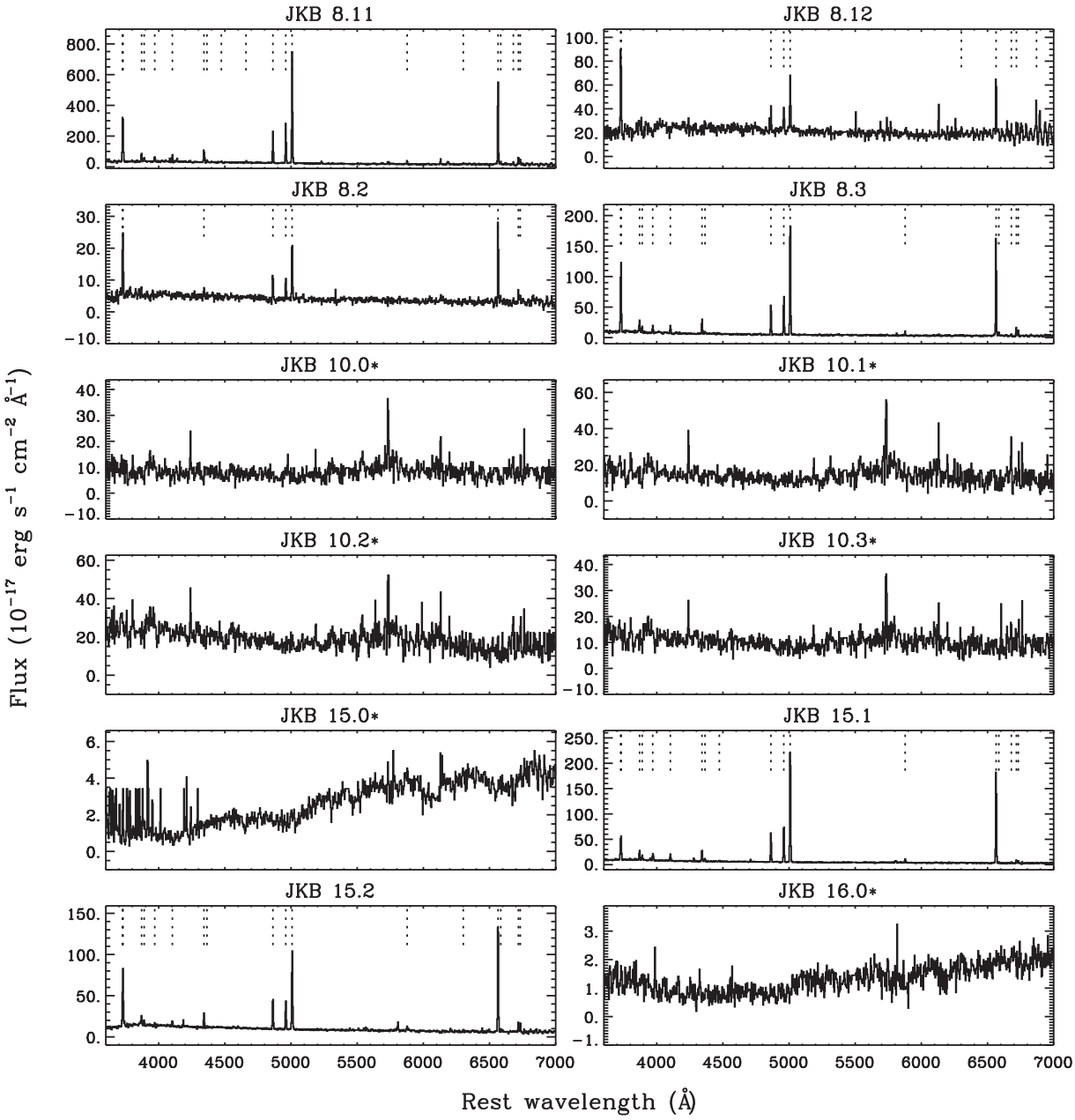

Figure B1 – *continued*

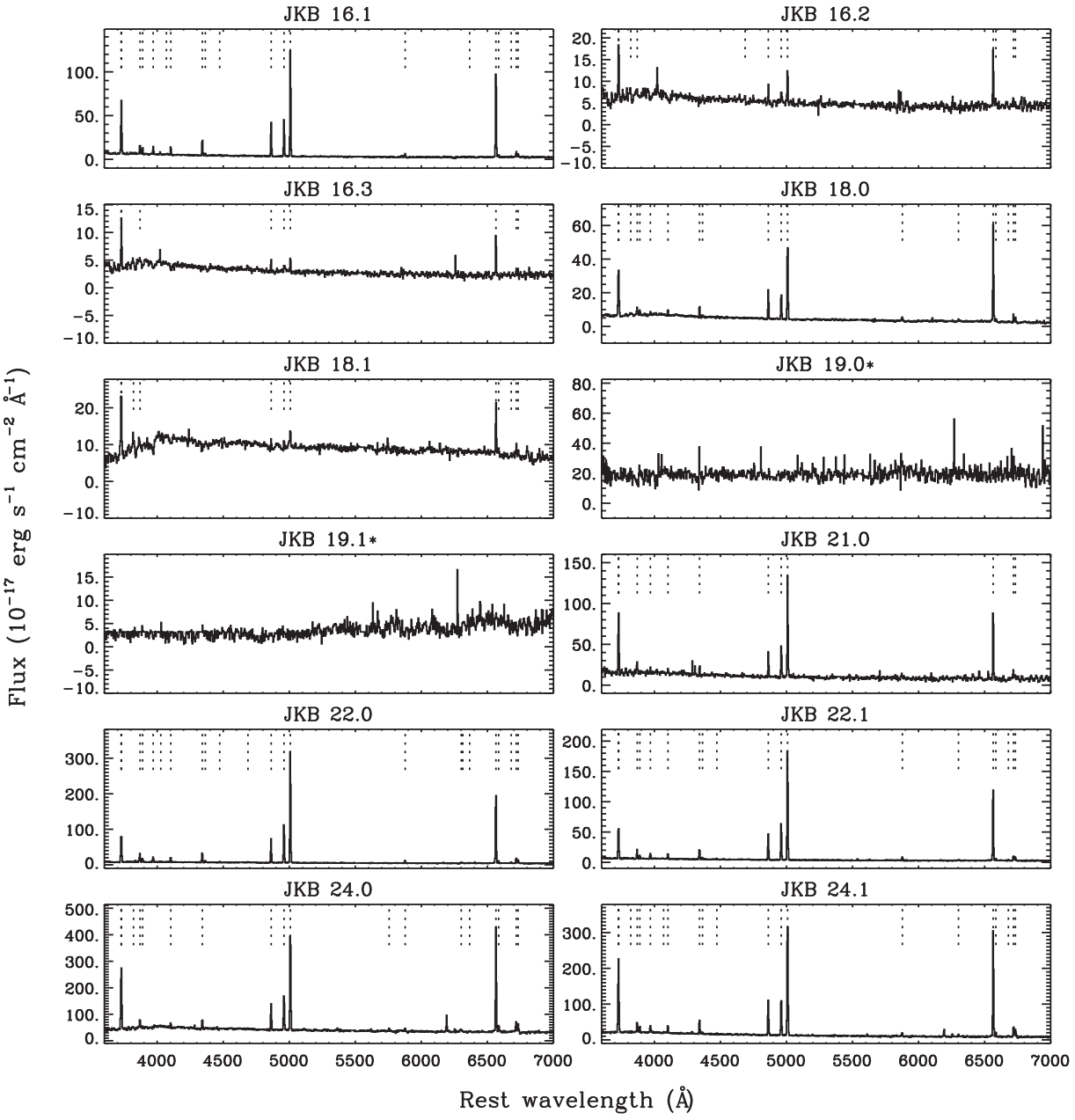

Figure B1 – *continued*

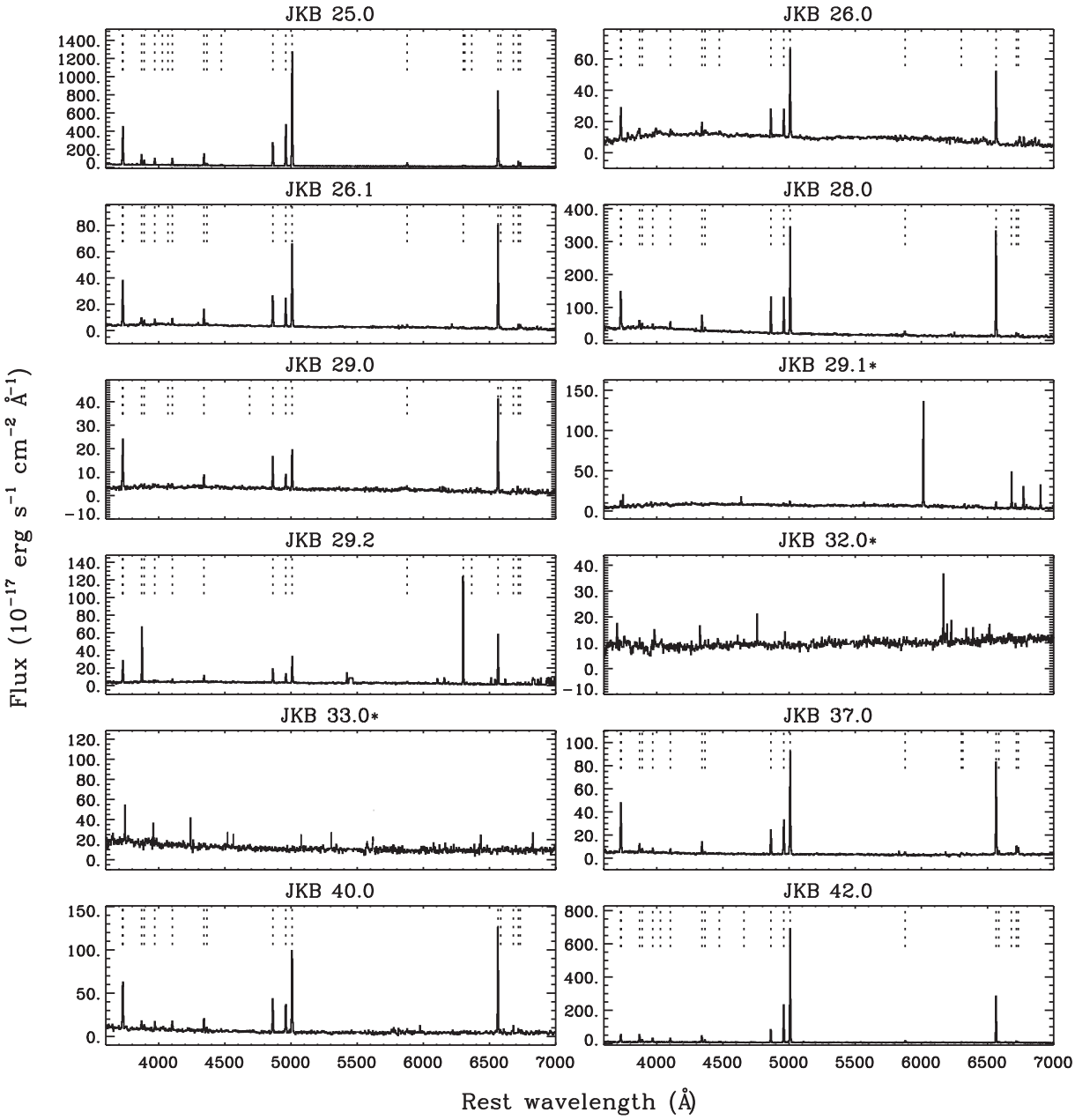

Figure B1 – *continued*

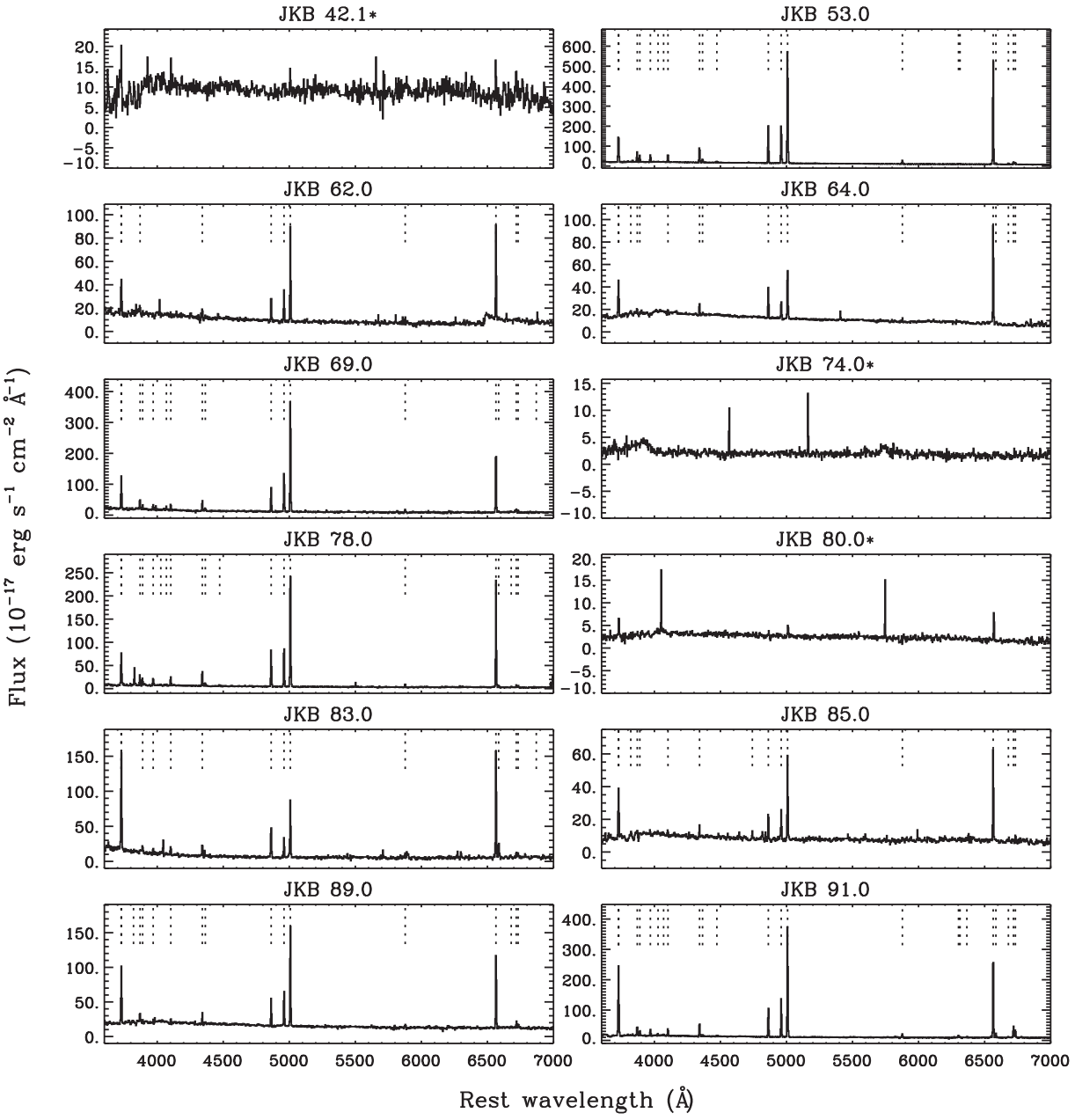

Figure B1 – *continued*

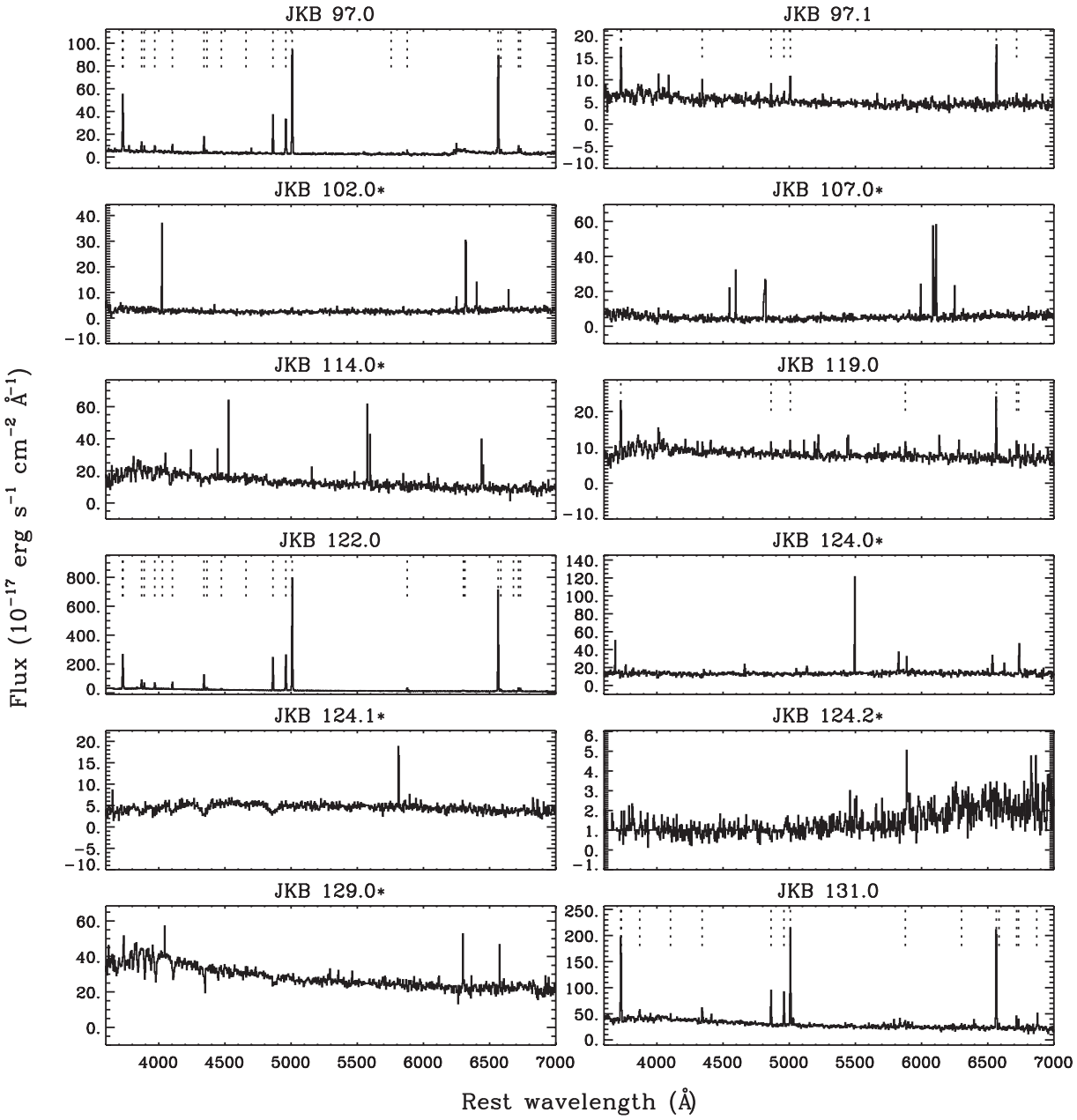

Figure B1 – *continued*

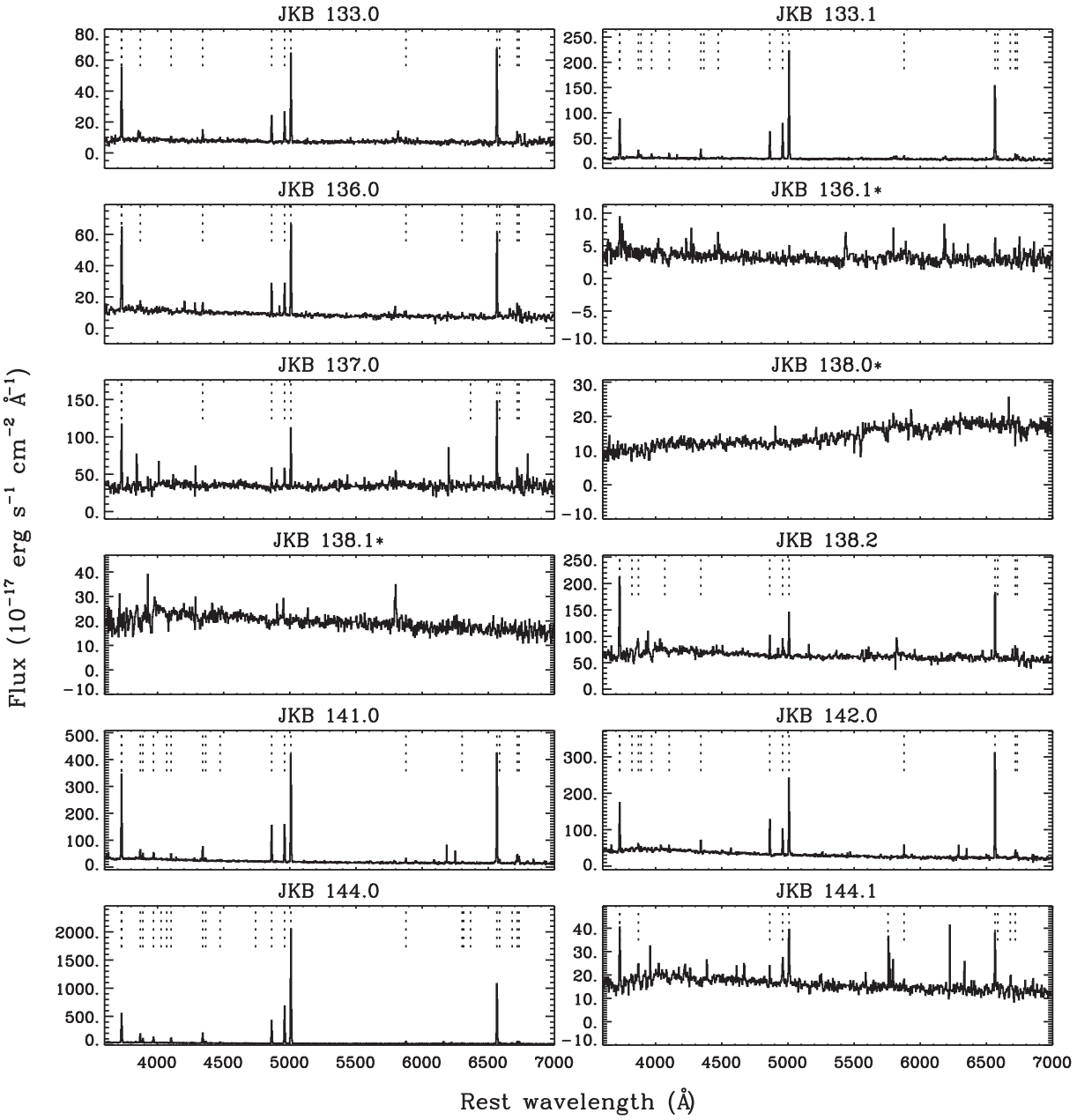

Figure B1 *– continued*

This paper has been typeset from a TEX/LATEX file prepared by the author.